九州大学学術情報リポジトリ
Kyushu University Institutional Repository

DESIGN AND TECHNO-ECONOMIC ANALYSIS OF LIGHT INTEGRATED GASIFICATION FUEL CELL

ビン ヌア, タウフィック

https://doi.org/10.15017/1543981

出版情報：九州大学, 2015, 博士（工学）, 課程博士
バージョン：
権利関係：全文ファイル公表済

Kyushu University

Graduate School of Engineering

DESIGN AND TECHNO-ECONOMIC ANALYSIS OF LIGHT INTEGRATED GASIFICATION FUEL CELL

By

Taufiq Bin Nur

A THESIS

Submitted in partial fulfillment of

The requirements for the degree of

[Doctor of Engineering]

DEPARTMENT OF HYDROGEN ENERGY SYSTEMS

GRADUATE SCHOOL OF ENGINEERING

KYUSHU UNIVERSITY

2015

ABSTRACT

Coal is one of the world`s primary energy resources, and it produces a large amount of carbon dioxide (CO_2) that contributes to global warming. Traditional coal gasification power plant technologies have not reach desirable level of electrical efficiencies. Nowadays, solid oxide fuel cell (SOFC) is a high efficiency power generation device that directly converts the chemical energy of a fuel to electricity. Typically, the major components of syngas produced from coal gasification include hydrogen, carbon monoxide, and methane are potential fuels for SOFCs, which make the possible integration between SOFCs and coal gasifier. Integration of SOFC in coal gasification power plant technology would be one of the promising technologies in the coal utilization for power generation. In this work, proposed plants consisting of coal gasifier and SOFC on the top of a steam turbine, called light integrated gasification fuel cell (L-IGFC), are investigated thermodynamically by using Aspen Plus software to evaluate their performance. The tubular SOFC configuration was selected. The analyses are based on the SOFC module considering ohmic, activation and concentration losses at a certain current density of the cell operating at the intermediate temperature. Since the syngas is also comprised of various impurities with concentration levels exceeding the tolerance of SOFC system, then the syngas must be cleanup in order to reduce these impurities to a level that SOFCs are able to tolerate safely. The impact of various working parameters of SOFC, such as fuel utilization and pressure, on the SOFC polarization and output are investigated. The system electrical efficiency of 39% in low heating value (LHV) achieves when employed wet gas cleanup unit as a syngas cleanup processes. Changing the syngas cleanup model by adopting dry gas cleanup concept

(DGC), contributes to increase the electrical efficiency of L-IGFC up to 46.35% in LHV. The parametric analysis of the performance of the L-IGFC system indicates that increasing the SOFC operating pressure improves system efficiency. The pressurized L-IGFC system with DGC gives the maximum electrical efficiency of 50.04% in LHV when operated at SOFC working pressure of 4 atm (4.053 bar). Reducing the moisture content of the fed coal to gasifier until 2 wt. % in a coal dryer contributes to increasing the electrical efficiency of L-IGFC plant up to 60.12% in LVH. The sensitivity analysis on the different working temperatures and pressures of SOFC then conducted where the maximum electrical efficiency of the system realized when SOFC operating conditions are 850 ºC and 3 atm. The electrical efficiency of L-IGFC plant at this condition is 60.32% in LHV.

ACKNOWLEDGMENT

First of all I wish to express my deepest gratitude to Professor Michihisa Koyama for his thoughtful, patient, and hearty guidance over the years throughout my PhD program at Kyushu University. Under his guidance I received a good training and grew up in the academic sense. It was a greats experience learning from him. I am also deeply grateful to Professor Takayoshi Ishimoto for his guidance and continuous encouragement during my PhD program.

I am deeply grateful to Professor Kuniaki Honda, International Institute for Carbon-Neutral Energy Research, Kyushu University, and Professor Yasunori Kikuchi, Presidential Endowed Chair for “Platinum Society”, The University of Tokyo, for their valuable advice and help in my research. Presenting this thesis would not have been possible without their hearty academic and intellectual support.

I am glad to thank to my thesis committee members Professor Kohei Ito and Professor Junichiro Hayashi for their involvement and the time they spared to review this thesis and for their constructive suggestions and comments.

Special thanks to the Indonesian Directorate General of Higher Education (DIKTI) for the financial support to continue my PhD studies at Kyushu University. Finally, I wish to thank my parents and family; without their support this thesis would not have been possible. I would like to give special thanks to my wife Triana Safitri for her patience and encouragement.

TABLE OF CONTENTS

NOMENCLATURE

BEC	bare erected eost ($)
C_i	cost of an advance component (sub-system)
$C_{i,ref}$	known cost of a reference component (sub-system) of the same type and same order of magnitude ($)
D	diffusion coefficient ($cm^2\ s^{-1}$)
E^0	fuel cell voltage under standard conditions (V)
E_{act}	activation energy ($kJ\ mol^{-1}$)
F	Faraday's constant ($96{,}485\ C\ mol^{-1}$)
ΔG	Gibbs free energy change ($J\ mol^{-1}$)
ΔH	enthalpy change ($J\ mol^{-1}$)
I_{tot}	total current (A)
i	current density ($A\ cm^{-2}$)
i_0	exchange current density ($A\ cm^{-2}$)
i_l	limiting current density ($A\ cm^{-2}$)
j	molar flow rate ($kmol\ hr^{-1}$)
M	molecular weight ($kg\ kmol^{-1}$)
n_e	number of electrons participating in the electrochemical reaction (-)
p	partial pressure (bar)
P_{ref}	reference pressure (bar)
P_{fresh}	fresh clean syngas pressure (bar)
P_{SOFC}	SOFC working pressure (bar)
Q	heat (J)

R	universal gas constant (8.314 J mol^{-1} K^{-1})
r_{pore}	electrode pore radius (μm)
$r_{cat,inner}$	inner radius of the cathode tube (cm)
$r_{cat,outer}$	outer radius of the cathode tube (cm)
ΔS	entropy change (J K^{-1} mol^{-1})
T	temperature (°C)
TPC	total plant cost ($)
TOC	total overnight cost ($)
$TACS$	total as-pent capital ($)
U_a	air utilization factor (%)
U_f	fuel utilization factor (%)
V	reversible open circuit voltage (V)
V_{cell}	cell voltage (V)
V_{Nernst}	Nernst potential (V)
V_{act}	activation polarization (V)
V_{conc}	concentration polarization (V)
V_{ohm}	ohmic polarization (V)
v	specific Fuller diffusion volume (-)
W_{SOFC}	work produced by SOFC (J)
$W_{expander}$	work produced by syngas expander (J)
$W_{turbines}$	work produced by steam turbine (J)
x_{O_2}	molar fraction of oxygen in air (-)
y_a^0	molar fraction of gaseous component *a* in bulk flow (-)
Z	mass flow rate (kg hr^{-1})

Greek letters

α	apparent charge transfer-coefficient (-)
ρ	material resistivity (Ω cm)
δ	thickness (cm)
γ	exchange current density constant (A cm^{-2})
ε	electrode porosity (%)
τ	electrode tortuosity (-)

Subscripts

an	anode
cat	cathode
elyt	electrolyte
int	interconnection

Superscripts

ex	exit
in	inlet

LIST OF TABLES

LIST OF FIGURES

CHAPTER 1
INTRODUCTION

1.1 Clean Coal Technology

The world energy consumption is expected to grow about 56% over the 2010 to 2040 period, and total world energy use will rise from 524 quadrillion British thermal unit (Btu) in 2010 to 630 quadrillion Btu in 2020 and then to 820 quadrillion Btu in 2030 [1]. Although renewable energy is increasing 2.5% per year, which resulted as one of the world`s fastest growing energy sources, however it is expected that fossil fuels (petroleum and other liquids fuels, natural gas, and coal) will continue to supply almost 80% of world energy use worldwide through 2040 [1]. Conventionally, these fuels have mainly been converted into electricity using thermal fossil fuel power plant technologies such as internal combustion engine, steam turbine, and gas turbine. However, global climate change and natural resource pollution cause significant worldwide concerns about the current trend in energy system development.

Among those various fossil fuel sources, coal continues to be the fuel most widely used in electricity generation. In 2010, coal-fired generation accounted for 40% of overall world electricity generation. The expected growth rate for coal-fired electricity generation is 1.8% annual rate from 2010 to 2040. Thus, predicted total world electricity generation from coal is 73% higher than the 2010 level [1]. Coal also has the highest carbon intensity among the fossil fuels. Emissions from coal usage accounted for 39% of total emission in 1990 and 44% in 2010. It is projected that the CO_2 emissions from coal use accounted for 45% by the year 2040. Although coal has the highest greenhouse gas emission of fossil fuels, it is the most abundant of the fuel. The leading countries for developing and producing coal technologies are Japan, Germany

and US, whereas China is the country with the highest demand for coal-based electricity production [2].

Coal-fired power plants generated electricity by burning coal, generating steam, and turning turbines. Coal-fired power generation, along with liquid natural gas (LNG)-fired power generation, is an important power source in Japan. The coal-fired thermal power plants accounts for around 28% of the volume of Japan`s electricity generation. Moreover, currently the nuclear power plants have suspended operation, resulting in an increasing dependence on LNG-fired power generation, and coal-fired power generation [3,4]. The desirable features for future energy solutions are diversity in primary energy sources and generation technologies, improve efficiency in energy conversion and use, and optimally matching energy technologies and resources to specific uses [5,6]. High power plant efficiency means that the use of fuel, such as coal, can be reduced. That lowers the power generation cost, and also at the same time reducing CO_2 emission. Because coal will likely be a major fuel for electrical power production in the future, more efficient and environmentally friendly production methods must be used.

There are several advanced pulverized-coal technologies for power generation such as fluidized-bed combustion, advanced combustion/heat engines (including pulverized coal combustors, slagging combustors and coal fired diesel engines), and integrated gasification combined cycles (IGCC) [7,8]. In the past two decades, IGCC power plants have been recognized as an attractive option for coal-based power production. The details on all the existing IGCC projects can be found elsewhere as summarized in Table 1.1.

Table 1.1 Major existing and planned IGCC commercial plants.

Plant (location)	Size (MW)	System features
Buggenum (Netherlands), 1994 [7,9].	253	- Feedstock: Coal and biomass. - Shell entrained-flow gasifier, Siemens V94.2 GT, overall plant efficiency of 43% without carbon capture and storage (CCS). - CCS technology: Pre-combustion (installed in 2011).
Wabash river (USA), 1995 [7,10].	262	- Feedstock: Bituminous coal and petroleum coke. - E-Gas technology two stage entrained-gasifier, General Electric's MS 7001 GT, overall plant efficiency of 40%. - CCS technology: No CCS included.
Tampa (USA), 1996 [7,10]	250	- Feedstock: Coal and petroleum coke. - Texaco entrained-blown gasifier, GE 7FA GT, overall plant efficiency of 38.2%. - CCS technology: No CCS included.
Pernis (Netherland), 1997 [7,11].	155	- Feedstock: Heavy oil residue. - Shell entrained-flow gasifier, GE MS6541B GT, overall plant efficiency of 36.7%. - CCS technology: to be added by 2015.
Priolo Gargallo (Italy), 1998 [7].	532	- Feedstock: Siemens V94.2 GT, Texaco entrained-flow gasifier, overall plant efficiency of 38% without CCS. - CCS technology: Amine based technology.
Puertollano (Spain), 1998 [7].	335	- Feedstock: Petroleum coke. - Siemens entrained-flow gasifier, Siemens V 94.3 GT, overall plant efficiency of 40% without CCS. - CCS technology: Amine based technology.

Sarlux (Italy), 2000 [7].	548	- Feedstock: Residual oil, tar, bitumen. - GE entrained-flow gasifier and GE MS9001E GT. - No CCS included.
Negishi (Japan), 2003 [7,12].	342	- Feedstock: Heavy oil, asphalt. - GE entrained-flow gasifier, Mitsubishi 701F GT, overall plant efficiency of 36%. - No CCS included.
Vresova (Czech), 2005 [7].	400	- Feedstock: Brown coal - Lurgi fixed-bed gasifiers, GE9171E GT, overall plant efficiency of 42.2%. - No CCS included.
Knox County (USA), 2013 [7,13]	618	- Feedstock: Mid-western coal. - Replaces 160 MW coal-fired power plant at the site, GE entrained-flow gasifier and two GE 7FB GT. - CCS technology: Projected CCS plant.
Kemper County (USA), 2014 [7,14].	582	- Feedstock: Lignite coal. - The plant started commercial combined cycle operations in August 2014 and is expected to be fully operational in second quarter of 2015. Non-slagging transport reactor integrated gasifier (TRIG) and two Siemens SGT6-5000F GT. - CCS technology: Pre-combustion technology.
Nakoso (Japan) 2014 [7,15].	500-600	- Feedstock: Bituminous coal. - Nakoso 250 MW demonstration project finished in end of March 2013 after achieving all of the targets [15]. - Mitsubishi Heavy Industries (MHI) gasifier, M701G GT, overall plant efficiency of 42%

	without CCS for the demonstration plant. - CCS technology: Amine based technology. - 540 MW constructions will start within 2016 [15].

As shown in Table 1, the IGCC power plants in Japan and the US have twice the power production size of the first IGCC power plants installed in the Netherland in 1994. The increase in power production has been achieved through the implementation of new technologies especially in the gas turbine systems. Also, note that the efficiency of the commercial IGCC power plants ranges between 36% and 42.2% in lower heating value (LHV) basis. The factors contributed to this difference is mostly due to the type of feedstock being used, which usually relies on the available fuel types and their properties, whether CO_2 capture technologies are considered or not in the process (and if so, the type of CO_2 technologies being used), conceptual and control system designs of the power plants, e.g., whether process integration was considered or not at the process design stage [7].

Increasing the thermal efficiency of power generation is an important issue not only to decrease the power generation costs from an economic standpoint, but also for suppressing CO_2 emissions [16]. However, utilizing coal sustainably and environmental friendly is a very challenging task. Coal has the highest carbon intensity fuel among the fossil fuels, besides also contains many impurities such as sulfur, chlorine, mercury, arsenic, etc. Conventional pulverized coal combustion also emits various pollutants and among them particulate matter, sulfur dioxide (SO_2), nitrogen oxides (NO_x), and mercury (Hg) have been identified as serious pollutants hazardous to human health and have to be carefully controlled and closely monitored [17,18]. This rising awareness of

the risk of climate change due to greenhouse gas (GHG) emissions has posed more stringent requirements on coal utilization and triggered development of `zero emission` clean coal technologies all over the world. Therefore, the innovative viable high efficiency power plant designs with very less CO_2 emissions, not simply extensions of conventional ones, will be necessary to significantly reduce CO_2 levels.

1.2 SOFC for Power Generation

Among the various plants for power generation technologies available, fuel cells provide a clear opportunity for potentially achieving high efficiency and significantly reducing CO_2 emissions. One such technology is the solid oxide fuel cell (SOFC) which offers a clean, less pollution and high electrical efficiency that could contribute to global sustainability through increased efficiency and flexibility in the use of resources [18-25]. They convert the fuel chemical energy directly into electrical energy through electrochemical reactions that are driven by the difference in the oxygen chemical potential between the anode and cathode of the cell. Capable of generating electricity with high efficiency, SOFCs are especially suitable for stationary electricity generation. Since the SOFC module operates at elevated temperatures (873 – 1273 K), it produces varying grades of waste that can be recovered for cogeneration application purpose. Thus, it can significantly impact the system efficiency and environmental issues.

The SOFC has been considered for a wide range of power generation applications. Potential applications and markets for the SOFC cover portable, transportation and stationary areas as listed in Table 1.2. One of the main advantages of

SOFC over other fuel cells is its ability to use wide range of hydrocarbon-based fuels [26,27].

Table 1.2 SOFC market and applications.

Market	Example of Application	Power Size	Status
Portable	Soldier power	20-100 W	Demonstration [28]
	Battery charger	500 W	Demonstration [28]
Transportation	Automobile and truck APU	5-50 kW	Demonstration [28]
	Aircraft APU	Up to 500 kW	Concept [28]
Stationary	Residential	700W	Commercialized [29]
	CHP and DG	100 kW-1 MW	Demonstration [30]
	Base load	100-500 MW	Concept [28]

As described in Table 1.2, SOFC can be integrated with a heat engine to form a hybrid cycle power system. In a typical hybrid combination, the heat energy of the SOFC exhaust is used to generate additional electricity in the heat engine. Due to high operation temperature of the SOFC module, great effort have been made to investigate the systems integration of SOFC and gas turbine (GT) for power plants applications using natural gas as fuels [22,31-41], meanwhile limited investigations have been done on integrated SOFC with steam turbine (ST) [42,43].

1.3 Integrated Coal Gasification Fuel Cell

In recent years, integrated SOFC with a coal gasification plant have become very popular as an alternative for high efficiency power plant with low CO_2 emissions compared to the traditional coal combustion power generation systems [18,41,44-59]. The capability of SOFC to internally reform hydrocarbon fuels provides SOFC-based system more flexibility in fuel input [60,61]. The concept of integrating coal gasification with high temperature fuel cell-based power generation, the integrated gasification fuel cell (IGFC) power plant, provides opportunity for potentially achieving efficiency up to 60% with very less emit CO_2.

1.3.1 Recent Progress on IGFC

Integrating gasifiers with high temperature fuel cell systems (molten carbonate fuel cell or MCFC, and SOFC) for power generation have been attracting significant research attention around the world since early 1990s. Early conceptual designs mostly focused on MCFC based system due to relative maturity of the MCFC technologies at that time [18]. The summarizes and compares the major IGFC power plants proposed and analyzed up to date are described in Table 1.3.

Table 1.3 Brief summary of literature study.

Researcher	Main features
Jansen, et al., (1992) [44].	- Gasifier: oxygen-blown, entrained-flow, dry feed, (Shell gasifier). - Syngas clean up[a]: HTGC. - Fuel cell type: MCFC (T = 650 ºC, P = 4 bar). - Gas Turbine: without gas turbine integration. - Carbon capture: downstream of the fuel cell, water gas shift

	reaction followed by ceramic membrane for CO_2 separation. - Efficiency: 53.1% (LHV basis) without carbon capture; 47.5% (LHV basis) with carbon capture.
Jansen, et al., (1994) [45].	- Gasifier: oxygen-blown, entrained-flow, slurry feed, (Texaco gasifier). - Syngas clean up[a]: HTGC or LTGC. - Fuel cell type: MCFC (T = 650 ºC, P = 4 bar). - Gas Turbine: without gas turbine integration. - Carbon capture: no carbon captures capability. - Efficiency: 53.2% (LHV basis) with HTGC; 49.2% (LHV basis) with LTGC.
EAGLE (2000) [46].	- Gasifier: oxygen-blown, entrained-flow, dry feed. - Syngas clean up[a]: LTGC. - Fuel cell type: MCFC. - Gas Turbine: with gas turbine integration. - Carbon capture: no carbon captures capability. - Efficiency: 53.3% (HHV basis).
EPRI (1992) [47].	- Gasifier: oxygen-blown, entrained-flow, dry feed (Shell gasifier). - Syngas clean up[a]: HTGC. - Fuel cell type: SOFC (T ≈ 1000 ºC, P = 1.27 bar). - Gas Turbine: without gas turbine integration. - Carbon capture: no carbon captures capability. - Efficiency: 49% (LHV basis).
Lobachyov, et al., (1997) [48].	- Gasifier: Conoco CO_2 acceptor gasification. - Syngas clean up[a]: no syngas cleaning process. - Fuel cell type: SOFC (T ≈ 939 ºC, P = 10 bar). - Gas Turbine: with gas turbine integration (turbine inlet temperature (TIT) = 1027 °C). - Carbon capture: no carbon captures capability. - Efficiency: 63.1% (HHV basis).
Kivisaari, et al., (2004) [49].	- Gasifier: oxygen blown, entrained-flow, dry feed. - Syngas clean up[a]: LTGC. - Fuel cell type: SOFC (T = 1000 ºC, P = 8 bar). - Gas Turbine: without gas turbine integration. - Carbon capture: No carbon captures capability.

	- Efficiency: 46.7% (LHV basis) electricity efficiency; 84.8% (LHV basis) overall efficiency for CHP.
Kuchonthara, et al., (2005) [50].	- Gasifier: oxygen blown, fluidized-bed gasifier. - Syngas clean up[a]: Not specified. - Fuel cell type: SOFC (T = 1000 ºC, P = 15 bar). - Gas Turbine: with gas turbine integration (TIT = 1270 °C). - Carbon capture: Upstream of the SOFC, water gas shift reaction followed by membrane for CO_2 separation. - Efficiency: 46.3% (HHV basis).
Rao, et al., (2005) [51].	- Gasifier: air blown, fluidized-bed gasifier. - Syngas clean up[a]: HTGC (warm gas cleaning). - Fuel cell type: SOFC (T ≈ 800 ºC, P ≈ 18.8 bar). - Gas Turbine: with gas turbine integration (TIT = 920 °C). - Carbon capture: No carbon captures capability. - Efficiency: 60.1% (HHV basis).
Rao, et al., (2005) [51].	- Gasifier: oxygen blown, fluidized-bed gasifier. - Syngas clean up[a]: HTGC (warm gas cleaning). - Fuel cell type: SOFC (T ≈ 800 ºC, P ≈ 18.8 bar). - Gas Turbine: with gas turbine integration (TIT = 920 °C). - Carbon capture: Downstream of the SOFC, water gas shift followed by H_2 separation membrane. - Efficiency: 49.6% (HHV basis).
Verma, et al., (2006) [52].	- Gasifier: oxygen blown, fluidized-bed gasifier. - Syngas clean up[a]: HTGC (warm gas cleaning). - Fuel cell type: SOFC (T = 800 ºC, P = 10 bar). - Gas Turbine: with gas turbine integration. - Carbon capture: Downstream of the SOFC, water gas shift followed by H_2 separation membrane. - Efficiency: 50.3% (HHV basis).
Ghost, et al., (2003; 2006) [53,54].	- Gasifier: oxygen blown, entrained-flow (Texaco gasifier). - Syngas clean up[a]: HTGC. - Fuel cell type: SOFC (T = 1050 ºC, P = 35 bar). - Gas Turbine: with gas turbine integration (TIT = 1250 °C). - Carbon capture: No carbon captures capability. - Efficiency: 54% (LHV basis).

Gerdes, et al., (2009) [55].	- Gasifier: Catalytic hydro-gasifier. - Syngas clean up[a]: HTGC (humid gas cleaning). - Fuel cell type: SOFC (T = 800 ºC, P = 18 bar). - Gas Turbine: without gas turbine integration. - Carbon capture: Downstream of the SOFC, oxygen combustion followed by water condensation. - Efficiency: 56.2% (HHV basis) with carbon capture; 61.8% (HHV basis) without carbon capture.
Li, et al., (2010) [18].	- Gasifier: Oxygen-blown, entrained-flow gasifier. - Syngas clean up[a]: LTGC. - Fuel cell type: SOFC (T = 850 ºC, P = 10 bar). - Gas Turbine: with gas turbine integration. - Carbon capture: Downstream of the SOFC (post anode CO_2 separation). - Efficiency: 60% (HHV basis) with carbon capture.
Spallina, et al., (2011) [56].	- Gasifier: Oxygen-blown, entrained-flow (Shell gasifier). - Syngas clean up[a]: LTGC. - Fuel cell type: SOFC (T = 800 ºC, P = 21 bar). - Gas Turbine: with gas turbine integration (TIT = 659.4 - 1268 °C). - Carbon capture: Downstream of the SOFC (O_2-fired). - Efficiency: 47.5% (LHV basis) with carbon capture; 53.3% (LHV basis) without carbon capture.
Braun, et al., (2012) [57].	- Gasifier: Oxygen-blown, entrained-flow (Shell gasifier). - Syngas clean up[a]: (not integrated and analyzed with the system). - Fuel cell type: SOFC (T = 775 ºC, P = 3-5 bar). - Gas Turbine: with gas turbine integration (TIT ~ 950 °C). - Carbon capture: Downstream of the SOFC (O_2-fired). - Efficiency: 48% (LHV basis) when the system includes entrained-flow gasifier and carbon capture.
Lanzini, et al., (2014) [58].	- Gasifier: Oxygen-blown, entrained-flow (Shell gasifier). - Syngas clean up[a]: LTGC. - Fuel cell type: SOFC (T = 800 ºC, P = 20 bar). - Gas Turbine: with gas turbine integration (TIT = 800 °C). - Carbon capture: Downstream of the SOFC (O_2-fired).

	- Efficiency: 52.1% (HHV basis) with carbon capture.
Siefert, et al., (2014) [59].	- Gasifier: CaO-$CaCO_3$ coal gasifier. - Ion transport membrane (ITM) O_2 separator. - Syngas clean up[a]: HTGC. - Fuel cell type: SOFC (T = 850 ºC, P = 2 bar). - Gas Turbine: with gas turbine integration (TIT = 1327 °C). - Carbon capture: CO_2 is removed inside of gasifier by lime, before entering to SOFC unit. - Efficiency: 60% (HHV basis) with carbon capture.

[a]By assuming the high-temperature gas cleaning (HTGC) has operating temperature above 250 °C, and low-temperature gas cleaning (LTGC) operating near ambient temperature [18]. The designations used by the original authors are listed in parentheses.

1.3.2 Key Issues and Main Features of the Approach

Utilizing coal sustainably and environmental friendly is a very challenging task. Integrating coal gasifiers with high temperature fuel cell systems i.e. MCFC or SOFC to develop high efficiencies power plant with low emissions have been attracting significant research attention around the world since early 1990s. However, due to SOFC have working temperature and fuel flexibility higher than MCFC, therefore efforts taken in this research work are focusing on integrated coal gasifier with SOFC. The efficiency of the existing design efforts done and published in the literatures are summarized in Figure 1.1. It is noted that an estimation conversion from LHV efficiency to HHV efficiency was applied for comparison in system efficiency, taking the difference in efficiency between HHV and LHV for bituminous coal is about 5% relative [62]. It can be seen that IGFC power plants offer advances in efficiency over others coal-fired power plants.

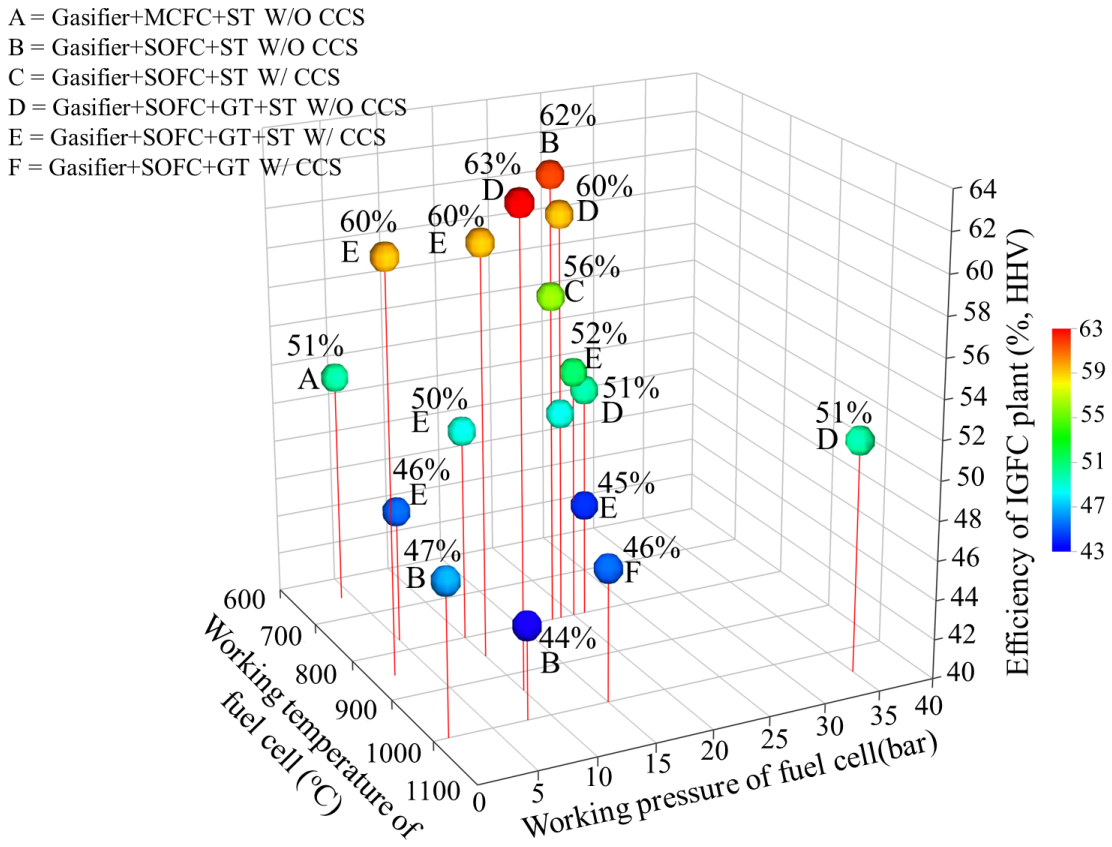

Figure 1.1 Fuel cell working temperature and pressure, and electrical efficiency of IGFC plant conditions.

Based on the literature survey, there are two models have been adopted in the application of integration coal gasifier with SOFC plants. In one model the SOFC module is operated at moderate conditions with low working pressure and low temperature (less than 900 °C). In this model, the high temperature exhaust exiting the SOFC module is delivered directly to a heat recovery system. Here, high temperature and high pressure steam is produced and then sent to a steam turbine system to generate electricity. The second model is the SOFC module operates at elevated pressures. In this mode, the air supplied for SOFC module is done by a compressor, the syngas is

delivered at the operating pressure, and the pressurized high temperature gases exiting the SOFC module are first delivered to a gas turbine and subsequently to the heat recovery system.

Adopting system configuration as following model one, the main heat thermal energy available during processes come from coal gasifier and SOFC module. The system configuration should provide adequate heat exchanger network to utilize the available heat. Allowing high temperature and high pressure syngas during process could enhance the efficiency of the system. However, the system configuration needs the components that able to work at these conditions to avoid waste thermal during process. This sufficient available thermal energy could help the heating process required in the system and at the same time reducing heat exchanger networks to decrease the complexity of the plant. EPRI [47] and Verma [53] demonstrated that by keeping high temperature syngas during process resulted in efficiency improvement.

Another effort related to high temperature syngas in system design was also demonstrated by Lobachyov et al [48] by using CO_2 acceptor gasification process for not only syngas production but also sulfur and other contaminants removal. The high temperature syngas coming out of the gasifier is used directly in the SOFC with minimal thermal energy loss. It can achieve the efficiency up to 63% (HHV basis), but however the feasibility of producing a syngas with contaminants removed to meet the stringent specification of SOFC module while utilizing such a gas cleanup process is not considered practically yet at this time. System design based on catalytic gasifiers can also achieve system efficiencies of ~60% (HHV basis) as demonstrated by Ref. [18] and Ref. [55].

Based on the important key finding from others conceptual design of IGFC power plant, then this research work attempted to design the innovative high efficiency plant with the target to reduce the complexity of the current plant. Moreover, this research work will contribute to knowledge since SOFCs have become a very high energy conversion system, in particular with its development in combined system.

1.4 Objectives

The main objective of this research work is to design, investigate and propose a system integrating the coal gasifier, intermediate temperature SOFC and steam turbine for power plant.

To avoid the confusion with existing general IGFC power plant, the term of light integrated gasification fuel cell (L-IGFC) will be used to refer to the proposed plant in this thesis. In this regard, special efforts were dedicated to:

1. Design the L-IGFC power plant configurations.
2. Simulate the coal gasifier unit by using Aspen Plus.
3. Develop a steady-state zero-dimensional tubular SOFC model by using Aspen Plus.
4. Simulate the tubular SOFC module by using Aspen Plus and analyze in MS Excel software.
5. Verify the results obtained with published references.
6. Investigate the performance and compare various innovative L-IGFC power plant configurations based on a non-dimensional SOFC model.
7. Compare the technical and economic analysis of the L-IGFC power plant with other fossil-based power plants, i.e. advanced supercritical pulverized coal (SCPC), IGCC and IGFC power plants.

1.5 Limitations

The main focus of this research work was on system modeling and analysis for integrated gasification with SOFC and steam turbine with special emphasis on the SOFC technology. Then, the system was thermodynamically modeled and analyzed along with continuous modifications of the working parameters each component in the system to enable the optimum performance. In addition, a part of the activities was related to techno-economic assessment of the proposed plant and others fossil based power plants. It should be highlighted that the lack of medium-scale IGFC plants system increases the level of uncertainty in economic indicators. Moreover, some of the major alternative plant`s components contributing to efficiency improvement have been identified and are presented in this thesis. Transient and dynamic simulation of the investigated cycles is also outside the scope of this thesis. The process integration was done by simulation without considering the pressure and temperature drop of each component.

1.6 Outline of Thesis

This section presents an outline of the thesis.

Chapter 1 – This chapter described briefly on the world energy situation and the need for high efficiency of energy system producing very less CO_2 emission. An overview of SOFC in particularly, and integrated coal gasifier with SOFC plants as stationary power generation then introduced to address this issue.

Chapter 2 – This chapter provided the general theory and modeling techniques for integrated coal gasifier and SOFC and balance of plants of the proposed plant. The Aspen plus simulation introduced at the first followed by the modeling processes for

each components of the plant.

Chapter 3 - This chapter introduces modeling and analysis of several system configurations of integrated coal gasifier with SOFC. Firstly, the system model introduced in previous Chapter was applied and verified with related result published in the literatures. Secondly, the models applied to design and analyze the proposed L-IGFC power plants. The results of several configurations that were carried out using the models discussed in this chapter.

Chapter 4 – This chapter describes the economic methodology selected for the techno-economic assessments as well as calculations performed for techno-economic studies within this PhD research.

Chapter 5 - General conclusion and recommendations for further research.

REFERENCES

[1]. Energy Information Administration (EIA), 2013, *International Energy Outlook 2013*, U.S. Department of Energy, Washington, D.C.

[2]. Horbach J, Chen Q, Rennings K, Vogele S. Do lead markets for clean coal technology follow market demand? A case study for China, Germany, Japan and the US. Environmental Innovation and Societal Transitions 2014; 10:42-58.

[3]. Nakamura T, Makino K, Shibata K, Harada M. Forecast of advanced technology for coal power generation towards the year of 2050 in CO2 reduction model of Japan. Energy Porcedia 2013; 37:7557-7564.

[4]. http://www.meti.go.jp/english/publications/pdf/journal2013_10a.pdf. Accessed June 2015.

[5]. McLarty D, Brouwer J, Samuelsen S. Hybrid fuel cell gas turbine system design and optimization. Journal of Fuel Cell Science and Technology ASME 2013; 10:041005 1-11.

[6]. Odukoya A, Carretero JA, Reddy BV. Thermodynamic optimization of solid oxide fuel cell-based combined cycle cogeneration plant. International Journal of Energy Research 2011; 35:1399-1411.

[7]. Sahraei M, McCalden D, Hughes R, Sandoval LAR. A survey on current advanced IGCC power plant technologies, sensors and control systems. Fuel 2014;137:245-259.

[8]. Espatolero S., Romeo L.M., Efficiency improvement strategies for the feedwater heaters network designing in supercritical coal-fired power plants. Applied Thermal Engineering 2014; 73:449-460.

[9]. Hannemann F, Koestlin B, Zimmermann G, Morehead H, Pena FG. Pushing forward IGCC technology at Siemens. Proceeding of Gasification Technologies Conference; October 12-15, 2003, San Francisco, California.

[10]. Figueroa JD, Fout T, Plasynski S, McIlvried H, Srivastava RD. Advances in CO_2 capture technology-The U.S. Department of Energy`s carbon sequestration program. Int J Greenh Gas Control 2008;2:9-10.

[11]. CO_2 Capture, transport and storage in Rotterdam. Rotterdam climate initiative executive summary; 2009.

[12]. IGCC State-of-the-art report. Department of mech & structural eng & material science. Norway: University of Stavanger; 2010.

[13]. Radcliffe D. Project overview of Edwardsport IGCC plant and proposed CCS project. Duke Energy; 2010.

[14]. http://www.power-technology.com/projects/kemper-county-integrated-gasification-combined-cycle-igcc-power-plant-mississippi/. Accessed June 2015.

[15]. Mitsubishi Hitachi Power System, LTD. MHPS IGCC power plant: IGCC. http://www.pl.emb-japan.go.jp/keizai/documents/E2_4%20Mitsubishi%20Hitachi%20Hashimoto.pdf. Accessed June 2015.

[16]. NEDO. Clean coal technologies in Japan, Technological innovation in the coal industry. New energy and industrial technology development organization (NEDO), 2006. Available at: http://www.jcoal.or.jp/eng/cctinjapan/. Accessed June 2015.

[17]. Li M, Brouwer J, Rao AD, Samuelsen GS. Application of a detailed dimensional solid oxide fuel cell model in integrated gasification fuel cell system design and analysis. J Power Sources 2011;196:5903-5912.

[18]. Li M, Rao AD, Brouwer J, Samuelsen GS. Design of highly efficient coal-based integrated gasification fuel cell power plants. J Power Sources 2010;195:5707-5718.

[19]. Gardner FJ, Day MJ, Brandon NP, Pashley MN, Cassidy M. SOFC technology development at Rolls-Royce. J Power Sources 2000;86:122-129.

[20]. Singhal SC. Advances in solid oxide fuel cell technology. Solid State Ionics 2000;135:305-313.

[21]. Chan SH, Low CF, Ding OL. Energy and exergy analysis of simple solid-oxide fuel-cell power systems. J Power Sources 2002;103:188-200.

[22]. Fukushima Y., Shimada M., Kraines S., Hirao M., Koyama M. Scenarios of solid oxide fuel cell introduction into Japanese society. J Power Sources 2004; 131:327-339.

[23]. Williams MC, Strakey JP, Singhal SC. U.S. distributed generation fuel cell program. J Power Sources 2004;131:79-85.

[24]. Zhao Y, Xia C, Jia L, Wang Z, Li H, Yu J, Li Y. Recent progress on solid oxide fuel cell: Lowering temperature and utilizing non-hydrogen fuels. Int J Hydrogen Energy 2013;38:16498-16517.

[25]. Kim DW, Yun UJ, Lee JW, Lim TH, Lee SB, Park SJ, Song RH, Kim G. Fabrication and operating characteristics of a flat tubular segmented-in-series solid oxide fuel cell unit bundle. Energy 2014;72:215-221.

[26]. Singhal SC. Solid oxide fuel cells for stationary, mobile, and military applications. Solid State Ionics 2002;152-153:405-410.

[27]. Ameri M, Mohammadi R. Simulation of an atmospheric SOFC and gas turbine hybrid system using Aspen Plus software. Int J Energy Res 2012;37:412-425.

[28]. Minh N. System technology for solid oxide fuel cells. In: Stolten D, Emonts B, eds. Fuel cells science and engineering-materials, systems, processes and technologies, Vol. 2. Germany: Wiley-VCH, Weiheim; 2012. Pp. 963-1010.

[29]. http://www.osakagas.co.jp/en/rd/fuelcell/sofc/technology/system.html

[30]. http://www.mhi-global.com/news/story/1309201714.html

[31]. Massardo AF, Lubelli F. Internal reforming solid oxide fuel cell-gas turbine combined cycles (IRSOFC-GT): part A-cell model and cycle thermodynamic analysis. ASME J Eng Gas Turbines Power 2000;122:27-35.

[32]. Chan SH, Ho HK, Tian Y. Modelling of simple hybrid solid oxide fuel cell and gas turbine power plant. J Power Sources 2002;109:111-120.

[33]. Liese EA, Gemmen RS. Performance comparison of internal reforming against external reforming in a solid oxide fuel cell, gas turbine hybrid system. ASME J Eng Gas Turbines Power 2005;127:86-90.

[34]. Araki T, Ohba T, Takezawa S, Onda K, Sakaki Y. Cycle analysis of planar SOFC power generation with serial connection of low and high temperature SOFCs. J Power Sources 2006;158:52-59.

[35]. Park SK, Oh KS, Kim TS. Analysis of the design of a pressurized SOFC hybrid system using a fixed gas turbine design. J Power Sources 2007;170:130-139.

[36]. Haseli Y, Dincer I, Naterer GF. Thermodynamic analysis of a combined gas turbine power system with a solid oxide fuel cell through exergy. Thermochimica Acta 2008;480:1-9.

[37]. Arsalis A, von Spakovsky MR, Calise F. Thermodynamic modeling and parametric study of hybrid solid oxide fuel cell-gas turbine-steam turbine power plants ranging from 1.5 MWe to 10 MWe. ASME J Fuel Cell Science and Technology 2009;6:1-12.

[38]. Costamagna P, Magistri L, Massardo AF. Design and part-load performance of a hybrid system based on a solid oxide fuel cell reactor and a micro gas turbine. J Power Sources 2001;96:352-368.

[39]. Tanaka K, Wen C, Yamada K. Design and evaluation of combined cycle system with solid oxide fuel cell and gas turbine. Fuel 2000;79:1493-1507.

[40]. Jia J, Abudula A, Wei L, Shi Y. Performance comparison of three solid oxide fuel cell power systems. Int J Energy Res 2013;37:1821-1830.

[41]. Koyama M, Kraines S, Tanaka K, Wallace D, Yamada K, Komiyama H. Integrated model framework for the evaluation of an SOFC/GT system as a centralized power source. Int. J. Energy Res. 2004; 28:13-30.

[42]. Dunbar WR, Lior N, Gaggioli RA. Combining fuel cells with fuel-fired power plants for improved exergy efficiency. Energy 1991;16(10):1259-1274.

[43]. Rokni M. Thermodynamic analysis of an integrated solid oxide fuel cell cycle with a rankine cycle. Energy Conv Manag 2010;51:2724-2732.

[44]. Jansen D, Oudhuis ABJ, van Veen HM. CO_2 reduction potential of future coal gasification based power generation technologies. Energy Conv Manag 1992;33:365-372.

[45]. Jansen D, van der Laag PC, Oudhuis ABJ, Ribberink JS. Prospects for advanced coal-fuelled fuel cell power plants. J Power Sources 1994;49:151-165.

[46]. Maruyama H, Takahashi S, Iritani J, Miki H. Status of the EAGLE project: coal gas production technology acceptable for fuel cells. 2000 Gasification Technologies Conference, San Francisco, California, 2000.

[47]. EPRI. Evaluation of the Westinghouse solid oxide fuel cell technology for electric utility applications in Japan. Prepared by Westinghouse Electric Corporation for the Electric Power Research Institute, TR-100713. Palo Alto, California, 1992.

[48]. Lobachyov KV, Richter HJ. High efficiency coal-fired power plant of the future. Energy Conv Manag 1997;38:1693-1699.

[49]. Kivisaari T, Bjornbom P, Sylwan C, Jacquinot, Jansen D, de Groot A. The feasibility of a coal gasifier combined with a high-temperature fuel cell. Chem Eng J 2004;100:167-180.

[50]. Kuchonthara P, Bhattacharya S, Tsutsumi A. Combination of thermochemical recuperative coal gasification cycle and fuel cell for power generation. Fuel 2005;84:1019-1021.

[51]. Rao AD, Verma A, Samuelsen GS. Engineering and economic analyses of a coal-fueled solid oxide fuel cell hybrid power plant. ASME Turbo Expo 2005: Power for Land Sea and Air, Reno-Tahoe, Nevada, 2005.

[52]. Verma A, Rao AD, Samuelsen GS. Sensitivity analysis of a vision 21 coal based zero emission power plant. J Power Sources 2006;158:417-427.

[53]. Ghosh S, De S. Thermodynamic performance study of an integrated gasification fuel cell combined cycle-an energy analysis. Proc Inst Mech Eng-A 2003;217:137-147.

[54]. Ghosh S, De S. Exergy analysis of a cogeneration plant using coal gasification and solid oxide fuel cell. Int J Energy Res 2006;30:647-658.

[55]. Gerdes K, Grol E, Keairns D, Newby R. Integrated gasification fuel cell performance and cost assessment, DOE/NETL-2009/1361, U.S. Department of Energy, Morgantown, WV, 2009.

[56]. Spallina V, Romano MC, Campanari S, Lozza G. A SOFC-based integrated gasification fuel cell cycle with CO_2 capture. ASME J Eng Gas Turbines Power 2011;133:1-10.

[57]. Braun RJ, Kameswaran S, Yamanis J, Sun E. Highly efficient IGFC hybrid power systems employing bottoming organic rankine cycles with optional carbon capture. J Eng Gas Turb Power 2012;134:1-15.

[58]. Lanzini A, Kreutz TG, Martelli E, Santarelli M. Energy and economic performance of novel integrated gasifier fuel cell (IGFC) cycles with carbon capture. Int J Greenh Gas Con 2014;26:169-184.

[59]. Siefert NS, Chang BY, Litster S. Exergy and economic analysis of a CaO-looping gasifier for IGFC-CCS. Appl Energy 2014;128:230-245.

[60]. Wachman ED, Marlowe CA, Lee KT. Role of solid oxide fuel cells in a balanced energy strategy. Energy Environ Sci 2012;5:5498-509.

[61]. Brett DJL, Atkinson A, Brandon NP, Skinner SJ. Intermediate temperature solid oxide fuel cells. Chem Soc Rev 2008;37:1568-78.

[62]. Beer JM. High efficiency electric power generation: The environmental role. Prog Energ Combust Sci 2007;33:107-134.

CHAPTER 2

MODELING APPROACH AND METHODOLOGY

An important goal of this thesis work is to perform L-IGFC designs that capture the unique synergies between coal gasification and SOFC module and can achieve high electrical efficiencies. This chapter introduces detailed design work on this topic. In order to be able to have a comparison between different process models, some general assumptions have to be made within the same calculation method. A commercial process simulator Aspen Plus™ is chosen to conduct the studies. Aspen Plus™ has many built-in model blocks that can directly be used in power plant simulation. Aspen Plus™ provides a flexible and robust calculation framework that ensures convergence of material and energy calculations in the multi-loop feed-back connectivities encountered in power plant cycles, and it has a versatile economic analysis package [1-5]. The combination with Excel worksheet was used in analyzing the SOFC performance. Peng-Robinson equation of state with Boston-Mathias alpha function (PR-BM) has been used to estimate all physical properties of the model. The modeling and simulation approach of several components and input data for the analysis are described below.

2.1 L-IGFC Plant Design

The layout of the L-IGFC power plant system is schematized in Figure 2.1. The system is based on the coal gasifier, the SOFC and the bottoming steam cycle. An entrained-flow, oxygen-blown, and dry feed gasifier that operates at 40 bar and 1500 °C is adopted in this study. A 99% purity oxygen flow is produced in standalone cryogenic

air separation unit (ASU) and compressed to the gasifier working pressure prior to entering the gasifier.

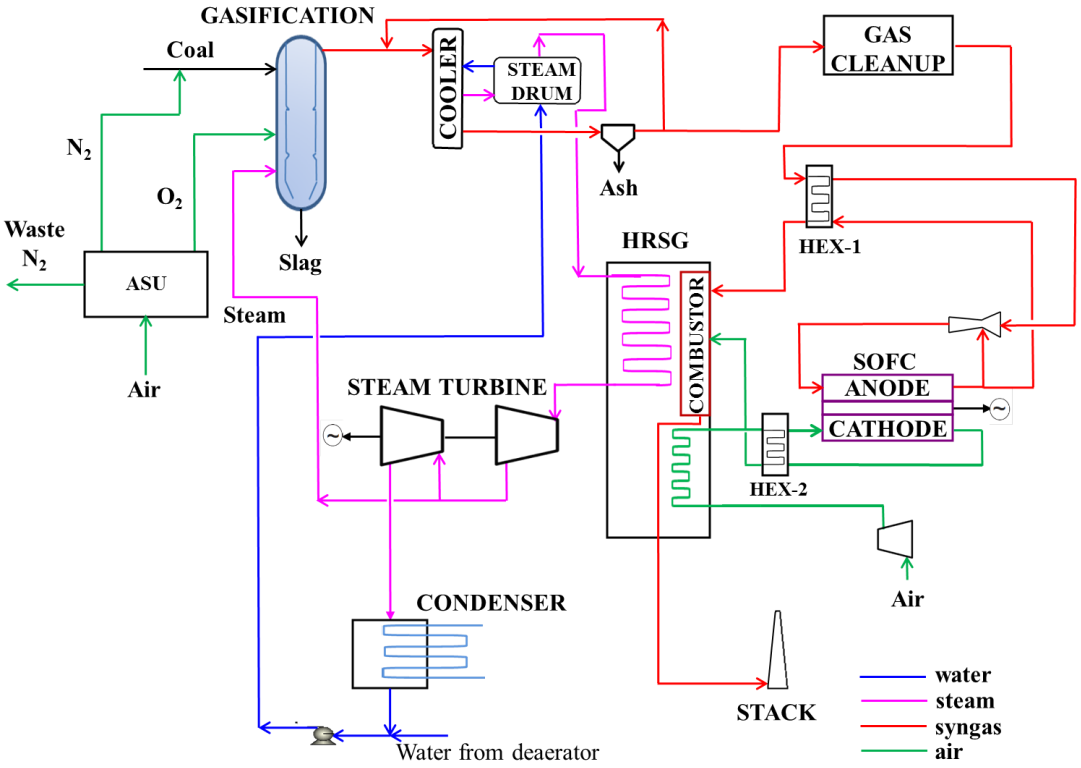

Figure 2.1 Flow diagram of the proposed L-IGFC power plant.

In gasifiers, carbon in the coal particles is converted to syngas, and the mineral matters in the coal are transformed to ash/slag. The high temperature converts the ash into molten slag, which flows down into a slag pool where it is quenched before removal through a lock hopper system. Meanwhile, about 30% smaller ash is entrained as fly ash with the raw syngas out of the gasifier into syngas quencher locating at right after the gasifier [6,7]. The high temperature raw syngas is quenched to 900 °C by means of cold syngas recirculation. The raw syngas is then cooled down in a convective syngas cooler, generating high pressure steam and heating up high pressure feed water

from a steam drum unit. Most of the ash entrained in the raw syngas leaving the syngas cooler is removed in a high pressure and high temperature filter [8]. The quenched raw syngas leaving convective syngas cooler then pass through syngas expander to reduce raw syngas pressure and temperature before entering a set of heat exchangers and gas cleanup unit. Meanwhile, the high pressure steam exiting steam drum is then sent to the heat recovery steam generator (HRSG) unit to raise the temperature up and finally expanded through a steam turbine (ST).

The raw syngas leaving the gasifier contains various impurities such as sulfur compound, chloride, ammonia, and particulate matter with concentration levels exceeding the tolerances of SOFC system. Sulfur is generally presented in coal-derived syngas as H_2S and COS. Therefore a gas cleanup process, i.e. the removal process of the gaseous species harmful to SOFC, is essential for the integrated system. The gas cleanup can be carried out by wet gas cleanup (WGC) and dry gas cleanup(DGC) as shown schematically in Figs. 2.2(a) and 2.2 (b), prior to entering the syngas expander and SOFC module.

The clean syngas fed to the SOFC undergoes the chemical and electrochemical reactions. A part of the exhaust fuel gases recycles to mix with the fresh syngas by the ejector. This recycle process is adopted for heating the fuel near the operating temperature of the SOFC and increasing the steam content to avoid the carbon deposition in the SOFC [8]. The rest of the anode exhaust enters the combustor unit where the reactions with the oxygen in the exhaust air proceed. The air stream fed to the cathode of SOFC by the blower is heated up to the temperature of 750 °C near the operation temperature of the SOFC with two steps. Here we note that we assumed the temperature of 750 °C to keep a maximum ΔT of 100 °C across the SOFC [9,10]. The

air is first heated up to 400 °C in pre-air heating in the HRSG unit followed by the heating process through a recuperator by means of hot exhaust air from the cathode section of SOFC up to 750 °C.

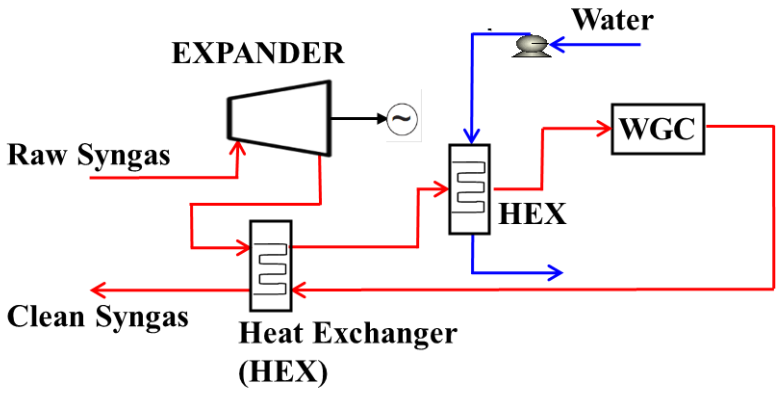

(a) wet gas cleanup unit

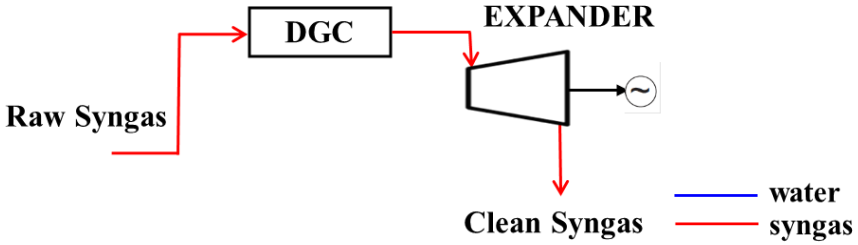

(b) dry gas cleanup unit

Figure 2.2 Schematic of the syngas cleanup unit.

The reactions in combustion unit release the thermal energy to generate the superheated steam. The superheated steam was then expanded in high pressure (HP) steam turbine (100 bar) and low pressure (LP) steam turbine (40 bar) to generate the electric power. The expanded steam after the LP turbine was then cooled down in a condenser to produce condensate before pumping again for the next cycle. The next several sections describe methods for process integration more detailed of each unit.

2.2 Gasification Unit

2.2.1 Gasification Theory

Gasification, which is a means to convert fossil fuels, biomass and wastes into either a combustible gas of a synthesis gas for subsequent utilization, offers the potential both for clean power and chemicals production [11]. The gasification will be the heart of a new generation of energy plants, possessing both feedstock and product flexibility, near zero emission of pollutants, high thermal efficiency and capture of carbon dioxide, and low cost for the feedstock and operation and maintenance (O&M) [12].

The most important coal gasification reactions are given in Eqs. (2-1) – (2-3), while the main syngas combustion reactions are shown in Eqs. (2-4) and (2-5) as follows [13]:

$$\mathrm{C} + CO_2 \rightarrow 2CO \quad \ldots (2\text{-}1)$$

$$\mathrm{C} + H_2\mathrm{O} \rightarrow \mathrm{CO} + H_2 \quad \ldots (2\text{-}2)$$

$$\mathrm{CO} + H_2O \rightarrow CO_2 + H_2 \quad \ldots (2\text{-}3)$$

$$2\mathrm{CO} + O_2 \rightarrow 2CO_2 \quad \ldots (2\text{-}4)$$

$$2H_2 + O_2 \rightarrow 2H_2O \quad \ldots (2\text{-}5)$$

In the practical of gasification processes, a broad range of reactor types can be used. If neglecting more exotic gasification techniques such as the molten bath gasifier, the tumbling-bed gasifier and underground gasification, the reactor types can be grouped into moving-bed gasifier, fluidized-bed gasifiers, and entrained-flow gasifiers. Each of these is defined on how the reactor brings about contact with the coal and the reactive gas [13,14].

The oldest gasifier is the moving bed (also called fixed bed) gasifier which can

handle lumps of non-caking coal in size of 5-80 mm. The gasifier is characterized by a bed in which the coal moves slowly downward under gravity as it is gasified, generally by a counter-current blast. In such a counter-current arrangement, the hot syngas from the gasification zone is used to preheat and pyrolyse the downward flowing coal. The gasifier generally has a rather linear temperature profiles, from about 250 °C at the product gas exit/coal inlet, up to about 1500 °C in the combustion zone located in the lower part of the gasifier. The coal is fed at the top of the gasifier, contributing to the gasifier bed. Since the volatiles liberated during pyrolysis and gasification come into contact with the fresh coal, no further thermal cracking of tars and phenols occur, which results in a product gas rich in these hydrocarbons that have to be removed prior to any use in a fuel cell. The outlet temperature of the syngas is generally low. Depending on the construction of the gasifier, the mineral-containing ash may be removed as a solid residue (dry ash) or as a slag. Typical moving-bed gasification processes include the Lurgi gasification process featuring dry ash and the British Gas/Lurgi (BGL) gasification process featuring slagging ash. The typical temperature profile of a moving-bed gasifier is shown in Figure 2.3(a).

Fluidized-bed gasifiers can only operate with solid crushed fuels (0.5-5 mm), with the exception of the transport reactor, which is midway between a fluidized bed and an entrained flow gasifier and as such operates with pulverized fuel (i.e. coal < 50 μm). The fluidized-bed gasifier is characterized by an even temperature distribution in the gasifier bed. The typical temperature profile of a fluidized-bed gasifier is shown in Figure 2.3(b). The crushed coal can be fed either at the top of the gasifier, or at the bottom together with the gasification and fluidization media. The operation of fluidized-bed gasifier is generally restricted to temperatures below the softening point of

the ash, since ash slagging will disturb the fluidization. The low gasifier temperature and the fact that a certain amount of only partially reacted fuel is inevitably removed with the ash result in a lower carbon conversion than for a gasifier operating at a higher temperature, but the tar content in the product gas is lower than for a moving-bed gasifier.

The entrained-flow gasifiers are the most versatile type of gasifiers as they can accept both solid and liquid fuels and operate at high temperature (above ash slagging temperatures) to ensure high carbon conversion and a syngas free of tars and phenols [11]. The gasifier is characterized by a step-wise temperature increase from the coal inlet to the product syngas outlet as shown in Figure 2.3(c). As a result of this temperature increase which gives an outlet temperature of about 1500 K (1227 ºC). Depending on the design of the entrained-flow gasifier, the powdered coal is either fed as water slurry or entrained in an inert gas stream. This feed is fed co-currently together with the oxidizing agents air/oxygen and steam. Almost all coals can be gasified in entrained-flow gasifier, making it more fuel flexible; but the high temperature operation creates a high oxygen demand. The majority of the most successful coal gasification processes that have been developed after 1950 are entrained-flow slagging gasifiers operating at pressure of 20-70 bar and at high temperature of at least 1400 °C. Some important entrained-flow gasification processes are Conoco-Phillips E-Gas, GE Energy (formerly Texaco), Shell, Prenflo^{TM}, Mitsubishi Heavy Industries (MHI), Siemens, and Multi-Purpose Gasifier (MPG) gasifiers.

In the coal gasification reactions, oxygen is necessary for accomplishing the gasification processes. The factors guiding whether oxygen or air to be used together with steam are commonly the operating temperature and pressure of the gasifier.

Air contains 79% nitrogen, and therefore the use of air requires a larger portion of the coal to be combusted in order to maintain the gasifier temperature than when oxygen is used [14]. In case when the gasifier is operated at an elevated pressure, the gasses fed to the gasifier have to be compressed to the operating pressure of the reactor, and thus the nitrogen present in air would increase the work needed for compression.

The oxygen-blown entrained-flow gasifiers are by far the most proven and matured technologies and have been most frequently chosen to pair with SOFC stack or modules. Due to the higher oxygen content in the gasifier and higher operating temperature, the syngas produced by such gasifiers generally features high CO and H_2 content, with only small amount of CH_4 [15].

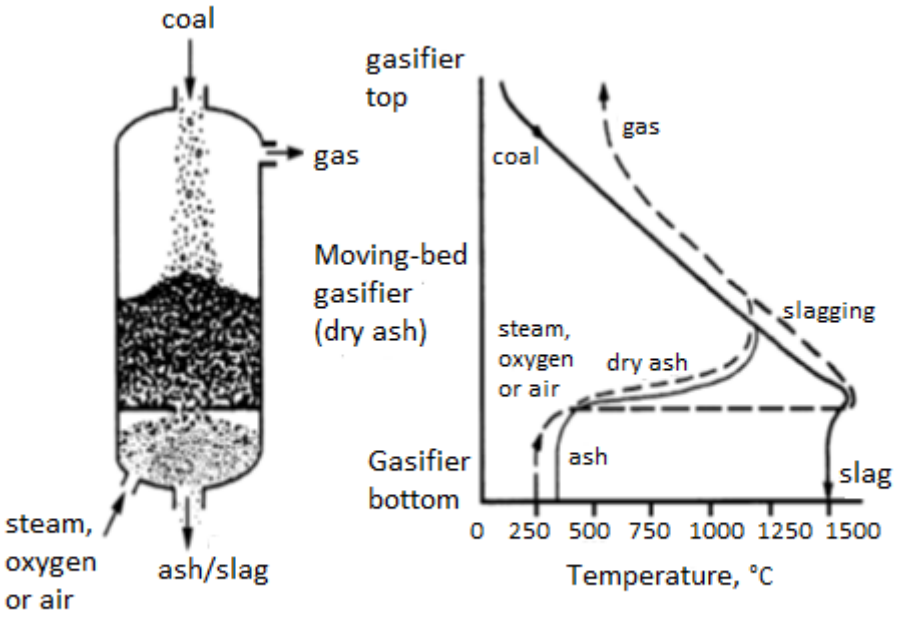

(a) A moving-bed gasifier

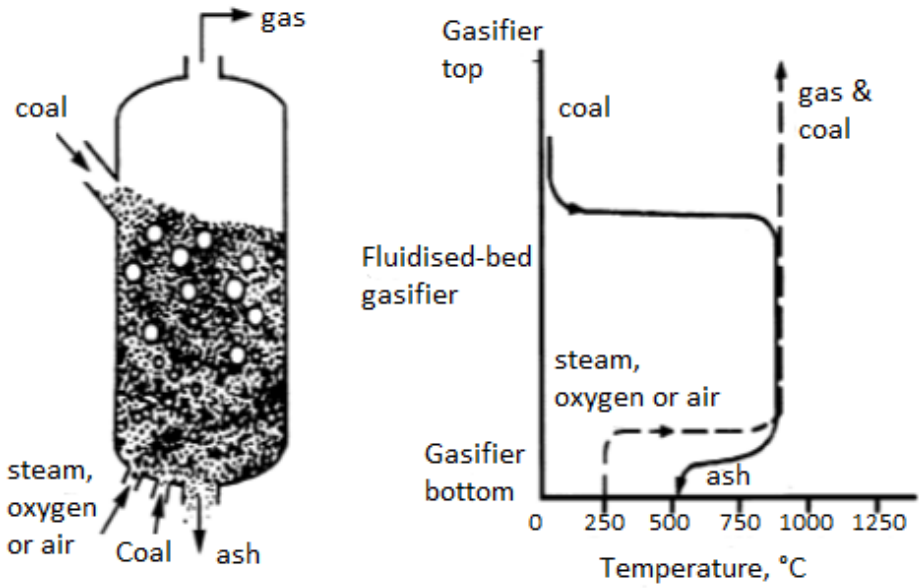

(b) A fluidized-bed gasifier

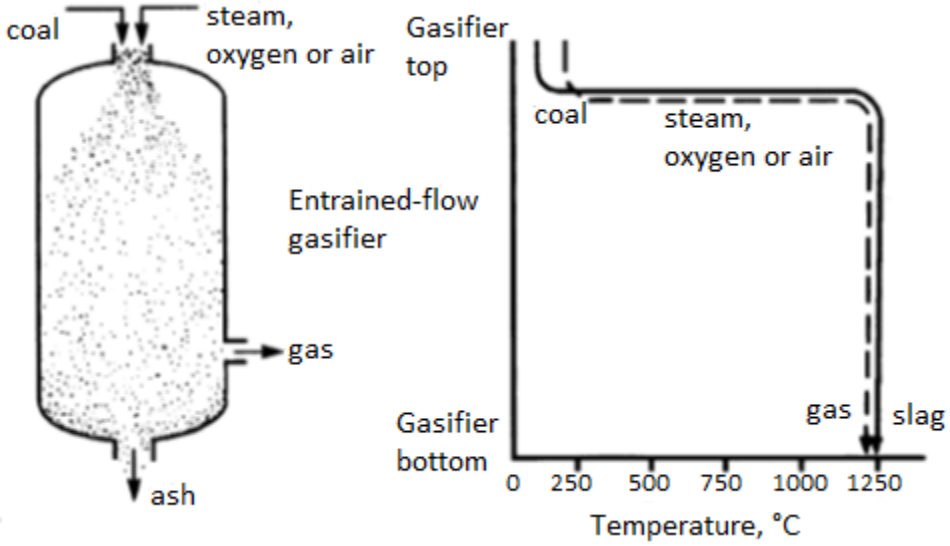

(c) An entrained-bed gasifier

Figure 2.3 Principles and temperature profiles of major gasifier reactors [14].

2.2.2 Gasification Model Description

The oxygen-blown entrained-flow gasifier fed with coal Illinois no. 6 as

feedstock was chosen in this study. Table 2.1 describes the composition of the coal. The modeling of the gasifier was based on the assumption that isothermal and the gaseous products reach chemical equilibrium [5,14].

Table 2.1 Composition of Illinois No. 6 coal [15,16].

Bituminous Illinois 6	
Proximate analysis (wt. %)	
Fixed carbon	47.05
Volatile matter	30.91
Moisture content	11.12
Ash content	10.91
Ultimate analysis (wt. %)	
Ash	10.91
C	71.72
H	5.06
O	7.75
N	1.41
S	2.82
Cl	0.33
Total	100
Heating values (kJ kg^{-1})	
Higher heating value	27139.90
Lower heating value	26139.21

Several Aspen Plus^{TM} unit operations have been used to simulate the gasifier as described in Table 2.2, while the detailed flowsheet of the gasifier is illustrated in Figure 2.4. The coal is defined as an unconventional component (processes with solids).

Table 2.2 Description of unit operation models for coal gasification unit.

Aspen Plus™ Name	Description
RYield	RYield reactor; decompose the coal into its elements (C, H, O, N, S, etc.)
RGibbs	Gibbs free energy reactor; calculates syngas composition by minimizing Gibbs free energy
Mixer	Mixer; simulates mixing of the recycled cooled raw syngas with hot raw syngas from gasifier
SSplit	Splitter; splits the slag material from gasifier unit Splitter; splits the ash material from raw syngas stream
FSplit	Splitter; splits the cooled raw syngas into a recycle stream and to the cleanup unit.
HeatX	Heat exchanger; to cool the raw syngas before sent it through cyclone
Flash2	Steam drum; to supply saturated water for syngas cooler, and evaporate the steam produced by syngas cooler to high quality of steam.

The property methods used for coal and ash to calculate the enthalpy and density of coal are HCOALGEN and DCOALIGT, respectively [17]. HCOALGEN model needs a component attribute definition for the coal, based on proximate analysis (PROXANAL), ultimate analysis (ULTANAL) and sulfur analysis (SULFANAL). The coal is first sent in a RYield reactor to decompose into its elements (C, H, O, N, S, etc.), where the stream class used is MIXCINC. The yield distribution was entered as mass

yield of component per total mass of feed and calculated from the ultimate analysis data [17, 18].

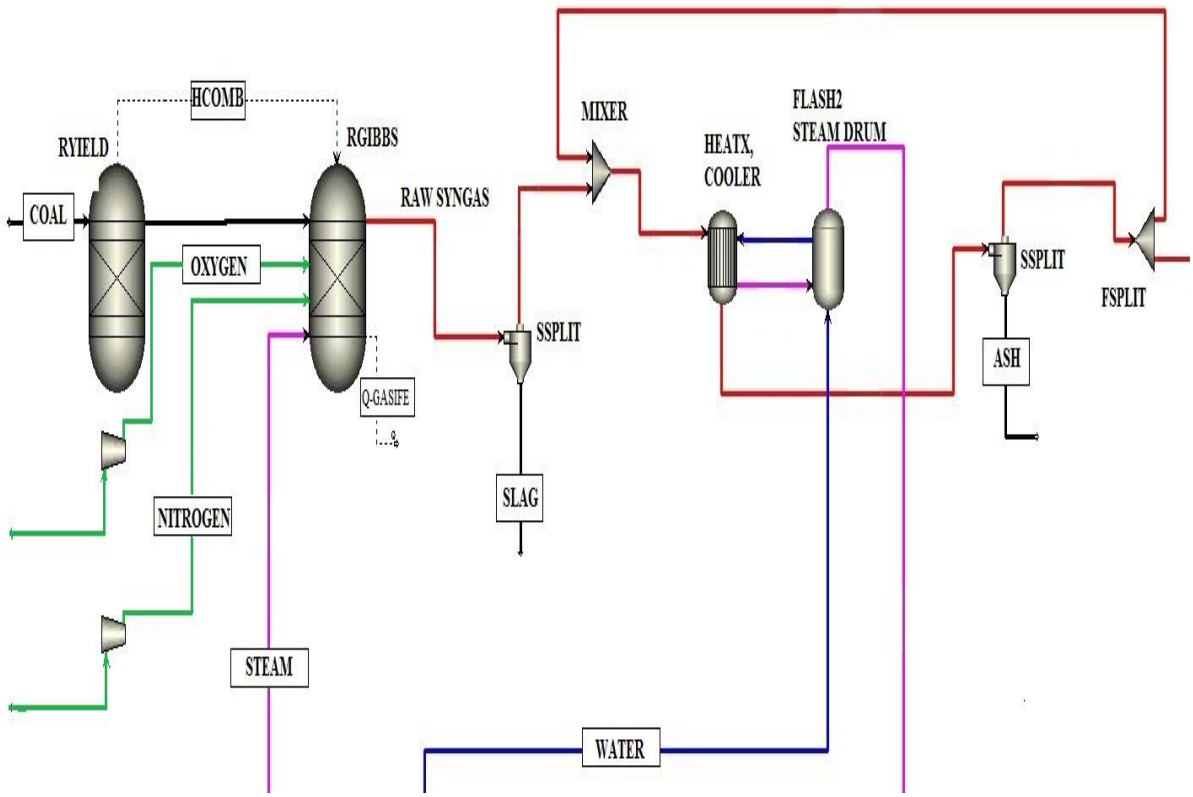

Figure 2.4 Aspen Plus^{TM} simulation model for coal gasifier unit.

For each unit feeding of coal, the RYield decompose reactor has a certain value corresponding to the element yield. In order to represent the decomposition of coal within the decompose reactor, it is required that a breakdown of mass basis should be calculated from the ultimate analysis data as follows [19]:

$$Yield\ H_2,\ m_{H_2} = (1 - X_{Moisture}) * X_H \quad \ldots (2.6)$$

$$Yield\ H_2O,\ m_{H_2O} = (X_{Moisture}) \quad \ldots (2.7)$$

$$Yield\ O_2,\ m_{O_2} = (1 - X_{Moisture}) * X_{O_2} \quad \ldots (2.8)$$

$$Yield\ N_2,\ m_{N_2} = (1 - X_{Moisture}) * X_{N_2} \quad \ldots (2.9)$$

$$Yield\ S,\ m_s = (1 - X_{Moisture}) * X_S \quad \ldots (2.10)$$

$$Yield\ C,\ m_C = (1 - X_{Moisture}) * X_C \quad \ldots (2.11)$$

$$Yield\ ASH,\ m_{ASH} = (1 - X_{Moisture}) * X_{ASH} \quad \ldots (2.12)$$

$$Yield\ Cl_2,\ m_{Cl_2} = (1 - X_{Moisture}) * X_{Cl_2} \quad \ldots (2.13)$$

RGibbs reactor is used to simulate gasification of coal. The decomposed elements will react with the steam and O_2 in the RGibbs reactor to extract the syngas. RGibbs reactor models chemical equilibrium by minimizing Gibbs free energy, which restricts individual equations to equilibrium and does not take account of the reaction kinetics. This type of reactor considers all the components as possible products, which is useful when there are many reactions between several components and reaction kinetics is unknown. The operating pressure, temperature, and O_2 to coal ratio are the key parameters required as input to the RGibbs reactor [20].

2.3 Air Separation Unit

In order to assure easier startup and higher flexibility, 99% purity oxygen flow is produced in standalone cryogenic air separation unit (ASU) and compressed to the gasifier working pressure prior to entering the gasifier. Nitrogen produced in ASU is partly used in lock hoppers for coal feeding and the remaining part vented to the atmosphere. ASU section was not simulated and assumption for its energy consumption was obtained from the information available in literature [21] as described in Table 2.3.

Table 2.3 Electricity consumption of ASU for gaseous Oxygen and Nitrogen.

Air separation plant product:	Oxygen	Nitrogen
Separation (kWh/tonne):	281	113
Compression @ 40 bar (kWh/tonne):	119	130
Total (kWh/tonne):	400	243

2.4 Gas Cleanup Unit

The raw syngas derived from coal gasification contains several impurities with levels exceeding the tolerances of SOFC system. Sulfur is generally presented in coal-derived syngas as H_2S and COS. Therefore a gas cleanup process which involves removal of fuel gas contaminants such as sulfur compounds, chloride, ammonia, particulate matter, alkali vapor and heavy metals, is essential for the integrated system.

Some known effects of these impurities on SOFC operations are briefly discussed as follows:

1. Sulfur compounds. Sulfur is generally presented in coal-derived syngas as H_2S, COS, SO_2, and CS_2. Sulfur is a poison for nickel steam reforming catalysts and for many anode catalysts including platinum. Sulfur can adhere to the catalytic nickel surface of the SOFC anode and reduce anode activity. Although many benefits are expected by reducing operating temperature of SOFC, it should be considered that at reduced temperatures sulfide impurities may easily adsorb on the surface of a SOFC fuel electrode to degrade its performance [22]. The hydrogen sulfide (H_2S) as main impurity in syngas at fuel electrode is expected to have the greatest impact on SOFC performance. The polarization resistance and the overvoltage of SOFC electrode increased when the H_2S concentrations in the fuel gas exceeded 0.05, 0.5 and 2 ppm

at SOFC operation of 1023, 1173 and 1273 K, respectively [23]. Thus for the SOFC operating at intermediate temperatures, a high grade desulfurization is necessary. However, many R&D have been made in order to develop an anode material that can withstand the sulfur content (particularly H_2S) present in the fuel. A comprehensive summary on those anode materials can be found in Refs. [22,24].

2. Chlorine and chloride. Chorine is the primary halogen in Coal, and its content is typically in the range of 0.01-0.1 mass%. During coal gasification process, a significant amount of the Cl is converted to HCL in the devolatilization process [25]. It has been reported that in high concentrations halogens (>100 ppm) may cause structural changes in SOFC [26]. The removal of HCL vapor from the feed-syngas can be beneficial in any power plant, especially in the MCFC and SOFC, and the IGCC power plant because of the great corrosion potential of the vapor in contact with metal components [27,28].
3. Ammonia. It was reported that the concentration of NH_3 plus HCN is typically on the range of 1800-5000 ppm, and the proportion of HCN is roughly 2%-10% of NH_3 [25,28]. In the IGCC power plant, most of total NOx emitted come from NH_3 which is transformed into NOx in the gas turbine. Since it is anticipated that the flue gas treatment to reduce the NOx emissions in the IGFC power plant, if needed, is probably an expensive option, the removal of NH_3 before the fuel cell is considered more attractive [25].
4. Particulate matter. Particulate matters also have a negative effect on the SOFC operation because they plug the porous components and thus increase diffusion losses.

The gas cleanup technologies available for IGFC application are the same as of

similar to those developed and applied in IGCC systems. However, the gas cleanup requirements for syngas from coal gasification fueled SOFC are generally more stringent than for other coal gasification based applications. The gas cleanup processes can be categorized into wet gas cleanup (WGC) process and dry gas cleanup (DGC) process [29].

2.4.1 Wet Gas Cleanup Process

A typical WGC process involves a series of venture water scrubbing to remove particulate matter, chlorides, and NH_3, followed by an absorption system using chemical or physical washes to remove sulfur compounds. After WGC processes, then the clean syngas often needs to be heated up again for downstream applications [30, 31]. Several Aspen Plus^{TM} unit operations have been used to simulate the WGC processes as described in Table 2.4 whereas the detailed flowsheet is illustrated in Figure 2.5.

Table 2.4 Description of Aspen Plus^{TM} unit operation blocks shown in Figure 2.5.

Aspen Plus^{TM} Name	Description
Compr	SYNGAS EXPANDER; decreases the pressure of the raw syngas. The discharge pressure of syngas expander will be adjusted to the requirement of pressure coming to the ejector. (Assume: P_{fresh}/P_{SOFC} = 3. If operating pressure of SOFC (P_{SOFC}) equal to 1.094 bar, then the discharge pressure of syngas expander (P_{fresh}) will be equal to 3.282 bar).
HeatX	HEX-1; to cool down raw syngas by mean of clean syngas from the WGC unit.

	HEX-2; to cool down raw syngas by mean of saturated water pumping from the plant.
Pump	PUMP-5; supplies water to cool down raw syngas prior entering to the physical absorption processes as a WGC unit.
Sep	WGC; simulates the Rectisol processes as a physical absorption/removal of undesired contaminants producing clean syngas. The separator model parameters were derived from data supplied by available published references.
Flash2	EFFLUSEP; for condensation of water and other condensates (e.g. tar) from the raw syngas by cooling the raw syngas below its dew point.

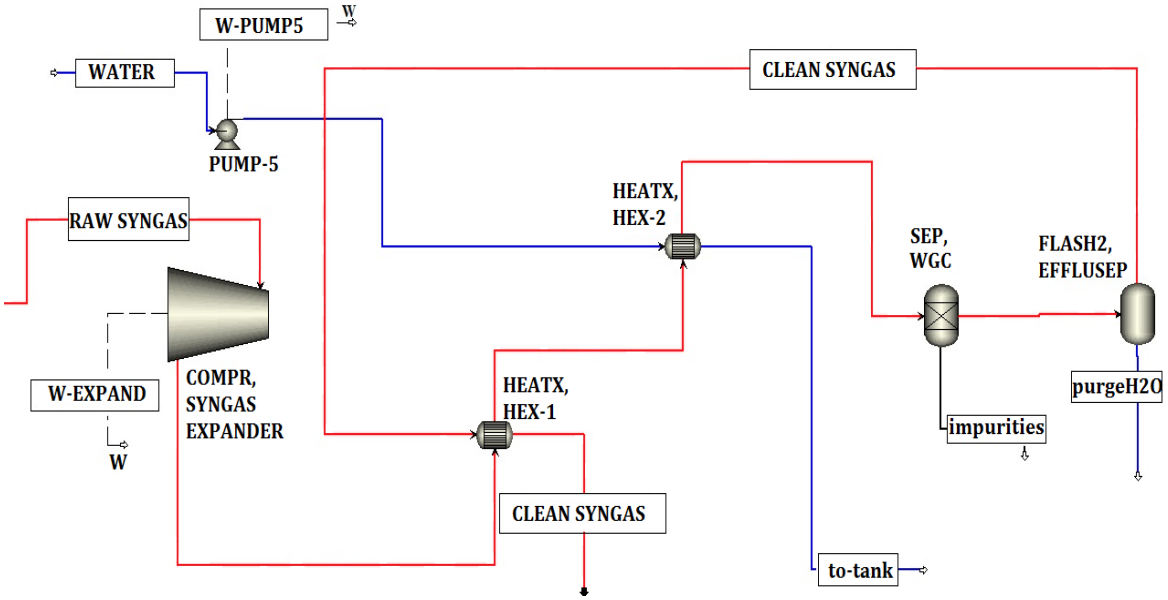

Figure 2.5 Aspen Plus™ simulation model WGC unit.

Main assumptions for the WGC unit used in this study are derived from the available literature [30]. The following utility consumptions are established for the WGC process; shaft power is 73.08 kW, low pressure (LP) steam is 323.74 kW and refrigeration duty is 131.42 kW, respectively, per kmol/h of sulfur compound removed to a trace level (for e.g. H_2S to less than 0.1 ppm) [30]. The total sulfur compound removed is calculated from the inlet and the outlet stream analysis.

2.4.2 Dry Gas Cleanup process

Due to the limitations of low temperature gas cleanup, efforts have been conducted to develop DGC process that will allow the removal of H_2S, HCN, HCl, particulate matter and alkali species from coal syngas at temperatures above 400 °C [25,27,31-35]. In DGC, syngas impurities are mostly removed by adsorption with solid state reactants at elevated temperatures. It consists of several stage processes: (i) stage of removing HCl by Na_2CO_3, (ii) stage of removing sulfur from the gas phase through adsorption by ZnO with regenerable processes, (iii) stage of removing trace metal contaminants (e.g., AsH_3) and ppb level H_2S by CuNi-SBA16, (iv) tar reforming stage and NH_3 decomposition by Ir/$MgAl_2O_4$ steam. Particulate matter can be removed by passing the raw syngas through a hot gas filter made of ceramic for separation of bulk of the entrained slag. A more detailed of removing processes is described below.

The chloride can be removed from the syngas in a picked bed Na_2CO_3 according to the following reaction [34]:

$$2HCl + Na_2CO_3 \rightarrow 2NaCl + CO_2 + H_2O \quad \ldots (2.14)$$

The H_2S and COS are removed from the syngas by contacting with ZnO sorbent. The desulfurization reactions are as follows [34,35]:

$$ZnO + H_2S \rightarrow ZnS + H_2O \quad \ldots (2.15)$$

$$COS + ZnO \rightarrow ZnS + CO_2 \quad \ldots (2.16)$$

The ZnS formed in the desulfurization process can be transferred to a regenerator where it contacts with air and is oxidized according to the reaction:

$$ZnS + \frac{3}{2}O_2 \rightarrow ZnO + SO_2 \quad \ldots (2.17)$$

The pressured off-gas leaving regenerator reactor will expand to compensate the power consumption of the regeneration stream compressor. The SO_2 gas that is generated can be recovered as element sulfur product by reacting with H_2 or CO. Meanwhile the energy consumption related to the treatment of the SO_2 gas was neglected since its effect on power balance was supposed to be quite limited [34,35]. A more detailed assessment of the configuration and processes on dry gas cleanup adopted in this study can be found in the literatures [34,35].

In the simulation model describing the DGC system, several Aspen Plus™ unit operations have been used to simulate the DGC processes as described in Table 2.5. The separator model as shown in Figure 2.6 was used to describe the gas cleanup unit by assigned a set of parameters available from the reference [35].

Table 2.5 Description of Aspen Plus™ unit operation blocks shown in Figure 2.6.

Aspen Plus™ Name	Description
Compr	SYNGAS EXPANDER; decreases the pressure of the raw syngas. The discharge pressure of syngas expander will be adjusted to the requirement of pressure coming to the ejector. (Assume: P_{fresh}/P_{SOFC} = 3. If operating pressure of SOFC (P_{SOFC}) equal to 1.094 bar, then the discharge pressure of syngas expander (P_{fresh}) will be equal to 3.282 bar).
Sep	DGC; simulates the DGC processes as a removal of undesired contaminants producing clean syngas. The separator model parameters were derived from data published in references.

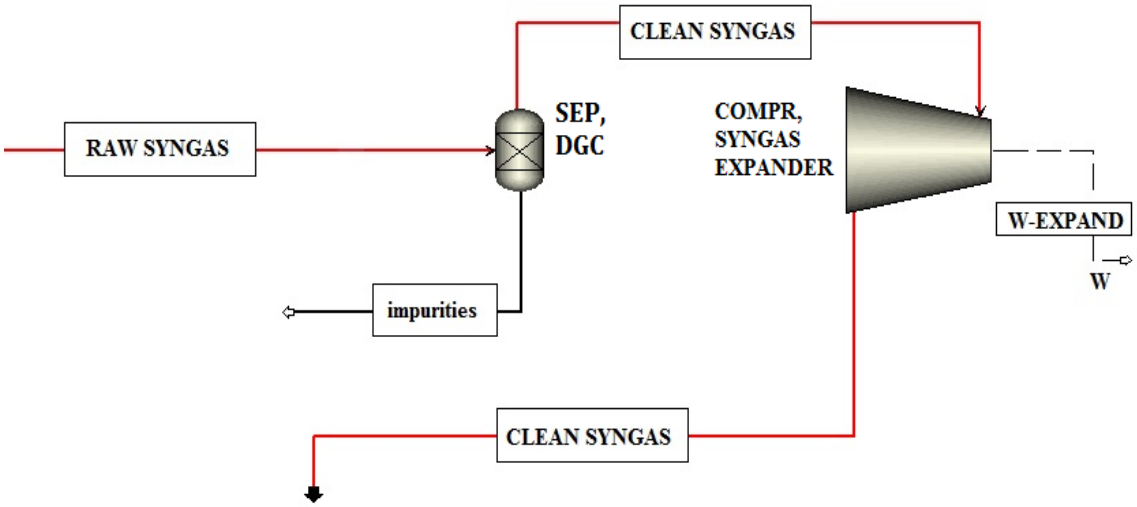

Figure 2.6 Aspen Plus™ simulation model DGC unit.

2.5 SOFC Module

2.5.1 Model description

The detailed Aspen Plus™ flowsheet of the tubular SOFC module is illustrated in Figure 2.7. A brief description of the unit operation blocks shown in Figure 2.7 is presented in Table 2.6. The model is based on the following assumptions: isothermal and steady state operation; zero-dimensional; all working fluids are treated as ideal gases; pressure drop are neglected; chemical reactions such as reforming and shift reactions reach the chemical equilibrium; ion cross over through the electrolyte cannot be modelled in Aspen Plus™, therefore the overall oxidation of H_2 was considered instead of the cell half reactions; and only H_2 reacted electrochemically, assuming that CH_4 and CO produce H_2 through the reforming and shift reactions, respectively [2-5,36-38].

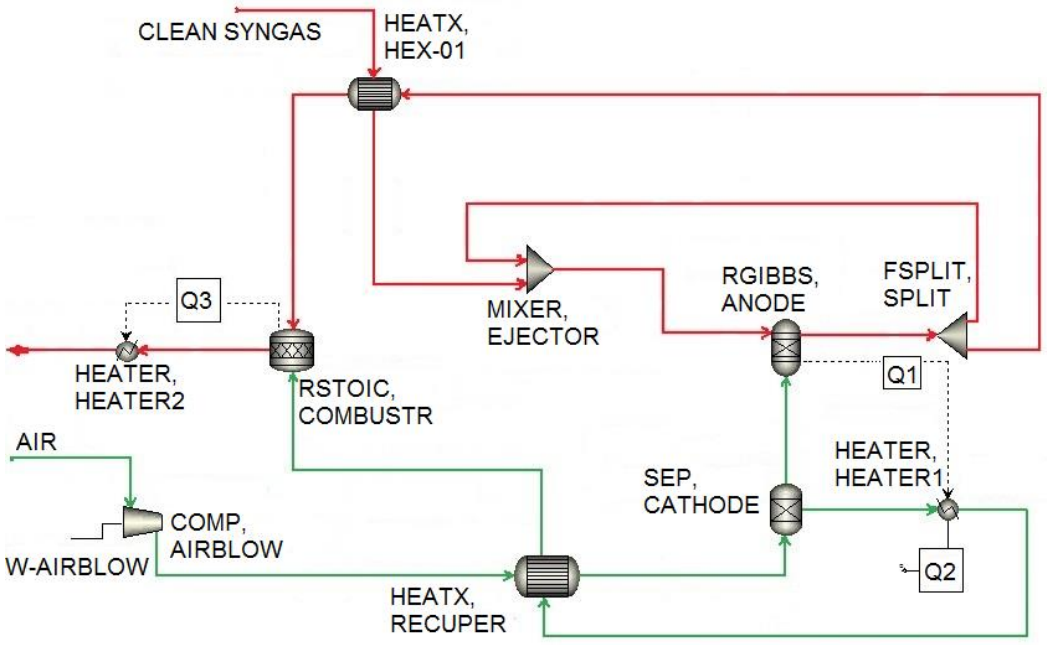

Figure 2.7. Aspen Plus™ SOFC module flowsheet.

(solid lines represent material streams and dotted lines represent energy streams)

Table 2.6 Description of Aspen Plus™ unit operation blocks shown in Figure 2.7.

Aspen Plus™ name	Block ID	Description
Compr	AIRBLOW	Blower; supply and increase the pressure of the input oxidant
Heater	HEATER1	Heater; increases the temperature of the exhaust oxidant stream to the anode exhaust temperature
	HEATER2	Heater; increases the temperature of the combustor unit products
Mixer	EJECTOR	Mixer; simulates mixing of the recycled exhaust fuel with fresh fuel (syngas) in the ejector
RGibbs	ANODE	Gibbs; Gibbs free energy reactor, simulates the reactions occurring at the anode
FSplit	SPLIT	Splitter; splits the exhaust fuel into a recycle stream sent to the ejector and a stream sent to the combustor unit
Sep	CATHODE	Separator; separates the O_2 required by the electrochemical reaction
RStoic	COMBUSTR	Stoichiometric reactor; simulates the complete combustion of the remaining fuel with the exhaust oxidant
HeatX	HEX-01	Heat exchanger; simulates preheating of the clean syngas by the exhaust fuel from anode section
	RECUPER	Heat exchanger; simulates preheating of the

	oxidant by the exhaust oxidant from cathode section

Referring to Figure 2.7, the fresh clean syngas is fed to the SOFC module being mixed with the recycled anode gas containing the electrochemical reaction products in the `EJECTOR` block. Here, the inlet fuel is heated up ny the heat exchange and the mixture with the recycled fuel. The discharge pressure of `EJECTOR` block was calculated using a pressure ratio: P_{fresh}/P_{SOFC} = 3 [2,4]. The stream from `EJECTOR` block goes to the `ANODE` block where the CH_4 reformed to H_2, CO shifted to H_2 and H_2 is oxidized by the electrochemical process. The reactions considered in the `ANODE` block are:

Steam reforming: $CH_4 + H_2O \leftrightarrow CO + 3H_2$ … (2.18)

Water-gas shift: $\mathrm{CO} + H_2O \leftrightarrow CO_2 + H_2$ … (2.19)

Electrochemical: $H_2 + O^{2-} \rightarrow H_2O + 2e^-$ … (2.20)

$H_2 + \frac{1}{2}O_2 \rightarrow H_2O$ overall reaction … (2.21)

The reduction of O_2 on the cathode side is as follows:

$$\frac{1}{2}O_2 + 2e^- \rightarrow O^{2-} \quad \text{… (2.22)}$$

The steam reforming reaction, water-gas shift reaction and overall reaction above are specified to reach thermodynamic equilibrium at a given temperature (T = 800 °C) while the exhaust temperature of `ANODE` block was estimated as 850 °C.

The electrochemical reaction of CO is neglected here. This is because most of CO participates in the water-gas shift reaction producing more H_2 and CO_2 [39,40]. Also, it was observed from a thermodynamic perspective that electrochemical oxidation

of both CO and H_2 at the anode yields the same Nernst potential in an SOFC as long as chemical equilibrium of the shift reaction is attained [41].

The air stream composition, temperature and pressure were inputted, and the molar flow rate is set by the air utilization factor. The compressed air is preheated by the hot exhaust from cathode section at `RECUPER` block. The compressed and preheated air enters the `CATHODE` block, whose function is to separate out the O_2 required for the electrochemical reaction $\left(jO_{2,consumed}\right)$ based on the anode fuel equivalent hydrogen molar flow rate $\left(jH_{2,equivalent}\right)$ and expected fuel utilization factor (U_f) as [2,4]:

$$jO_{2,consumed} = 0.5\left(U_f\right)\left(jH_{2,equivalent}\right) \quad \ldots (2.23)$$

where the fuel utilization factor (U_f) is defined as:

$$U_f = \frac{jH_{2,consumed}}{jH_{2,equivalent}} \quad \ldots (2.24)$$

The $jH_{2,equivalent}$ is the equivalent hydrogen contained in the fresh syngas, and can be calculated as:

$$jH_{2,equivalent} = jH_{2,in} + 1(jCO_{in}) + 4\left(jCH_{4,in}\right) + 7\left(jC_2H_{6,in}\right) + \cdots \quad \ldots (2.25)$$

On the cathode side, an air utilization factor (U_a) is defined as follows:

$$U_a = \frac{jO_{2,consumed}}{jO_{2,in}} \quad \ldots (2.26)$$

The required O_2 is directed to the `ANODE` block. The temperature of the exhaust air is assumed to be the same with `ANODE` block exhaust temperature. To keep the thermodynamic balance, the heat produced during electrochemical reaction is supplied to `HEATER1` block and simulated by taking a heat stream (Q1) from `ANODE` to `HEATER1` [2,4]. The exhaust fuel enters the block `SPLIT`, whose function is to split the stream into a recycle and a stream directed to the combustion unit. The recycle fraction was defined to reach the minimum temperature of 750 ºC (if the working temperature of SOFC is 800 ºC for example). The exhaust fuel and oxidant are fed to `COMBUSTR` block where complete combustion of the remaining fuel occurs. The reactions specified in the `COMBUSTR` block are as follows [2,4]:

Hydrogen oxidation: $H_2 + \frac{1}{2}O_2 \rightarrow H_2O$ … (2.27)

Carbon monoxide oxidation: $\mathrm{CO} + \frac{1}{2}O_2 \rightarrow CO_2$ … (2.28)

The heat generated by combustion reactions is represented by the heat stream Q3, which is fed to the block `HEATER2`, whose function is to calculate the combustion products temperature. The temperatue combustion products enter the HRSG unit to serve heat for steam cycle and preheat the compressed air for SOFC.

2.5.2 Voltage calculation

When the fuel cell operates at a steady-flow process, neglected the changes in kinetic and gravitational potential energies of working fluids, the energy balance based on first law of thermodynamic can be expressed as [42]:

$$\Delta H = Q + W_{SOFC} \quad \ldots (2.29)$$

Assuming that the cell operates reversibly and isothermally,

$$Q = T\,\Delta S \quad \text{and} \quad \Delta H = T\,\Delta S + \Delta G = T\Delta S + W_{SOFC} \quad \ldots (2.30)$$

where *ΔH* is the enthalpy change and *ΔS* is the entropy change.

The maximum electrical work obtainable in a fuel cell operating at constant temperature and pressure is given by the change in Gibbs free energy (*ΔG*) of the electrochemical reaction as:

$$W_{SOFC} = \Delta G = -n_e F V \quad \ldots (2.31)$$

where Δ denotes a property change of reaction, *n* is the number of electrons participating in the electrochemical reaction, *F* is Faraday's constant, and *V* is the reversible open circuit voltage.

When the SOFC is not connected to an external load, there is no current flow outside of the module and the operating voltage is equal to the open circuit voltage. To define the operating voltage, we need to consider the polarizations. The actual cell voltage was calculated by first applying the Nernst equation to determine the reversible Nernst voltage (V_{Nernst}) and then subtracting the various polarizations, including ohmic, activation and concentration polarizations. In this study, we calculated the average Nernst voltage using partial pressure of gas species at cell inlet and exit to consider the inhomogeneity of cell voltage from the inlet to the exit of the cell. Thus, Nernst voltage can be written as follows [43]:

$$V_{Nernst} = \frac{V_{Nernst}^{in} + V_{Nernst}^{ex}}{2} \quad \ldots (2.32)$$

$$V_{Nernst}^{i} = E^0 + \Delta E = \frac{-\Delta G^0}{n_e F} + \frac{-\Delta G}{n_e F} = E^0 + \frac{RT}{2F} ln\left(\frac{{p_{H_2}}^{in} . {p_{O_2}}^{0.5^{in}}}{{p_{H_2O}}^{in}}\right) \quad \ldots (2.33)$$

$$V_{Nernst}^{e} = E^0 + \Delta E = \frac{-\Delta G^0}{n_e F} + \frac{-\Delta G}{n_e F} = E^0 + \frac{RT}{2F} ln\left(\frac{{p_{H_2}}^{ex} . {p_{O_2}}^{0.5^{ex}}}{{p_{H_2O}}^{ex}}\right) \quad \ldots (2.34)$$

where $E^0 = 1.2723 - 2.7645x10^{-4}T$ is the fuel cell voltage under standard conditions as a function of the cell temperature, n_e is the number of electrons participating in the electrochemical reaction, R is universal gas constant, T is the cell temperature and p partial pressure of respective species. The actual cell voltage can be defined as follows:

$$V_{cell} = V_{Nernst} - V_{ohm} - V_{act} - V_{conc} \quad \ldots (2.35)$$

The ohmic polarization is caused by the resistance to the oxide ion conduction through the electrolyte and resistance to the electron conduction in the electrodes and the interconnector. Figure 2.8 shows the current passing through the electrolyte and interconnector in the radial direction, and that through the anode cathode in the circumferential direction, where (A)-(C) indicate current flows that induce ohmic polarization [44].

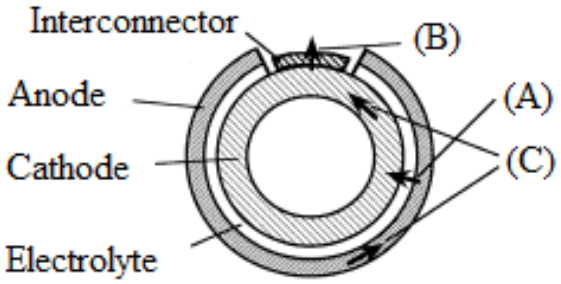

Figure 2.8 Cross-section of tubular SOFC

For tubular SOFC, the ohmic polarization can be calculated as follows [44]:

$$V_{ohm} = V_{ohm(A)} + V_{ohm(\boldsymbol{B})} + V_{ohm(C)} \quad \ldots (2.36)$$

$$V_{ohm} = i\rho_{elyt}\delta_{elyt} + id\pi\rho_{int}\frac{\delta_{int}}{w_{int}} + id\frac{\pi}{2}\left(\frac{\rho_{cat}}{\delta_{cat}} + \frac{\rho_{an}}{\delta_{an}}\right)\frac{1}{2}d\frac{\pi}{2} \quad \ldots (2.37)$$

where δ, ρ, w, and d are thickness (cm), resistivity (Ω cm), width (cm), and cell diameter (cm), respectively. The subscripts *elyt* and *int* represent electrolyte and interconnector, respectively. The loss from the current collector is negligible due to the low resistivity of Ni.

The electrode potential loss to overcome the activation energy of electrode reactions is called the activation polarization [43,45]. The relation between activation polarization, V_{act}, and the current density is expressed in implicit form by using the Butler-Volmer equation written as follows:

$$i = i_0\left[exp\left(\alpha\frac{n_eF}{RT}V_{act}\right) - exp\left(-(1-\alpha)\frac{n_eF}{RT}V_{act}\right)\right] \quad \ldots (2.38)$$

where i_0 and α are the exchange current density and the apparent charge transfer-coefficient, respectively. The exchange current density for anode ($i_{0,an}$) and cathode($i_{0,cat}$) can be expressed by [43]:

$$i_{0,an} = \gamma_{an}\left(\frac{p_{H_2}}{P_{ref}}\right)\left(\frac{p_{H_2O}}{P_{ref}}\right)exp\left(-\frac{E_{act,an}}{RT}\right) \quad \ldots (2.39)$$

$$i_{0,cat} = \gamma_{cat}\left(\frac{p_{O_2}}{P_{ref}}\right)^{0.5}exp\left(-\frac{E_{act,cat}}{RT}\right) \quad \ldots (2.40)$$

where γ is the exchange current density constant, P_{ref} is reference pressure and was taken as 1.013 bar, and E_{act} is the activation energy. The subscripts of *an* and *cat* represent anode and cathode, respectively. If we assume that the charge transfer coefficient for anode and cathode is 0.5 and substitute this value in the Butler-Volmer equation, then activation polarization can be calculated as follows:

$$V_{act} = \frac{2RT}{n_e F}\ sinh^{-1}\left(\frac{i}{2i_0}\right) \quad \ldots (2.41)$$

$$V_{act} = V_{act,an} + V_{act,cat} = \frac{2RT}{n_e F}\ sinh^{-1}\left(\frac{i}{2i_{0,an}}\right) + \frac{2RT}{n_e F}\ sinh^{-1}\left(\frac{i}{2i_{0,cat}}\right) \quad \ldots (2.42)$$

The concentration polarization is caused by the resistance to mass transport through the electrodes. Concentration polarization involves the difference in partial pressures between the electrode-electrolyte interface and bulk of the gas streams and can be calculated by using the following equation [10,46]:

$$V_{conc} = V_{conc,an} + V_{conc,cat}$$
$$= \left[-\frac{RT}{2F} ln\left(1 - \frac{i}{i_{l,an}}\right) + \frac{RT}{2F}\ ln\left(1 + \frac{p_{H_2}^{ex}.i}{p_{H_2O}^{ex}.i_{l,an}}\right)\right] + \left[-\frac{RT}{4F}\ ln\left(1 - \frac{i}{i_{l,cat}}\right)\right] \quad \ldots (2.43)$$

where $i_{l,an}$ is limiting current density for the anode [46] which can be estimated as follows:

$$i_{l,an} = \frac{2F\ .\ p_{H_2}^{ex}\ .\ D_{an(eff)}}{RT\ .\ \delta_{an}} \quad \ldots (2.44)$$

The O_2 diffusion induced concentration polarization of tubular cell has been previously studied. A general form of $P_{O_2}(c)$ shown in Figure 2.9 as a result of the concentration polarization is given by:

$$P_{O_2}(c) = P_t - P_t(1-x)^{1-i/i_{l,cat}} \quad \ldots (2.45)$$

where P_t is the total cell pressure; x = molar fraction of O_2 in air; and $P_{O_2}(b)/P_t$ is the partial pressure of oxygen in bulk air at P_t = 1 atm; and i and $i_{l,cat}$ are the current density and limiting current density, respectively [48]. The limiting current density for the cathode $\left(i_{l,cat}\right)$ as described in Eq. (2.43), at which $P_{O_2}(c)$ becomes zero, then takes form as [47,48]:

$$i_{l,cat} = \frac{-\ln\left(1-x_{O_2}^{ex}\right)}{ln\left(\frac{r_2}{r_1}\right)} \frac{4F \,.\, D_{cat(eff)(T)}}{RT \,.\, r_2} P_t \quad \ldots (2.46)$$

where r_2 and r_1 are the outer and inner radii of the cathode tube, respectively.

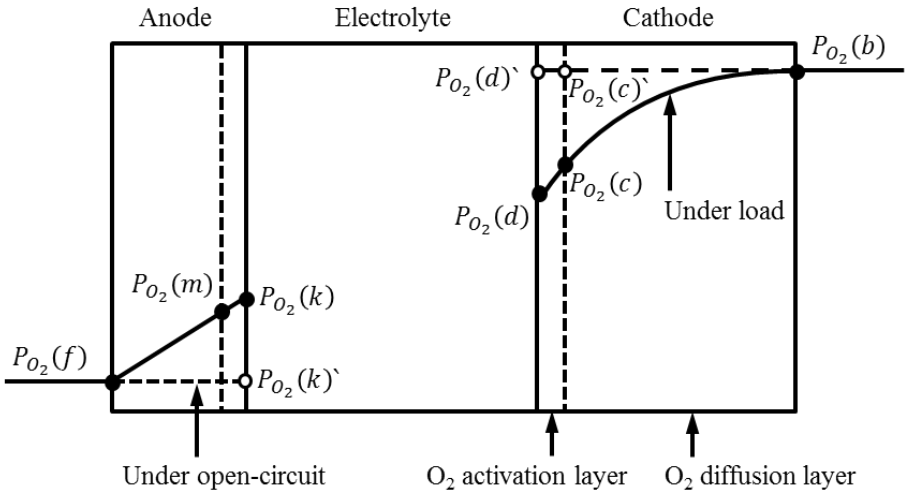

Figure 2.9 Schematic of P_{O_2} distributions across the functional layers of an SOFC. Dashed lines: Under oper circuit and solid lines: Under load [48].

The mass flux of the reactants and the product, i.e. H_2, H_2O, and O_2, through a porous solid is diffusive in nature and may involve only ordinary molecular and Knudsen diffusions. The latter is important when the mean free path is much bigger than the pore size, and molecules collide with the solid walls more often than with other molecules [47-49]. In this study, small pore size was adopted for anode thus both the ordinary molecular and Knudsen diffusions should be considered in the anode section.

Based on the established analysis developed for thick cathode supported SOFC with a relatively large pore diameter, it showed that Knudsen diffusion is negligible compared to molecular diffusion [47,48]. Therefore, only ordinary O_2 molecular diffusion is considered for the cathode in this study.

The ordinary binary diffusion coefficient for both anode and cathode can be calculated [43,50]:

$$D_{ab} = \frac{0.00143T^{1.75}}{M_{ab}^{1/2}\left[v_a^{1/3} + v_b^{1/3}\right]^2 P} \quad \ldots (2.47)$$

where

$$M_{ab} = 2[(1/M_a) + (1/M_b)]^{-1} \quad \ldots (2.48)$$

Here subscripts *a* and *b* represent the gaseous components that make up the binary gas mixture (H_2-Balance at anode and O_2-N_2 at cathode), P is partial pressure (bar), v is the specific Fuller diffusion volume, and M is the molecular weight. In a multi component gaseous system, molecular diffusion coefficient of the components ($D_{a,m}$) can be calculated as [51]:

$$D_{H_2,m} = \frac{1-y^0_{H_2}}{\frac{y^0_{H_2O}}{D_{H_2-H_2O}}+\frac{y^0_{CO}}{D_{H_2-CO}}+\frac{y^0_{CO_2}}{D_{H_2-CO_2}}+\frac{y^0_{N_2}}{D_{H_2-N_2}}} \quad \ldots (2.49)$$

$$D_{CO,m} = \frac{1-y^0_{CO}}{\frac{y^0_{H_2}}{D_{H_2-CO}}+\frac{y^0_{H_2O}}{D_{H_2O-CO}}+\frac{y^0_{CO_2}}{D_{CO-CO_2}}+\frac{y^0_{N_2}}{D_{CO-N_2}}} \quad \ldots (2.50)$$

$$D_{H_2O,m} = \frac{1-y^0_{H_2O}}{\frac{y^0_{H_2}}{D_{H_2-H_2O}}+\frac{y^0_{CO}}{D_{H_2O-CO}}+\frac{y^0_{CO_2}}{D_{H_2O-CO_2}}+\frac{y^0_{N_2}}{D_{H_2O-N_2}}} \quad \ldots (2.51)$$

$$D_{CO_2,m} = \frac{1-y^0_{CO_2}}{\frac{y^0_{H_2}}{D_{H_2-CO_2}}+\frac{y^0_{CO}}{D_{CO-CO_2}}+\frac{y^0_{H_2O}}{D_{H_2O-CO_2}}+\frac{y^0_{N_2}}{D_{CO_2-N_2}}} \quad \ldots (2.52)$$

$$D_{N_2,m} = \frac{1-y^0_{N_2}}{\frac{y^0_{H_2}}{D_{H_2-N_2}}+\frac{y^0_{CO}}{D_{CO-N_2}}+\frac{y^0_{H_2O}}{D_{H_2O-N_2}}+\frac{y^0_{CO_2}}{D_{CO_2-N_2}}} \quad \ldots (2.53)$$

The effective ordinary molecular diffusion coefficient is given by:

$$D_{a,m(eff)} = D_{a,m}\left(\frac{\varepsilon}{\tau}\right) \quad \ldots (2.54)$$

The Knudsen diffusion and the effective Knudsen diffusion coefficient for the anode gases can be calculated as:

$$D_{K,a} = 97 r_{por}(T/M_i)^{0.5} \quad \ldots (2.55)$$

$$D_{K,a(eff)} = D_{K,a}\left(\frac{\varepsilon}{\tau}\right) \quad \ldots (2.56)$$

where subscript a represents the gaseous component (H_2 - balance), r_{por} is the anode pore radius, M_i is the molecular weight of the gaseous, ε is porosity and τ is tortuosity

of the anode. The overall effective diffusion coefficient for each gas can be calculated as:

$$\frac{1}{D_{a(eff)}} = \frac{1}{D_{a,m(eff)}} + \frac{1}{D_{K,a(eff)}} \quad \ldots (2.57)$$

Finally, the anode and cathode diffusion coefficients were calculated using the following equations [2]:

$$D_{an(eff)} = \left(\frac{y^0_{H_2O}.P_{SOFC}}{P_{SOFC}}\right) D_{H_{2(eff)}} + \left(\frac{y^0_{H_2}.P_{SOFC}}{P_{SOFC}}\right) D_{H_2O_{(eff)}} \quad \ldots (2.58)$$

$$D_{cat(eff)} = D_{O_{2(eff)}} \quad \ldots (2.59)$$

where y_a^0 terms in Eqs. (2.49-2.53) and Eq. (2.58) is the molar fractions in the bulk flow, taken as the average values of the anode and the cathode inlet and outlet streams.

After calculating the mentioned voltage losses, the fuel cell power output is the product of the cell voltage and the current. The total current and the direct current (DC) output power of each cell can be expressed as follows [4]:

$$I_{tot} = \frac{\left(jH_{2,equivalent}\left(\frac{mol}{h}\right)\right)\left(2\ U_f\ F\left(\frac{C}{mol}\right)\right)}{\left(\frac{3600\ s}{h}\right)} = \frac{jH_{2,equivalent}U_f}{0.018655} \quad \ldots (2.60)$$

$$\mathrm{W}_{SOFC-DC} = V_{cell}\ x\ I_{tot} \quad \ldots (2.61)$$

The alternating current (AC) power of the cell module can be specified using:

$$W_{SOFC-AC} = W_{SOFC-DC}\ x\ \eta_{inv} \quad \ldots (2.62)$$

where η_{inv} is the inversion efficiency of direct to alternating current.

The SOFC only converts part of the chemical energy of syngas fuel into electrical power, and the rest will become heat as a result of losses in the system. The net heat duty for the 'ANODE' block is calculated in Aspen Plus™ as [4]:

$$Q_2 = Q_r + Q_s + Q_e - Q_g \quad \ldots (2.63)$$

where Q_r, Q_s, and Q_e are the reaction heats for reactions appeared in Eqs. (2.18, 2.19, and 2.21), and $Q_g$represents the heat given to the fuel and air streams, which includes the heat stream feed into the block (Q_1).

2.6 Steam Power Generation Cycle

2.6.1 Rankine Cycle

A flowsheet and T-S diagram of an ideal Rankine cycle is shown in Figure 2.10 and Figure 2.11, respectively. The condensate from process 4-1 is pumped isentropically from 1 to 2 before being evaporated to saturated vapor from 2-3. Then, an isentropic expansion is performed through a turbine from saturated vapor to condenser pressure in process 3-4. Water droplets can erode the turbine blades, and it is therefore desirable to keep the outlet steam quality as high as possible. The heat supplied to the system is most commonly supplied by the combustion of coal or other fired boiler model. From 4 to 1 the two-phase mixture is condensed to saturated liquid by cooling water in a

cooling tower. It is possible to superheat the steam in order to improve the performance. Superheat increases the steam quality at the outlet and the work output form the steam turbine.

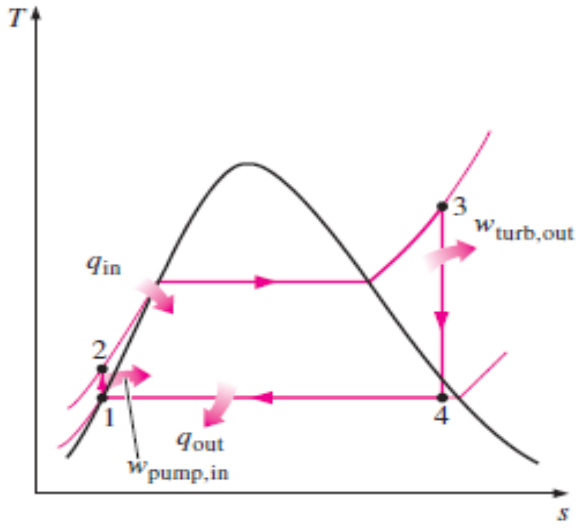

Figure 2.10 Flow diagram of ideal Rankine Cycle [52].

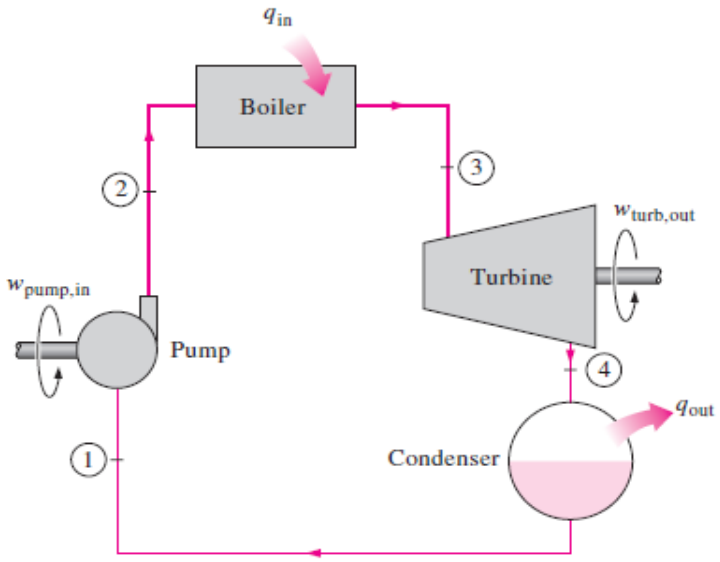

Figure 2.11 T-S Diagram of ideal Rankine Cycle [52].

2.6.2 Steam Cycle Model Description

The excess of heat from exhaust SOFC module and combustor unit is recovered by using HRSG to produce sufficient high pressure steam before expanded in a high pressure and low pressure steam turbine for power generation. The steam turbine cycle is based on the theoretical Rankine cycle, in which a liquid is compressed, evaporated, expanded and condensed. Each step in the cycle takes place in a different component. The detailed Aspen Plus™ flowsheet of the steam turbine cycle is illustrated in Figure 2.12. A brief description of the unit operation blocks shown in Figure 2.12 is presented in Table 2.7.

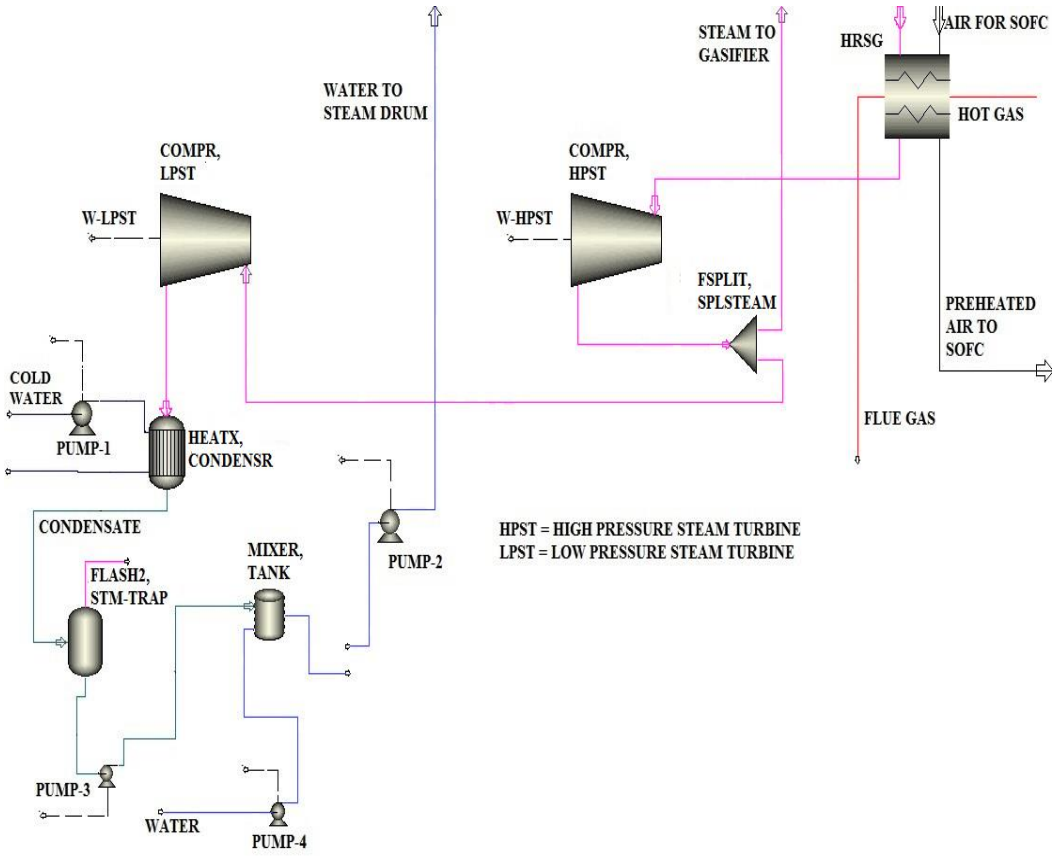

Figure 2.12 Aspen Plus™ Rankine cycle Flowsheet.

(solid lines represent material streams and dotted lines represent energy streams)

Table 2.7 Description of Aspen Plus™ unit operation blocks shown in Figure 2.12.

Aspen Plus™ Name	Description
MHeatX	HRSG; simulates heat transfer between hot exhaust gas from combustion unit (hot stream) and steam from steam drum (hot stream) and compressed air for SOFC unit (cold stream).
Compr	HPST; simulates the high pressure steam turbine (HPST) producing electricity. LPST; simulates the low pressure steam turbine (LPST) producing electricity.
Pump	PUMP-1; to supply the saturated water for condenser unit. PUMP-2; to supply the water for steam drum and syngas cooler, producing steam for Rankine cycle. PUMP-3; to pump the condensate produced by condenser into the water supply tank. PUMP-4; to supply water for the power plant purpose via water supply tank.
Heatx	CONDENSER; simulates the condensing process of vapor into liquid.
Flash2	STM-TRAP (steam trap); to discharge condensate and non-condensable gases with loss of live steam.
Mixer	TANK (water supply tank); to supply the water for the plant.
FSplit	SPLSTEAM (split steam); to split the steam into LPST and coal gasifier.

2.7 System performance

The total electrical efficiency of L-IGFC power plant system can be calculated as follow:

$$\eta_{electrical} = \frac{(W_{SOFC}+W_{expander}+W_{turbines})-E_{int,consumed}}{Z_{coal}LHV_{coal}} \quad \ldots (2.64)$$

where W_{SOFC}, $W_{expander}$, $W_{turbines}$, are the power produced by SOFC, syngas expander, and steam turbines, respectively.

2.8 Input Data

The integration study has many degrees of freedom, and exploring all possible interactions in the power plant will be time consuming. In order to simplify the integration study and obtain a fair comparison between the system integration, it is necessary to make some common assumptions and constrains for the integration schemes. The main assumptions and constraints are listed as follows:

- The raw syngas is quenched to 900 °C prior to entering convective syngas cooler to prevent the fly ash from having sticky surfaces.
- About 30% ash is entrained as fly ash with the raw syngas out of the gasifier into syngas quencher.
- SOFC operates at steady state (detailed assumption for SOFC modules were described in Section 2.5).
- Pressure drops and heat loss in the system analysis are not taken into account.
- The temperature difference (ΔT) between inlet and outlet of anode, and inlet and outlet of cathode will be set constant at 100 °C, respectively for all integration

schemes.

The input parameters for the plant calculation are summarized in Table 2.8. The input parameters are categorized into free input design variables (I), and outsource data mechanism (M) as input parameters collected from published references.

Table 2.8 Design and operating parameter assumptions for plant calculation

Item	Value	
Gasifier		
Gasification pressure, bar [53]	40	(M)
Gasification temperature, °C [14]	1500	(M)
Coal feed, kg hr^{-1} [14]	5986	(M)
Oxygen feed (99% purity), kg hr^{-1} [14]	5722	(M)
Nitrogen feed (carrier gas and purge), kg hr^{-1} [14]	526	(M)
Steam feed, kg hr^{-1} [14]	571	(M)
Air separation unit (ASU) [21]		
Energy consumption, kWh/tonne-O_2	400	(M)
Wet Gas Cleanup [30]		
Energy consumption per kmol/hr sulphur , kW	528.24	(M)
Dry Gas Cleanup [35]		
Cleanup temperature, °C	460	(M)
Cleanup pressure, bar	40	(M)
Miscellaneous BOP, % input LHV [8]	0.15	(M)
SOFC		
Temperature of the inlet fuel to anode, °C	750	(I)

Temperature of the inlet air to cathode, °C	750	(I)
Operating temperature of the SOFC, °C	800	(I)
Operating pressure of the SOFC, bar	1.09	(I)
Fuel utilization factor (U_f), %	80	(I)
Air utilization factor (U_a), %	30	(I)
Steam cycle		
HP/LP turbine pressure levels, bar	100/40	(I)
HP/LP turbine temperature level, °C	565/440	(I)
Condensing pressure, bar	0.4	(I)
Steam mass flow rate to HP turbine, kg hr^{-1} (Plant with coal as received).	55000	(I)
DC to AC inverter efficiency, % [9]	95	(M)
Electric generator efficiency, % [8]	98.7	(M)

Detailed input parameter for SOFC to calculate ohmic, activation, concentration polarizations are given in Table 2.9.

Table 2.9 Input parameters for SOFC unit

Geometry	
Cell diameter (d), cm [44]	1.6
Cathode thickness (δ_{cat}), μm [44,54]	2×10^3
Electrolyte thickness (δ_{elyt}), μm [44,13]	20
Anode thickness (δ_{an}) , μm [44,13]	100
Interconnector thickness (δ_{int}), μm [44]	20

Interconnector width (w_{int}), cm [44]	0.5
Inner radius of the cathode tube (r_1), cm	0.588
Outer radius of the cathode tube (r_2),cm	0.788
Properties of SOFC components [55]	
Cathode resistivity (ρ_{cat}), Ω cm	0.008114exp(600/T)
Electrolyte resistivity (ρ_{elyt}), Ω cm	0.00294exp(10350/T)
Anode resistivity (ρ_{an}), Ω cm	0.00298exp(-1392/T)
Interconnector resistivity (ρ_{int}), Ω cm	0.1256exp(4690/T)
Parameters for activation polarization	
Activation energy ($E_{act,an}$ / $E_{act,cat}$), kJ mol^{-1} [43]	110 / 120
Exchange current density constant ($\gamma_{an}, \gamma_{cat}$), A cm^{-2} [43,56]	7 x 10^5
Parameters for concentration polarization	
Anode pore radius (r_{por}), μm [56]	1
Electrode porosity (ε), % / tortuosity (τ) [56]	50 / 3

REFERENCES

[1]. Ong`iro A, Ugursal VI, Al Taweel AM, Lajeunesse G. Thermodynamic simulation and evaluation of a steam CHP plant using aspen plus. Appl Therm Eng 1996;16(3):263-271.

[2]. Doherty W, Reynolds A, Kennedy D. Computer simulation of a biomass gasification-solid oxide fuel cell power system using Aspen Plus. Energy 2010;35:4545-4555.

[3]. Tanim T, Bayless D, Trembly JP. Modeling a 5 kWe planar solid oxide fuel cell based system operating on JP-8 fuel and a comparison with tubular cell based system for auxiliary and mobile power applications. J Power Sources 2014;245:986-997.

[4]. Zhang W, Croiset E, Douglas PL, Fowler MW, Entchev E. Simulation of a tubular solid oxide fuel cell stack using AspenPlus^{TM} unit operation models. Energy Conv Manag 2550;46:181-196.

[5]. Ramzan N, Ashraf A, Naveed S, Malik A. Simulation of hybrid biomass gasification using Aspen Plus: A comparative performance analysis for food, municipal solid and poultry waste. Biomass and Bioenergy 2011;35:3962-3969.

[6]. Wang P, Massoudi M. Slag behavior in gasifiers. Part I: influence of coal properties and gasification conditions. Energies 2013;6:784-806.

[7]. Ni J, Yu G, Guo Q, Dai Z, Wang F. Modeling and comparison of different syngas cooling types for entrained-flow gasifier. Chem Eng Sci 2011;66:448-459.

[8]. Spallina V, Romano MC, Campanari S, Lozza G. A SOFC-based integrated gasification fuel cell cycle with CO_2 capture. ASME J Eng Gas Turbines Power 2011;133:1-10.

[9]. Ameri M, Mohammadi R. Simulation of an atmospheric SOFC and gas turbine hybrid system using Aspen Plus software. Int J Energy Res 2012;37:412-425.

[10]. Colpan CO, Dincer I, Hamdullahpur F. Thermodynamic modeling of direct internal reforming solid oxide fuel cells operating with syngas. Int J Hydrogen Energy 2007;32:787-795.

[11]. Minchener AJ. Coal gasification for advanced power generation. Fuel 2005;84:2222-2235.

[12]. Stiegel GJ, Maxwell RC. Gasification technologies: the path to clean, affordable energy in the 21st century. Fuel processing technology 2001;71:79-97.

[13]. Emun F, Gadalla M, Majozi T, Boer D. Integrated gasification combined cycle (IGCC) process simulation and optimization. Computers & Chemical Engineering 2010;34:331-338.

[14]. Kivisaari T, Bjornbom P, Sylwan C, Jacquinot, Jansen D, de Groot A. The feasibility of a coal gasifier combined with a high-temperature fuel cell. Chem Eng J 2004;100:167-180.

[15]. Verma A, Rao AD, Samuelsen GS. Sensitivity analysis of a vision 21 coal based zero emission power plant. J Power Sources 2006;158:417-427.

[16]. Haslbeck JL, Hamilton BA, Kuehn NJ, et al. Cost and performance baseline for fossil energy plants, volume 1: bituminous coal and natural gas to electricity. DOE/NETL-2010/1397.

[17]. Aspen Plus. Getting started modeling processes with solids. Aspen Technology Inc., 2010.

[18]. http://wp.auburn.edu/eden/wp-content/uploads/2012/03/4470-Lecture-5-2013.pdf

[19]. Zhou L, Zhang Z, Chivetta C, Agarwal R. Process simulation and validation of chemical-looping with oxygen uncoupling (CLOU) process using Cu-Based Oxygen carrier. Energy Fuels 2013;27:6906-6912.

[20]. Mukherjee S, Kumar P, Hosseini A, Yang A, Fennell P. Comparative assessment of gasification based coal power plants with various CO2 capture technologies producing electricity and hydrogen. Energy Fuels 2014;28:1028-1040.

[21]. European Industrial Gases Association AISBL. Indirect CO_2 emissions compensation: benchmark proposal for air separation plants. Position paper PP-33-December 2010.

[22]. Trembly JP, Marquez AI, Ohrn TR, Bayless DJ. Effects of coal syngas and H_2S on the performance of solid oxide fuel cells: Single-cell tests. J Power Sources 2006;158:263-273.

[23]. Matsuzaki Y, Yasuda I. The poisoning effect of sulfur-containing impurity gas on a SOFC anode: Part I. Dependence on temperature, time, and impurity concentration. Solid State Ionics 2000;132:261-269.

[24]. Tsipis EV, Kharton VV. Electrode materials and reaction mechanisms in solid oxide fuel cells: a brief review. III. Recent trends and selected methodological aspects. J Solid State Electrochem 2011;15:1007-1040.

[25]. Ohtsuka Y, Tsubouchi N, Kikuchi T, Hashimoto H. Recent progress in Japan on hot gas cleanup of hydrogen chloride, hydrogen sulfide and ammonia in coal-derived fuel gas. Powder Technol 2009;190:340-347.

[26]. Jansen D, van der Laag PC, Oudhuis ABJ, Ribberink JS. Prospects for advanced coal-fuelled fuel cell power plants. J Power Sources 1994;49:151-165.

[27]. Dou B, Wang C, Chen H, Song Y, Xie B, Xu Y, Tan C. Research progress of hot gas filtration, desulphurization and HCL removal in coal-derived fuel gas: A review. Chem Eng Res Des 2012;90:1901-1917.

[28]. Leppalahti J, Koljonen T. Nitrogen evolution from coal, peat and wood during gasification: Literature review. Fuel Process Technol 1995;43:1-45.

[29]. Japan Coal Energy Center (JCOAL). http://www.jcoal.or.jp/eng/cctinjapan/cct_english.pdf

[30]. Sadhukhan J, Zhao Y, Shah N, Brandon NP. Performance analysis of integrated biomass gasification fuel cell (BGFC) and biomass gasification combined cycle (BGCC) systems. Chem Eng Sci 2010;65:1942-1954.

[31]. Gerdes K, Grol E, Keairns D, Newby R. Integrated gasification fuel cell performance and cost assessment, DOE/NETL-2009/1361, U.S. Department of Energy, Morgantown, WV, 2009.

[32]. Gupta RP, O`Brien WS. Desulfurization of hot syngas containing hydrogen chloride vapors using zinc titanate sorbents. Ind Eng Chem Res 2000;39:610-619.

[33]. Woolcock P, Brown RC. A review of cleaning technologies for biomass-derived syngas. Biomass Bioenergy 2013;52:54-84.

[34]. Howard CJ, Dagle RA, Lebarbier VM, Rainbolt JE, Li L, King DL. Progress toward biomass and coal-derived syngas warm cleanup: proof-of-concept process demonstration on multicontaminant removal for biomass application. Ind Eng Chem Res 2013;52:8125-8138.

[35]. Giuffrida A, Romano MC, Lozza GG. Thermodynamic assessment of IGCC power plants with hot fuel gas desulfurization. Appl Energy 2010;87:3374-3383.

[36]. Costamagna P, Magistri L, Massardo AF. Design and part-load performance of a hybrid system based on a solid oxide fuel cell reactor and a micro gas turbine. J Power Sources 2001;96:352-368.

[37]. Doherty W, Reynolds A, Kennedy D. Simulation of a tubular solid oxide fuel cell stack operating on biomass syngas using aspen plus. J Electrochem Soc 2010;157:B975-B981.

[38]. Li M, Powers JD, Brouwer J. A finite volume SOFC model for coal-based integrated gasification fuel cell systems analysis. J Fuel Cell Sci Technol 2010;7:1-12.

[39]. Holtappels P, De Haart LGJ, Stimming U, Vinke IC, Mogensen M. Reaction of CO/CO2 gas mixtures on Nu-YSZ cermet electrodes. J App Electrochem 1999;29(5):561-568.

[40]. Ho TX, Kosinski P, Hoffmann AC, Vik A. Modeling of transport, chemical and electrochemical phenomena in a cathode-supported SOFC. Chem Eng Sci 2009;64:3000-3009.

[41]. Li PW, Chyu MK. Electrochemical and transport phenomena in solid oxide fuel cells. J Heat transfer 2005;127(12):1344-1362.

[42]. Smith JM, Van Ness HC, Abbott MM. Introduction to chemical engineering thermodynamics, 7th edition, McGraw-Hill, NY, 2005.

[43]. Akkaya AV. Electrochemical model for performance analysis of a tubular SOFC. Int J Energy Res 2007;31:79-98.

[44]. Tanaka K, Wen C, Yamada K. Design and evaluation of combined cycle system with solid oxide fuel cell and gas turbine. Fuel 2000;79:1493-1507.

[45]. Chan SH, Khor KA, Xia ZT. A complete polarization model of a solid oxide fuel cell and its sensitivity to the change of cell component thickness. J Power Sources 2001;93:130-140.

[46]. Kim JW, Virkar AV, Fung KZ, Mehta K, Singhal SC. Polarization effects in intermediate temperature, anode-supported solid oxide fuel cells. J Electrochem Soc 1999;146(1):69-78.

[47]. Huang K. Gas-diffusion process in a tubular cathode substrate of an SOFC. J Electrochem Soc 2004;151(5):A716-A719.

[48]. Huang K, Zampieri A, Ise M. Cathode polarizations of a cathode-supported solid oxide fuel cell. J Electrochem Soc 2010;157(10):B1471-B1478.

[49]. Shi Y, Cai N, Li C. Numerical modeling of an anode-supported SOFC button cell considering anodic surface diffusion. J Power Sources 2007;164:639-648.

[50]. Todd B, Young JB. Thermodynamic and transport properties of gases for use in solid oxide fuel cell modelling. J Power Sources 2002;110:186-200.

[51]. Hajimolana SA, Hussain MA, Soroush M, Wan Daud WMA, Chakrabarti MH. Modeling of a tubular-SOFC: the effect of the thermal radiation of fuel components and CO participating in the electrochemical process. Fuel Cells 2012;12(5):761-772.

[52]. Cengel YA, Boles MA. Thermodynamics: An engineering approach, 5th edition, McGraw-Hill, New York, NY, USA, 2006.

[53]. http://www.thyssenkrupp-industrial-solutions.com/fileadmin/documents/brochures/gasification_technologies.pdf

[54]. Fukushima Y, Shimada M, Kraines S, Hirao M, Koyama M, Scenarios of solid oxide fuel cell introduction into Japanese society. J Power Sources 2004; 131:327-339.

[55]. Jia J, Abudula A, Wei L, Shi Y. Performance comparison of three solid oxide fuel cell power systems. Int J Energy Res 2013;37:1821-1830.

[56]. Campanari S, Iora P. Definition and sensitivity analysis of a finite volume SOFC model for a tubular cell geometry. J Power Sources 2004;132:113-126.

CHAPTER 3

L-IGFC DESIGN AND ANALYSIS

This chapter explains a proposed design of a system integrating coal gasifier fuel cell system for high efficiency power generation. A commercial process simulator Aspen Plus™ is chosen to conduct the studies. One challenge when using Aspen Plus™ for a power generation cycle including a SOFC module is the SOFCs have not been included in its built in models such as turbines or compressors unit operation models. Moreover, we need to link with Fortran application or Microsoft Excel in order to analyze the performance of SOFC module. However, as early mentioned in the previous chapter, the approach introduced in this thesis is to develop a SOFC model by using existing Aspen Plus™ V8.4 functions and unit operation models combining with Excel to analyze the SOFC performance and L-IGFC system performance. It can easily be extended to study the entire process, consisting SOFC and balance of plant. Based on literature review, several IGFC design concepts were proposed and evaluated although most of them are still in a conceptual stage. They can be categorized based on the SOFC working pressure: atmospheric and pressurized, and also gas cleanup models: WGC and DGC.

3.1 Verification of the developed model of Coal Gasifier

In the previous chapter, an Aspen Plus™ coal gasification module model was introduced based on literature descriptions. In this section, the model is extended to study the entire power generation process. Before integrated the coal gasifier unit with SOFC module and others BOP, the model was validated against published data. The

coal gasification unit was simulated by referring to coal composition and others parameters from reference [1]. Gasification unit is based on a dry feed, oxygen-blow, and entrained flow Prenflo type. The composition of the coal and operating condition for the gasifier are given in Table 3.1 and Table 3.2.

Table 3.1 Data for Pittsburg No. 8 coal [1].

Pittsburg No. 8 Coal	
Ultimate analysis (%)	
Carbon	74.9
Hydrogen	5.1
Oxygen	5.2
Nitrogen	1.5
Sulphur	2.4
Chlorine	0.09
Fluorine	0.009
Ash	10.8
Proximate analysis (%)	
Moisture	1.0
Ash	9.0
Fixed Carbon	52.3
Volatile matter	37.7
Lower heating value (MJ kg^{-1} (mf))	30.4
Higher heating value (MJ kg^{-1} (mf))	31.5

Table 3.2 Data for the Prenflo gasifier [1].

Gasifier outlet temperature (^{O}C)	1450
Gasifier pressure (bar)	20
Coal feed (including 1% moisture) (kg hr^{-1})	5986
Oxygen feed (99% purity) (kg hr^{-1})	5868

Nitrogen feed (carrier gas and purge) (kg hr^{-1})	526
Steam feed (kg hr^{-1})	571

Major calculation results and some comparisons between the simulation results and literature data are listed in Table 3.3. It shown the model results are in good agreement with published work.

Table 3.3 Raw syngas composition obtained from the gasifier, prior to gas cleanup unit.

	Reference[1]	This study (Aspen V. 8.4)
Gasifier outlet temperature, ºC	1500	1500
Gasifier pressure, bar	20	20
Gasifier outlet flow, kg hr^{-1}	12446	12420.7
Molar composition, %		
H_2	26.3	25.9
N_2	4.2	3.8
H_2O	5.7	6.1
CO	59.6	59.6
CO_2	3.4	3.8
H_2S	0.6	0.7
CH_4 (ppm)	20	19
H_3N	16.7	16
Cl_2 (ppm)	5.4	57
COS	0.05	0.057
Ash+Slag, kg hr^{-1}	505	530.3

3.2 Verification of the developed SOFC module

The Aspen Plus™ SOFC module flowsheet was introduced based on literature descriptions of a tubular direct internal reforming SOFC technology in the previous

chapter. In this section, this model is extended to study the entire power generation process consisting of the SOFC module and balance of plant (BOP). Before integrated the SOFC module with coal gasifier and others BOP, the model was validated against published data. Some assumptions as input parameters were defined according to the reference [2]. These assumptions for the SOFC model simulation are listed in Table 3.4.

Table 3.4 Assumptions for SOFC model simulation.

Inlet fuel composition (mole basis)	CH_4 81.3%, C_2H_6 2.9%, C_3H_8 0.4%, C_4H_{10} 0.2%, N_2 14.3%, CO 0.9%.
Temperature of inlet fuel, °C [2]	200
Operating temperature of the SOFC, °C [2]	910
Temperature of inlet air, °C [2]	630
Temperature of the inlet fuel to anode, °C	810
Temperature of the inlet air to cathode, °C	810
Operating pressure of the SOFC, bar [2]	1.094
Ejector fresh fuel pressure ratio [2]	3
Steam to carbon ratio (S/C ratio) [2]	2.5
Pressure drops inside the SOFC [2]	0
Fuel utilization factor (U_f), % [2]	85
ΔT between inlet and outlet of anode, °C	100
ΔT between inlet and outlet of cathode, °C	100
DC to AC inverter efficiency, % [2]	92

Major calculation results and some comparisons between the simulation results and literature data are listed in Table 3.5. It shown the model results are in good agreement with published work. There is only a slight difference for actual voltage and current density due to the different method for calculating them between reference and this study. The reference used semi-empirical correlations developed using a reference

polarization curve. It has been reported that these correlations may not be valid for other fuels [3,4]. The method of voltage calculation applied in this study is considered to be more accurate as the employed equations consider changes in pressure, temperature, cell geometry and properties, and could be applied to diverse fuels. Other differences in comparison with the reference also include the approach of oxygen flow rate consumed or required by electrochemical reaction was set and also the fuel reforming type. In this thesis work, the oxygen required was set by using a specified U_a whereas reference applied a heat balance assuming a certain amount of heat loss. Also, the direct internal reforming (DIR) SOFC was selected for this study instead of indirect internal reforming (IIR) which was adopted by reference.

Table 3.5 Comparison results.

	Literature [1]	Model results
Voltage, V	0.70	0.697
Current density, mA cm^{-2}	178	165
Cathode inlet temperature, ºC	821.32	810
Module exhaust temperature, ºC	833.85	836.40
Anode exhaust gas molar composition, %	11.6% H_2, 7.4% CO, 50.9% H_2O, 24.9% CO_2, 5.1% N_2	11.8% H_2, 7.6% CO, 50.7% H_2O, 24.8% CO_2, 5.1% N_2
Cathode exhaust gas molar composition, %	17.7% O_2, 82.3% N_2	17.7% O_2, 82.3% N_2
Module exhaust gas molar composition, %	4.5% H_2O, 2.3% CO_2, 15.9% O_2, 77.3% N_2	4.5% H_2O, 2.3% CO_2, 15.9% O_2, 77.3% N_2

3.3 Atmospheric L-IGFC Plant

The layout of the proposed L-IGFC power plant system was introduced in Chapter 2. The L-IGFC system configured with atmospheric SOFC by using different type of syngas cleanup process: WGC and DGC will be discussed detailed in the following discussions.

3.3.1 Atmospheric L-IGFC Plant with WGC

3.3.1.1 System Performance

The process scheme of this design is shown in Figure 3.1. The characteristic of this design is that the various impurities in the raw syngas such as sulfur compound, chloride, ammonia, and particulate matter were removed by using WGC unit.

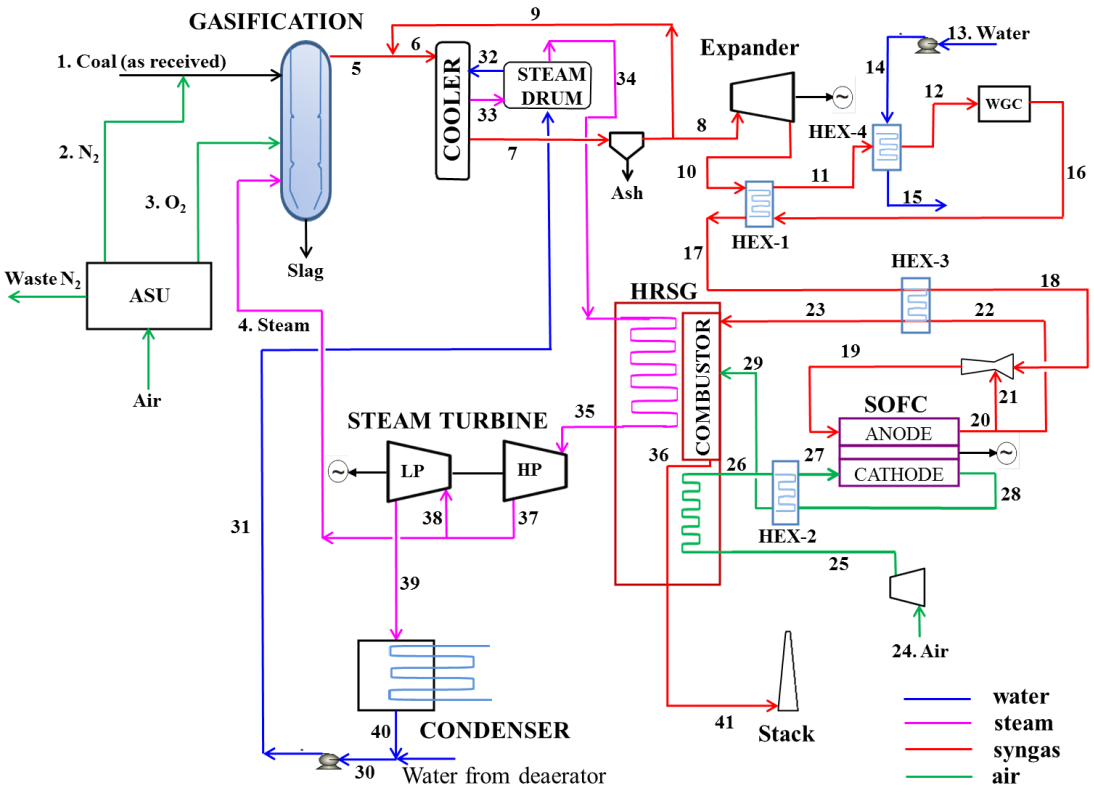

Figure 3.1 Flow diagram of the proposed L-IGFC power plant with WGC.

The L-IGFC power plant with WGC was simulated in Aspen Plus™ by using the input data as described in Table 2.8 of Chapter 2. The stream properties for this plant are presented in Table 3.6. The raw syngas composition leaving the gasifier (stream 5) is 12.93 ppm CH_4, 21.28% H_2, 49.03% CO, 9.63% CO_2, 15.18% H_2O, 3.96% N_2, 0.86% H_2S, 457.94 ppm Cl_2, 24.01 ppm NH_3. The electrical power output produced by syngas expander ($W_{expander}$), SOFC (W_{SOFC}), and steam turbines ($W_{turbines}$) are 1296.40 kW, 8353.62 kW, and 12,929.92 kW, respectively. The net internal energy consumption ($E_{int,consumed}$) by ASU, pumps, air blower, WGC unit and auxiliaries is 5420.44 kW. The net electrical power output of the plant is 17,159.5 kW, giving a system efficiency of 39.48%. The largest energy consumption during processes occurred in WGC unit which approximately of 2471 kW.

Table 3.6 Stream properties for the L-IGFC power plant with WGC.

stream	T	P	Z	Molar composition (%)							
	(°C)	(bar)	(kg/h)	H_2	O_2	N_2	H_2O	CO	CO_2	H_2S	CH_4
1	25	1.013	5986	Coal as received, see Table 2.1 Chapter 2							
2	710.5	40	526	0	0	100	0	0	0	0	0
3	664.4	40	5722	0	99	1	0	0	0	0	0
4	440	40	571	0	0	0	100	0	0	0	0
5	1500	40	12398	21.3	0	4	15.2	49	9.6	0.9	0
6	900	40	32608.60	21.3	0	4	15.2	49	9.6	0.9	0
7	509.9	40	32608.60	21.3	0	4	15.2	49	9.6	0.9	0
8	509.9	40	12224.55	21.3	0	4	15.2	49	9.6	0.9	0
9	509.9	40	20209.91	21.3	0	4	15.2	49	9.6	0.9	0
10	246.9	3.28	12224.55	21.3	0	4	15.2	49	9.6	0.9	0
11	115	3.28	12224.55	21.3	0	4	15.2	49	9.6	0.9	0
12	81.6	3.28	12224.55	21.3	0	4	15.2	49	9.6	0.9	0

13	20.0	1.013	3000	0	0	0	100	0	0	0	0
14	20.1	3.04	3000	0	0	0	100	0	0	0	0
15	75.0	3.04	3000	0	0	0	100	0	0	0	0
16	25.0	3.28	10634.82	25.2	0	4.7	0.8	58	11.4	0	0
17	186.5	3.28	10634.82	25.2	0	4.7	0.8	58	11.4	0	0
18	409.1	3.28	10634.82	25.2	0	4.7	0.8	58	11.4	0	0
19	750	1.09	48272.8	10.7	0	4.7	15.3	25.3	44	0	0
20	850	1.09	53145.48	4.7	0	4.7	21.2	11.9	57.4	0	0
21	850	1.09	37637.63	4.7	0	4.7	21.2	11.9	57.4	0	0
22	850	1.09	15507.85	4.7	0	4.7	21.2	11.9	57.4	0	0
23	700	1.09	15507.85	4.7	0	4.7	21.2	11.9	57.4	0	0
24	25	1.013	69734	0	21	79	0	0	0	0	0
25	34.2	1.09	69734	0	21	79	0	0	0	0	0
26	400	1.09	69734	0	21	79	0	0	0	0	0
27	750	1.09	69734	0	21	79	0	0	0	0	0
28	850	1.09	64861.33	0	15.7	84.3	0	0	0	0	0
29	481.5	1.09	64861.33	0	15.7	84.3	0	0	0	0	0
30	77.20	1.20	55000	0	0	0	100	0	0	0	0
31	79.30	100	55000	0	0	0	100	0	0	0	0
32	309.9	100	55000	0	0	0	100	0	0	0	0
33	309.9	100	55000	0	0	0	100	0	0	0	0
34	309.9	100	55000	0	0	0	100	0	0	0	0
35	565	100	55000	0	0	0	100	0	0	0	0
36	750.4	1.09	80369.18	0	11.8	71.9	4.4	0	11.8	0	0
37	440	40	55000	0	0	0	100	0	0	0	0
38	440	40	54429	0	0	0	100	0	0	0	0
39	82.90	0.4	54429	0	0	0	100	0	0	0	0
40	77.80	1.20	54429	0	0	0	100	0	0	0	0
41	34.2	1.09	80369.18	0	11.8	71.9	4.4	0	11.8	0	0

The WGC used in the concept of L-IGFC shown in Figure 3.1 works at near or slightly higher than room temperature and the process poses relatively bigger efficiency penalty on the whole system. This is because the hot raw syngas from the coal gasifier must be quenched to low temperature to accommodate the temperature range of the gas cleanup processes. Then, the clean syngas needs to be heated up again prior to entering the SOFC unit. The process results in significant waste of thermal energy and requires expensive and complex heat exchanger equipment. It has been observed that by reducing syngas temperature below its dew point may cause condensation of water and in the end will reduce the total mass of clean syngas as a fuel for SOFC unit.

3.3.1.2 Pinch Points and Utility

The starting point is a stream-by-stream breakdown of the heat sources and sinks within the process. The breakdown shows the enthalpy change ΔH and temperatures T of all heat sinks (cold stream) and all heat sources (hot streams) in a given process. Consider the characteristics of a heat-exchanger network (HEN) that is to achieve the energy targets, subject to a given ΔT_{min} requirement. ΔT_{min} is the minimum permissible temperature difference for heat transfer. The rules of Pinch analysis are: (i) do not recover process heat across the pinch, (ii) do not apply hot utilities to process streams below the pinch, and (iii) do not apply cold utilities to process streams above the pinch [5].

In order to ensure a heat transfer between cold and hot flows, the combined curves of the hot material flows must lie over those of the cold flows in all points. The constraint set by ΔT_{min} is defined as the minimal temperature difference between the flows. Then the pinch point, where the distance between the hot and cold curves is

minimal, denotes the possible optimal internal heat transfer between the hot and cold flows [6]. By approximating hot and cold streams as linear correlations, these curves can be illustrated in enthalpy-temperature diagrams (H-T). The necessary data are temperatures, heat duty, and heat capacity of each stream and available utility data.

In the case of L-IGFC plant with WGC, by using the Aspen Plus™, the pinch point takes place at 82.9 ºC for the hot streams and 52.9 ºC for the cold streams as shown in Figure 3.2 for composite curve and Figure 3.3 for grand composite curve. It indicates that the design has ΔT_{min} = 30 ºC.

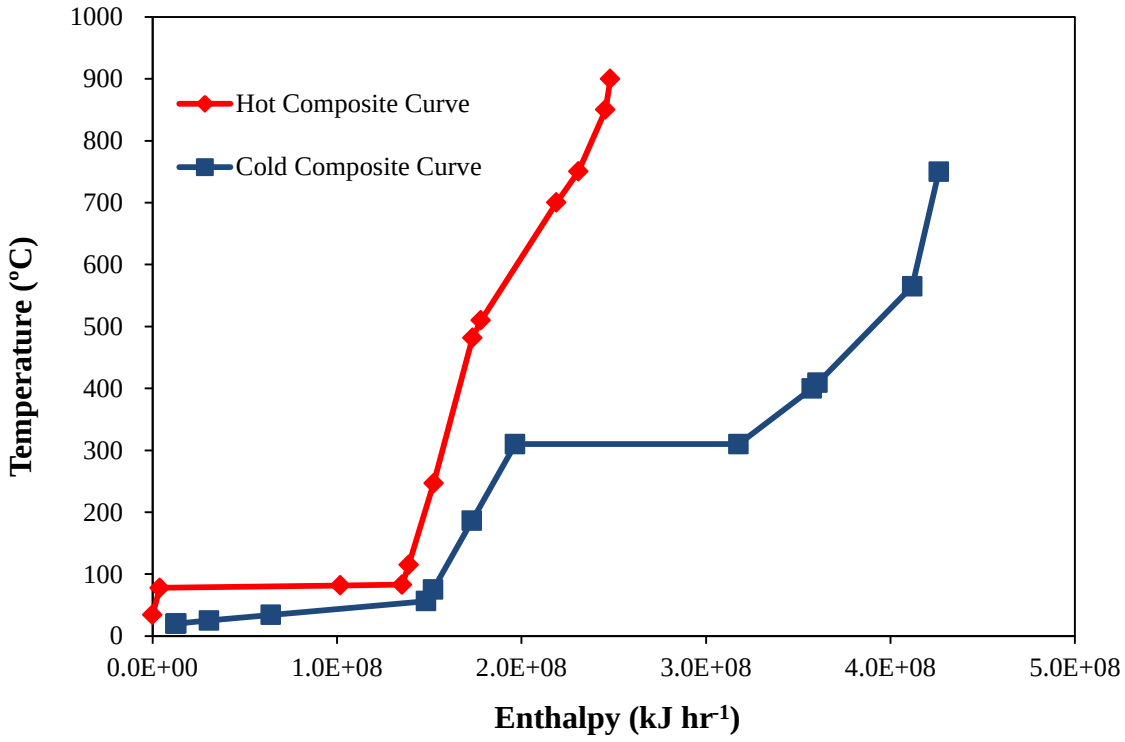

Figure 3.2 Composite curves of the L-IGFC with WGC.

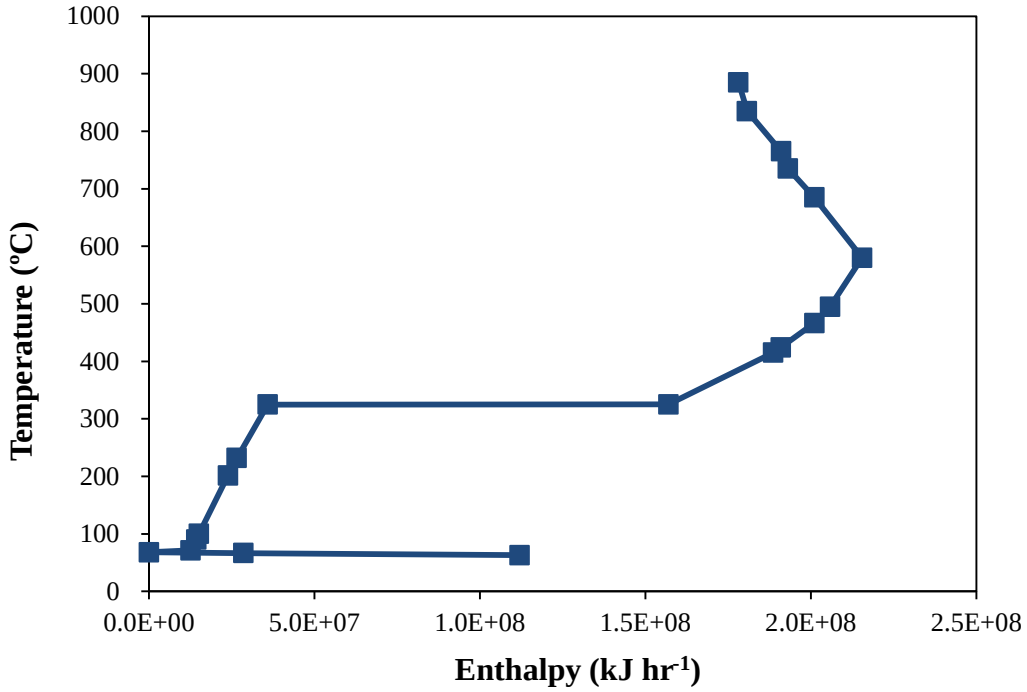

Figure 3.3 Grand composite curves of the L-IGFC with WGC.

3.3.2 Atmospheric L-IGFC Plant with DGC

3.3.2.1 System Performance

An evolution of the L-IGFC power plant adopting the DGC process, which operates at higher temperature, is shown in Figure 3.4. The configuration is rather simplified without requirement of complex heat exchangers for cooling the high temperature raw syngas before cleanup processes.

By using the same input data as described in Table 2.8 of Chapter 2, a system efficiency of 46.35% was calculated for L-IGFC power plant with DGC, which is about 6.87% points higher than the L-IGFC with conventional WGC unit. The electrical powers produced from the L-IGFC with DGC are: 1197.58 kW by syngas expander, 8966.13 by SOFC, and 12,929.92 kW by steam turbines. The net internal energy consumption is 2948.66 kW, where the largest energy is consumed by ASU. Thus the

net electrical power output is 20,144.97 kW. This proposed system reduces the complexity by avoiding heavy system integration implemented in most of current design of IGFC power plants.

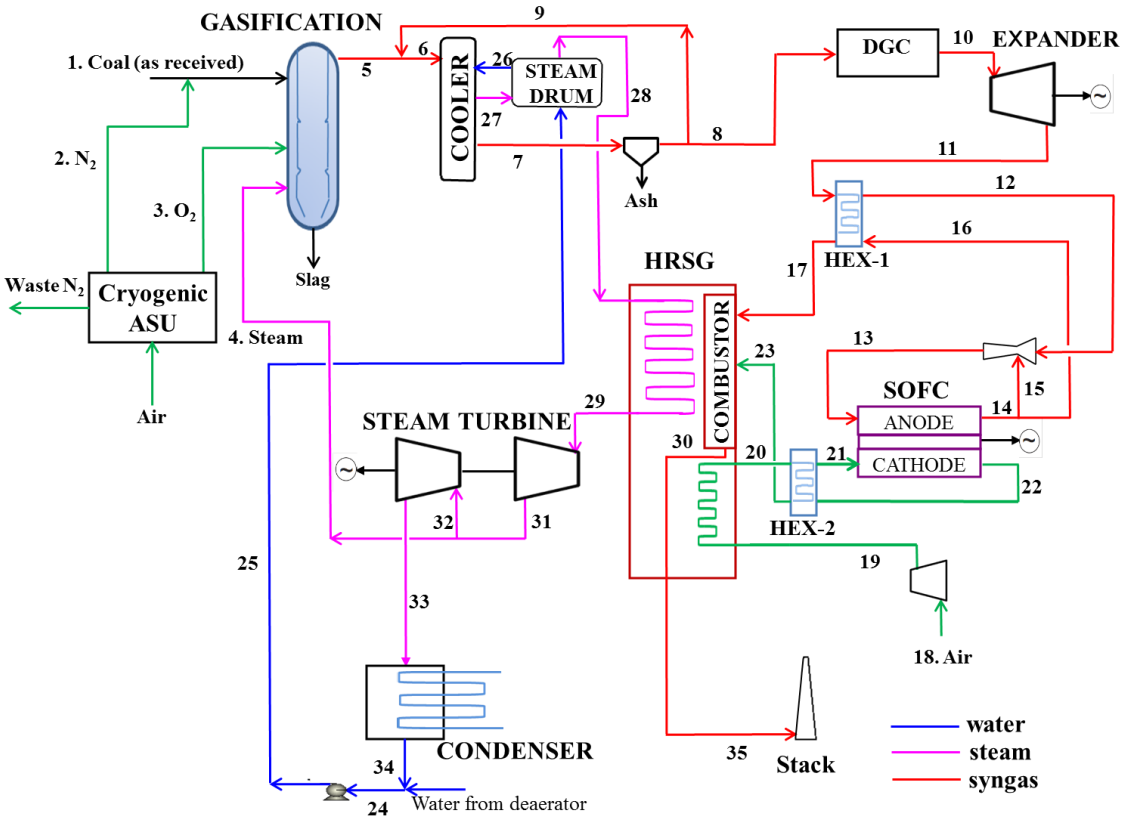

Figure 3.4 Flow diagram of the proposed L-IGFC power plant with DGC.

For a better description of L-IGFC plants with DGC unit, the characteristics of the main stream are shown in Table 3.7. It can be seen that the system maintains high temperature raw syngas without necessity of complex heat exchanger prior entering to the gas cleanup unit. The DGC that can work at high temperatures and minimum energy usage during the cleanup processes is generally beneficial to the L-IGFC system performance. From the simulation results, it can be observed that the output thermal

energy of the combustion unit (stream 30) is used only to generate high quality steam for steam turbine application by avoiding the heating process for the low temperature gas necessary in WGC-based system.

Table 3.7. Stream properties for the L-IGFC power plant with DGC.

point	T	P	Z	Molar composition (%)							
	(°C)	(bar)	(kg/h)	H_2	O_2	N_2	H_2O	CO	CO_2	H_2S	CH_4
1	25	1.013	5986	Coal as received, see Table 2.1 Chapter 2							
2	710.5	40	526	0	0	100	0	0	0	0	0
3	664.4	40	5722	0	99	1	0	0	0	0	0
4	440	40	571	0	0	0	100	0	0	0	0
5	1500	40	12398.68	21.3	0	4	15.2	49	9.6	0.9	0
6	900	40	30402.99	21.3	0	4	15.2	49	9.6	0.9	0
7	459.9	40	30402.99	21.3	0	4	15.2	49	9.6	0.9	0
8	459.9	40	12224.55	21.3	0	4	15.2	49	9.6	0.9	0
9	459.9	40	18004.31	21.3	0	4	15.2	49	9.6	0.9	0
10	459.9	40	12047.31	21.5	0	4	15.3	49.5	9.7	0	0
11	211.4	3.28	12047.31	21.5	0	4	15.3	49.5	9.7	0	0
12	532.7	3.28	12047.31	21.5	0	4	15.3	49.5	9.7	0	0
13	750.0	1.09	39571.71	11.7	0	4	25.1	24.1	35.1	0	0
14	850.0	1.09	44444.39	5.7	0	4	31.1	8.6	50.6	0	0
15	850.0	1.09	27524.40	5.7	0	4	31.1	8.6	50.6	0	0
16	850.0	1.09	16919.98	5.7	0	4	31.1	8.6	50.6	0	0
17	620.0	1.09	16919.98	5.7	0	4	31.1	8.6	50.6	0	0
18	25	1.013	69734.0	0	21	79	0	0	0	0	0
19	34.2	1.09	69734.0	0	21	79	0	0	0	0	0
20	400	1.09	69734.0	0	21	79	0	0	0	0	0
21	750	1.09	69734.0	0	21	79	0	0	0	0	0
22	850	1.09	64861.33	0	15.7	84.3	0	0	0	0	0
23	481.5	1.09	64861.33	0	15.7	84.3	0	0	0	0	0

24	77.20	1.20	55000	0	0	0	100	0	0	0	0
25	79.30	100	55000	0	0	0	100	0	0	0	0
26	309.9	100	55000	0	0	0	100	0	0	0	0
27	309.9	100	55000	0	0	0	100	0	0	0	0
28	309.9	100	55000	0	0	0	100	0	0	0	0
29	565	100	55000	0	0	0	100	0	0	0	0
30	726.2	1.09	81781.30	0	11.5	69.9	7.1	0	11.5	0	0
31	440	40	55000	0	0	0	100	0	0	0	0
32	440	40	54429	0	0	0	100	0	0	0	0
33	82.90	0.4	54429	0	0	0	100	0	0	0	0
34	77.80	1.20	54429	0	0	0	100	0	0	0	0
35	41.1	1.09	81781.30	0	11.5	69.9	7.1	0	11.5	0	0

3.3.2.2 Effect of SOFC Performance on the System

The L-IGFC plant is designed on the basis of the SOFC module, thus the SOFC design or operation parameter will influence significantly the performance of the overall system. The contribution of each polarization term on cell voltage loss at standard operating condition is shown in Figure 3.5. The SOFC under investigation is dramatically affected by the ohmic polarization. It can be seen that the ohmic polarization is much higher than the other losses. Contributions of electrolyte, electrodes, and interconnect resistance to the ohmic polarization are 11.78%, 62.33% and 25.89%, respectively. Such polarization depends on the temperature in the solid components (anode, cathode, electrolyte, and interconnection). In fact, the higher the cell operating temperature, the lower the resistivity of the components. It is also found that the activation polarization increases steeply at low current density and gradually at high current density. Meanwhile, the magnitude of the concentration polarization is much lower than the others polarizations. It should be noted that the concentration

polarization curve exhibits a concave curvature at high current density. Whether a concave curvature is observed at high current density (in the cell voltage-current density line) or not, depends on the magnitude of the ohmic and activation polarizations. Therefore, it is apparent that, the lower current density is beneficial for the SOFC to increase the cell voltage, i.e. the cell efficiency, while it results in the larger cell area leading to the higher manufacturing cost. This trade-off between efficiency and output power density cannot be avoided in SOFC. Consequently, the ways to increase the cell efficiency are to decrease the ohmic polarization and activation polarization in order to realize a higher output density at a given cell voltage.

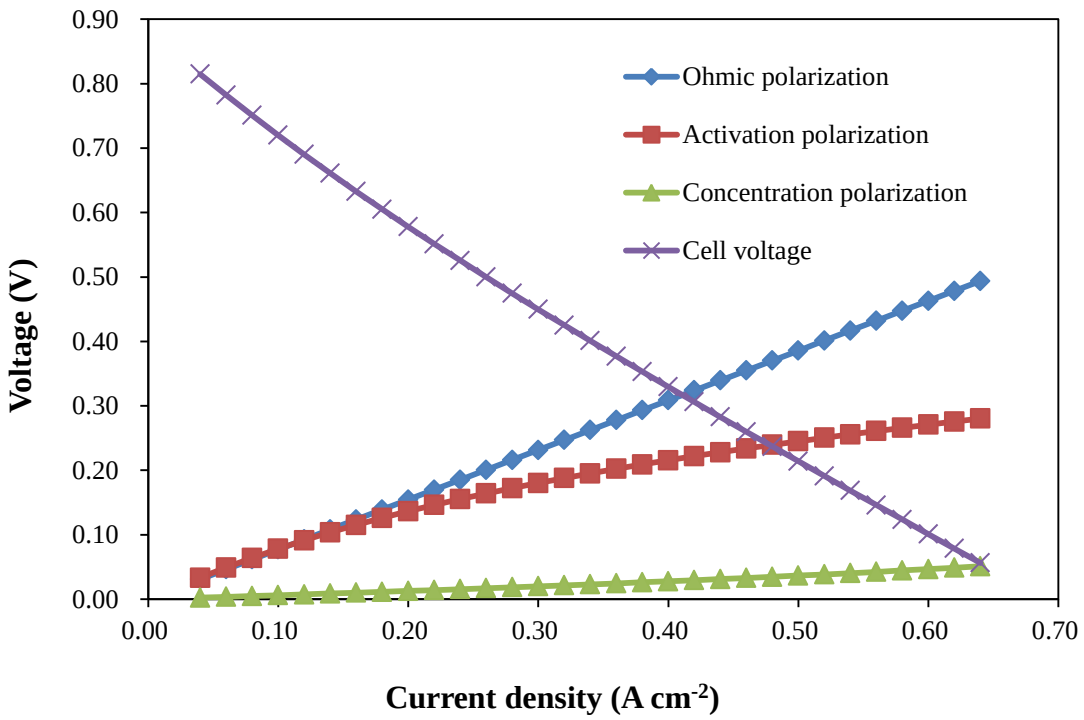

Figure 3.5 SOFC cell voltage and polarizations characteristics vs current density of L-IGFC with DGC.

Another observation is the influence of SOFC's fuel utilization factor on the system performance of L-IGFC plant, which is shown in Figure 3.6. In whole analysis for SOFC module in this research work, the fresh clean syngas is fed to the SOFC module being mixed with the recycled anode gas containing the electrochemical reaction products in the ejector block (as described in the Chapter 2). This recycle ratio of anode is defined as the fraction of the anode outlet molar flow that is recirculated back to the ejector block, that is always be less than or equal to 1. Operating SOFC in different fuel utilization contributes to different values of the recycle ratio due to fixed $\Delta T = 100$ °C for outlet and inlet of SOFC and change slightly the syngas composition in the inlet of anode providing different Nernst voltage.

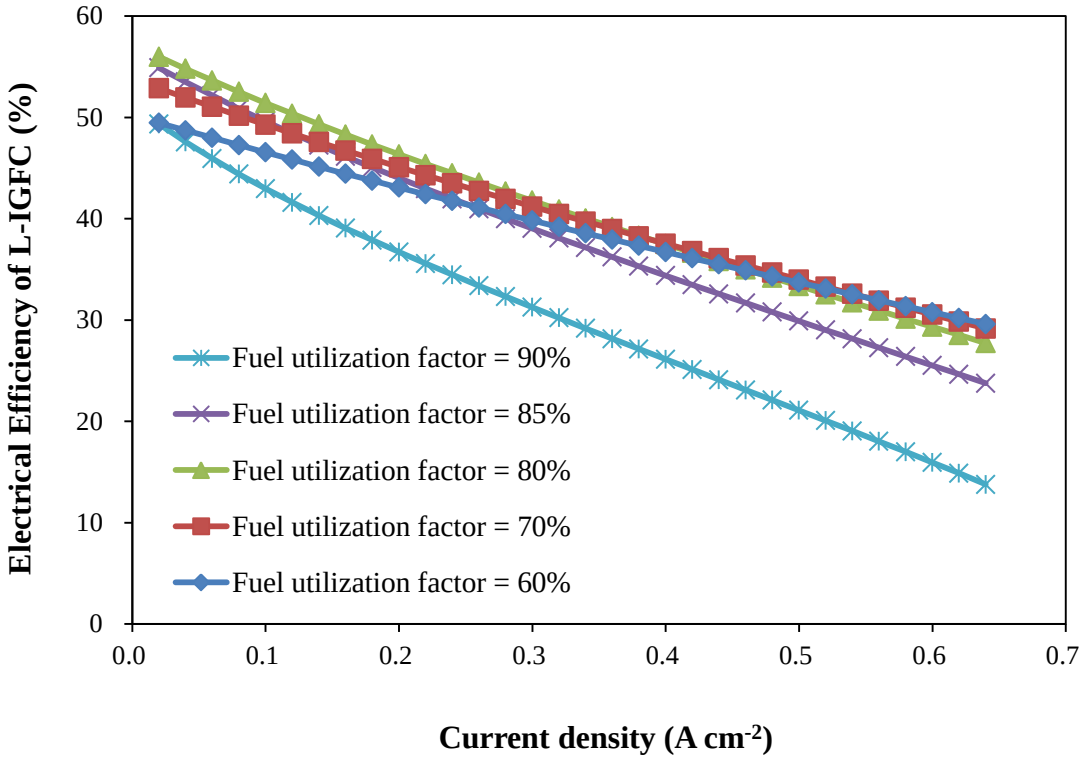

Figure 3.6. Effect of fuel utilization on total electrical system efficiency of L-IGFC with DGC.

Increasing the fuel utilization factor, while the input fuel flow rate remain fixed, means that more chemical energy is being converted into electrical energy, thus can lead to the increased efficiency of the overall system. As we observed, increase in the fuel utilization factor is beneficial at lower current density while it may result in lower efficiency at higher output density. Although fuel cell efficiency continuously increases with increasing fuel utilization factor, however it should remain below 90% to avoid risk of fuel depletion in the fuel cell [7]. Meanwhile, in lower fuel utilization factor, fuel is converted mainly in the combustor unit producing high temperature for HRSG inlet unit. For comparison, with the same input parameters of the system for different fuel utilization factors, the output stream from combustor to HRSG have temperatures of 1033 °C, 864 °C, 726 °C, 666 °C, and 611°C at fuel utilization factor of 60%, 70%, 80%, 85%, and 90%, respectively. Those high temperature cold increases the system efficiency by increasing the steam temperature and steam mass flow rate for steam turbine. However, due to material temperature limit on HRSG, the fuel utilization factor of 80% was confirmed as the best performance among the studied conditions due to high efficiency of the SOFC and at the same time it provides sufficient thermal energy to generate high quality of steam to drive steam turbine to produce electricity.

3.3.2.3 Pinch Points and Utility

The L-IGFC plant configured with DGC unit has the simple layout compared to the plant design adopted WGC unit for syngas clean-up process. The changes in temperature conditions and mass flow of the process streams have an effect in the behavior of the composite curve. However, in this design, the composite curve obtained at ΔT_{min} equal to 30 ºC, as shown in Figure 3.7. The pinch points takes place at

82.9 ºC for the hot fluids and 52.9 ºC for the cold fluids, as also the same points appeared at L-IGFC with WGC plant.

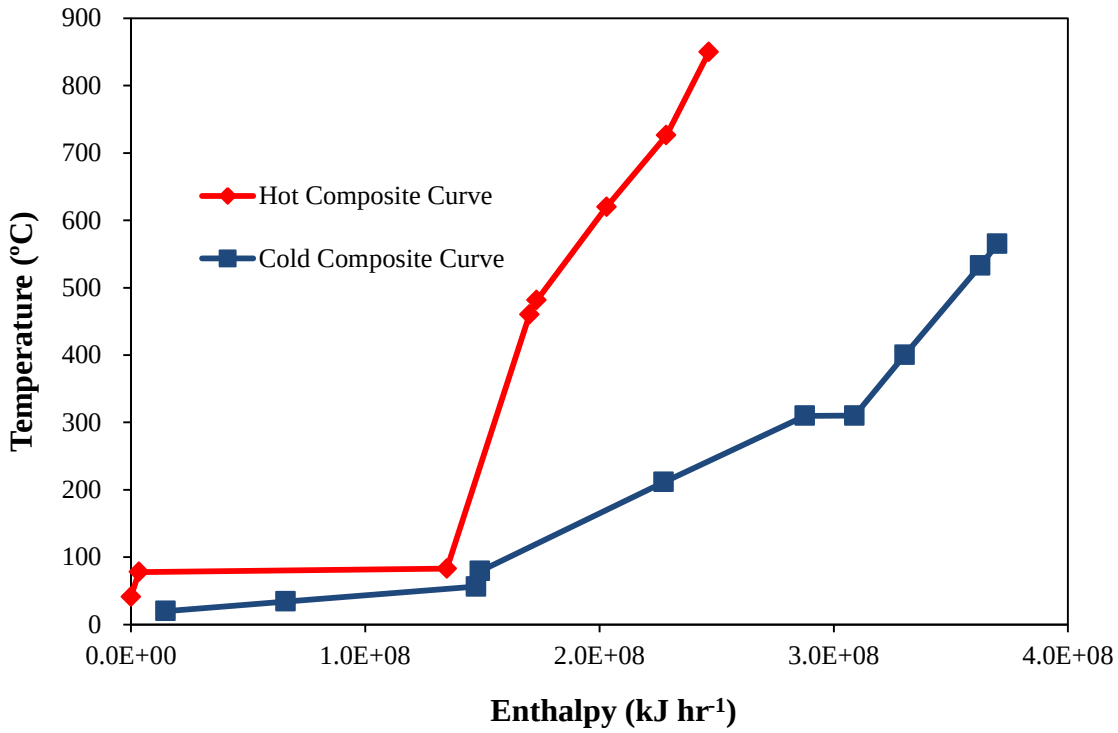

Figure 3.7 Composite curves of the L-IGFC with DGC.

3.4 Pressurized L-IGFC Plant with DGC

The SOFC technology has demonstrated its potential to produce power at high efficiencies with very low levels of emissions. The SOFC performance is estimated to improve with increase in working pressure as Nernst voltage increases with pressure. In this section, the performances of L-IGFC system configured with pressurized SOFC are discussed. The layout of the pressurized L-IGFC power plant system is quite similar to the atmospheric L-IGFC system, which are described in section 3.3. However, in order to utilize waste heat efficiently, two heat exchangers and one gas expander after HRSG

were added to the pressurized L-IGFC system as shown in Figure 3.8.

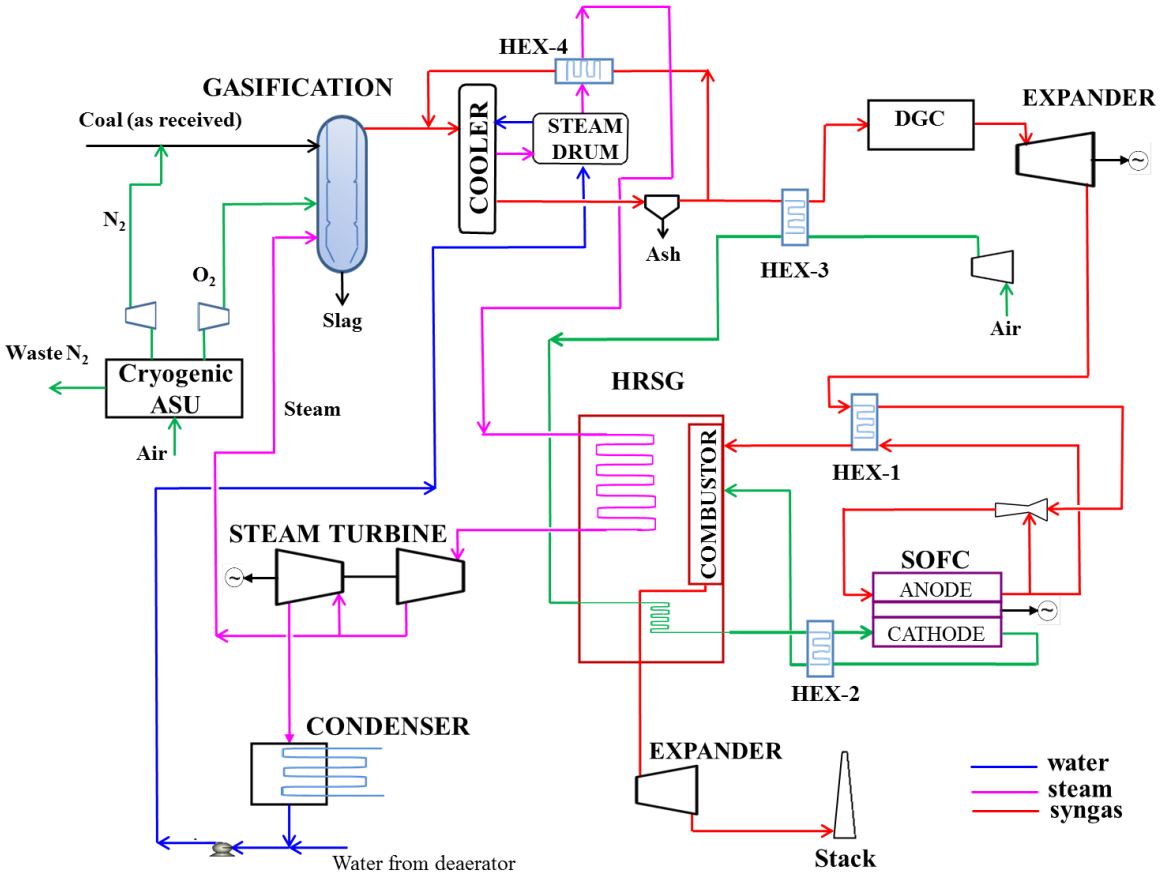

Figure 3.8. Flow diagram of the pressurized L-IGFC power plant with DGC.

The effect of the SOFC working pressure on the system efficiency at different current density and constant temperature is shown in Figure 3.9. It can be seen that the system efficiency is considerably improved when increasing the SOFC working pressure from 2.027 bar (2 atm) to 4.053 bar (4 atm). The increased pressure increases the partial pressure of H_2 in the fuel channel and O_2 in the air channel, and thus increases the exchange current density resulting in decreased activation polarization. Furthermore, the transport of gases to the electrolyte-electrode interfaces is improved,

thereby reducing the concentration polarization. These factors lead to the improvement of SOFC performance.

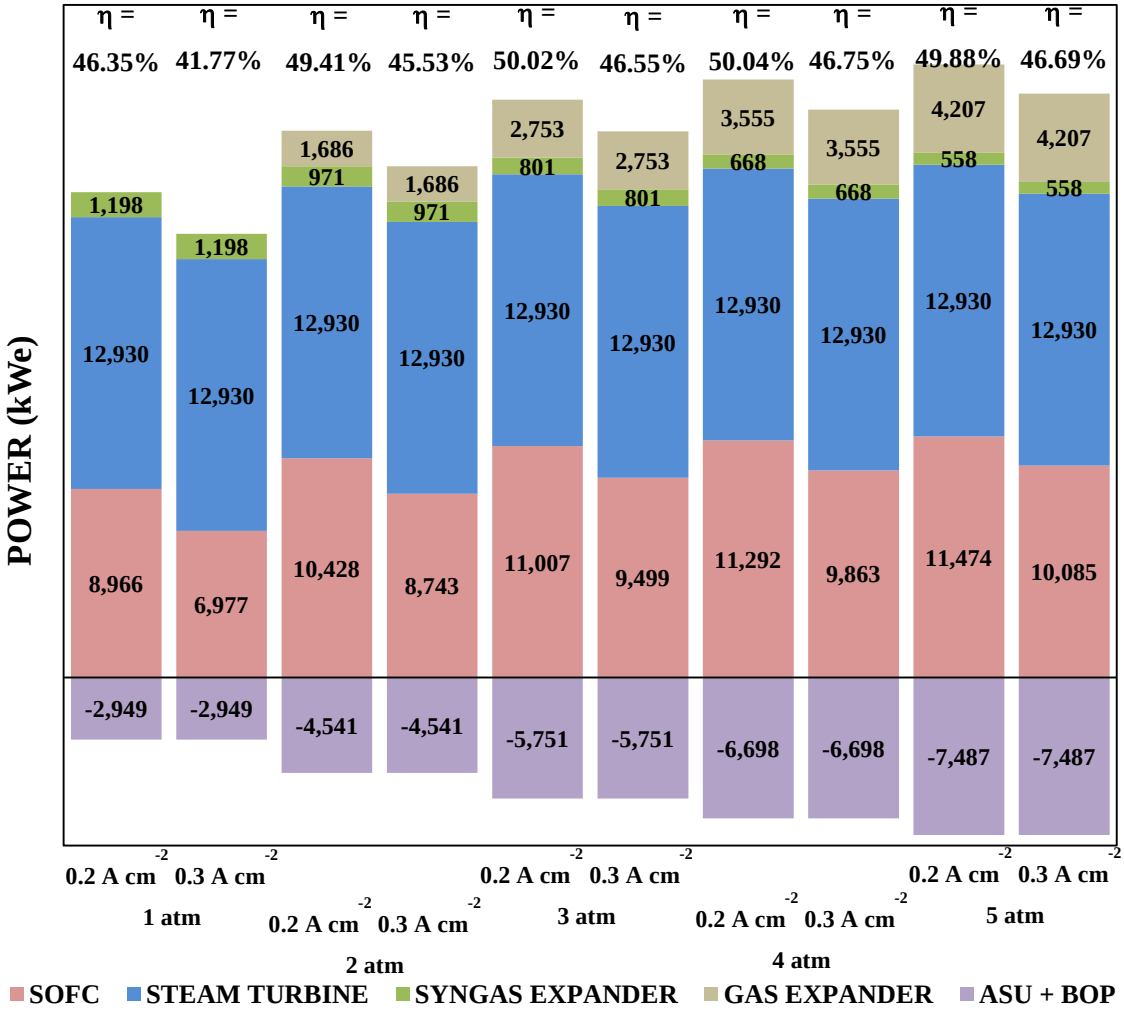

Figure 3.9. Effect of SOFC working pressure on total electrical system efficiency (η) of L-IGFC with DGC.

However, it is found that the L-IGFC efficiency decreases when the working pressure SOFC is higher than 4 atm. This is caused by that the air compressor consumes more power at the high pressure operation, while the power produced by the syngas

expander slightly decreases. As a result, the pressurized L-IGFC system with DGC gives the maximum electrical efficiency of 50.04% when operated at SOFC working pressure of 4.053 bar and current density of 0.2 A cm^{-2}.

3.4.1 Pinch Points and Utility

The L-IGFC plant design operated at SOFC working pressure of 4 atm has the pinch points at 82.9 ºC for the hot fluids and 52.9 ºC for the cold fluids with overall ΔT_{min} equal to 30 ºC as shown in Figure 3.10.

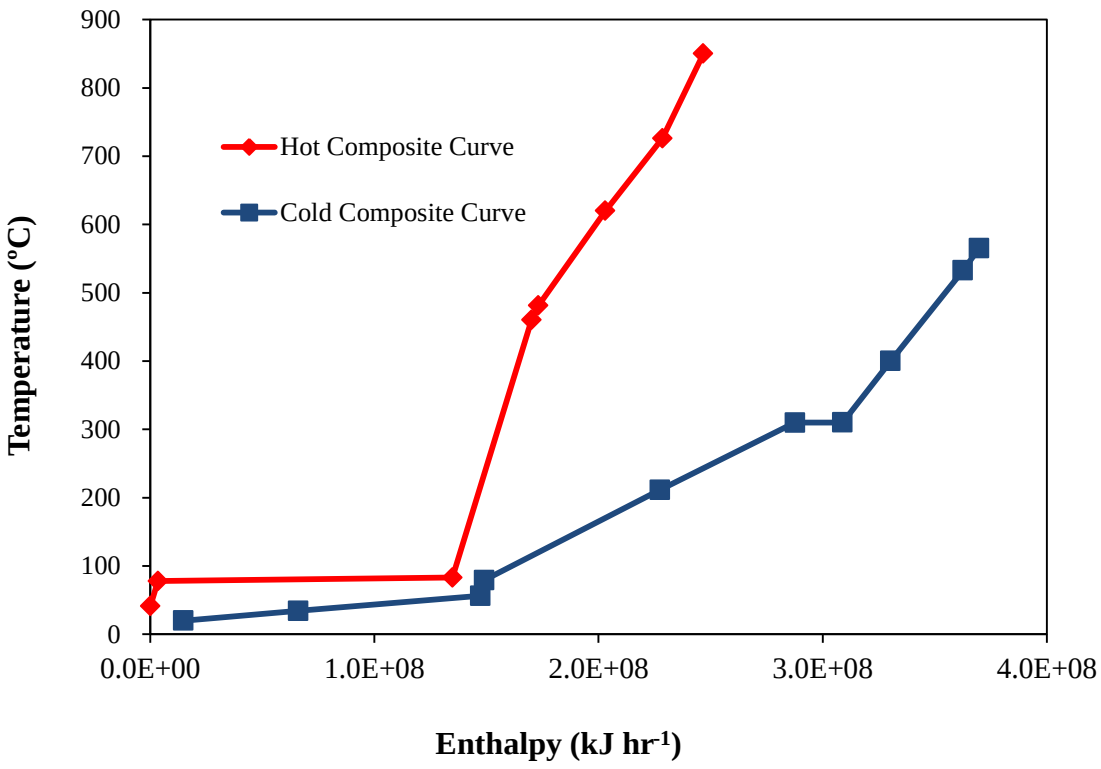

Figure 3.10 Composite curves of the L-IGFC with DGC.

The pinch point, whereas the closest approximation between hot composite curve and cold composite curve, divides the curve in 2 different zones. These zones are;

(i) temperature `above the pinch`, where there is a deficit of thermal load and the service required is only hot utility, and (ii) temperature `below the pinch`, where there is an excess of thermal load and the service required is only cold utility. From all of the L-IGFC designs analyzed as also shown in the previous section, it shown that those design did not transfer heat across the pinch.

3.4.2 Effect of Coal Moisture Content on the System

The effect of various coal properties such as mineral matter, moisture, fixed carbon, and calorific value can impact the gasification process and plant efficiency. Some important properties of coal in relation to the gasification process are (1) coal type; (2) proximate analysis – determination of moisture, ash, volatile matter, and fixed carbon; (3) ultimate or elementary analysis – determination of the elemental composition of the coal; and (4) calorific value or heat content.

Coal moisture content influences latent and sensible heat losses which can impact significantly on efficiency of the power plant. A high amount of moisture in coal is undesirable for a number of reasons such as it increases the stickiness of coal, resulting in blocked chutes and hang-ups in bunkers; it adds to storage and transportation costs, and increased moisture content reduces calorific values and also causes the decrease of ignition characteristics [8].

Apart from efficiency reduction, high moisture increases coal handling feed rate, demands more auxiliary power for coal-handling systems and pulverizes, and leads to higher plant operating and maintenance costs [9]. Therefore, a unit of coal dryer has been added to the L-IGFC plant design as illustrated in Figure 3.11. The coal feeders provide coal to the coal dryer unit where the coal is pulverized and dried to reduce its

moisture content by the use of high temperature nitrogen. In this section, 2 different coal moisture contents will be used for L-IGFC power plant configured with pressurized SOFC. The plant fed with the coal contains moisture around 11.12 wt.% (as received) is denoted as a baseline plant (BP), whereas the plant with a coal drying unit to reduce the moisture content from the coal prior to entering the gasifier denoted as an improved plant (IP).

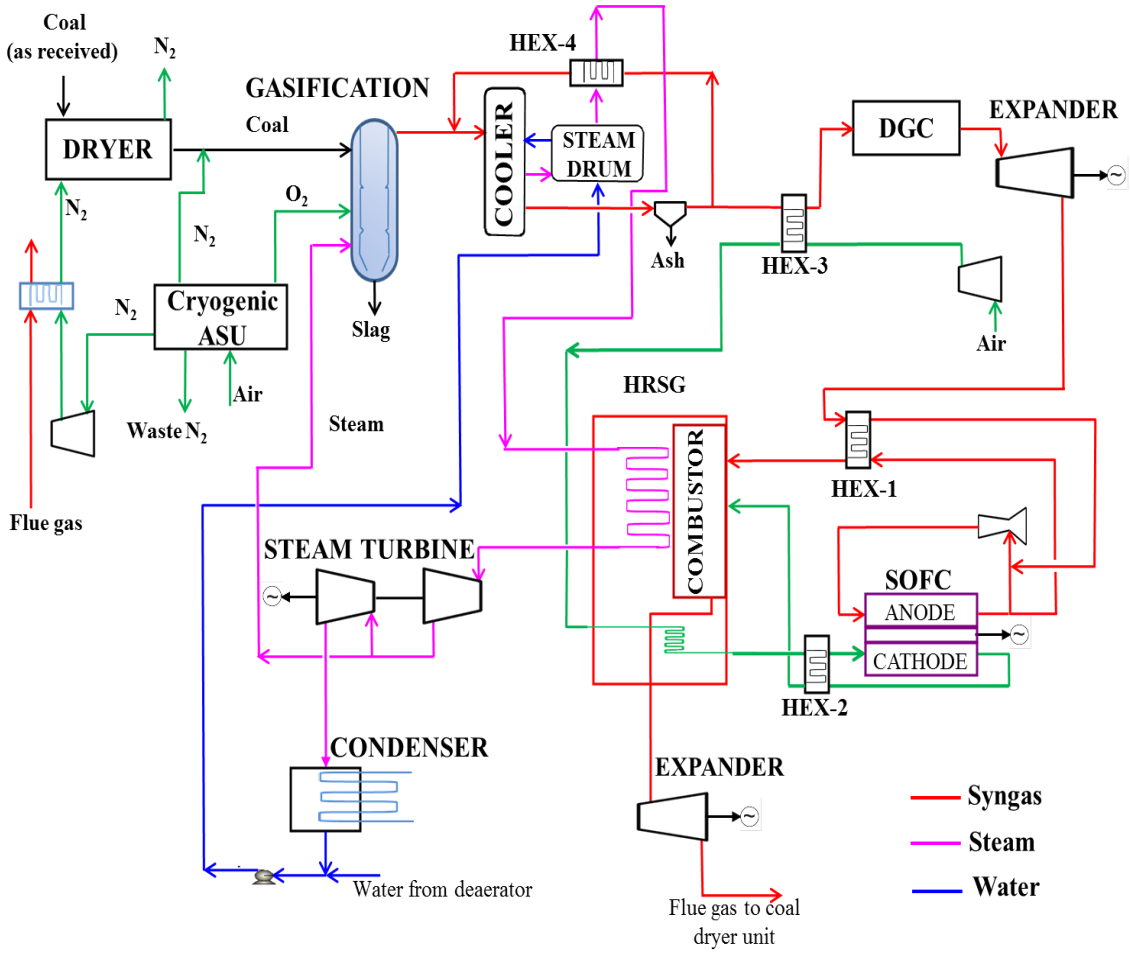

Figure 3.11 Flow diagram of the pressurized L-IGFC power plant with a coal dryer as coal dried plant (IP) design.

The effect of coal moisture content on unit performance is presented in Figure 3.12. The electrical power output produced by syngas expander ($W_{SE\text{-}BP}$), SOFC ($W_{SOFC\text{-}BP}$) at 3 atm, steam turbine ($W_{ST\text{-}BP}$), and gas expander ($W_{GE\text{-}BP}$) are 0.80 MW, 11.01 MW, 12.93MW, and 2.75 MW, respectively. The net internal energy consumption ($E_{int,consumed}$) by ASU, pumps, air blower, and auxiliaries is 5.75 MW. Thus the net electrical power output is 21.74 MW with electrical efficiency of the L-IGFC plant is 50.02% in lower heating value (LHV).

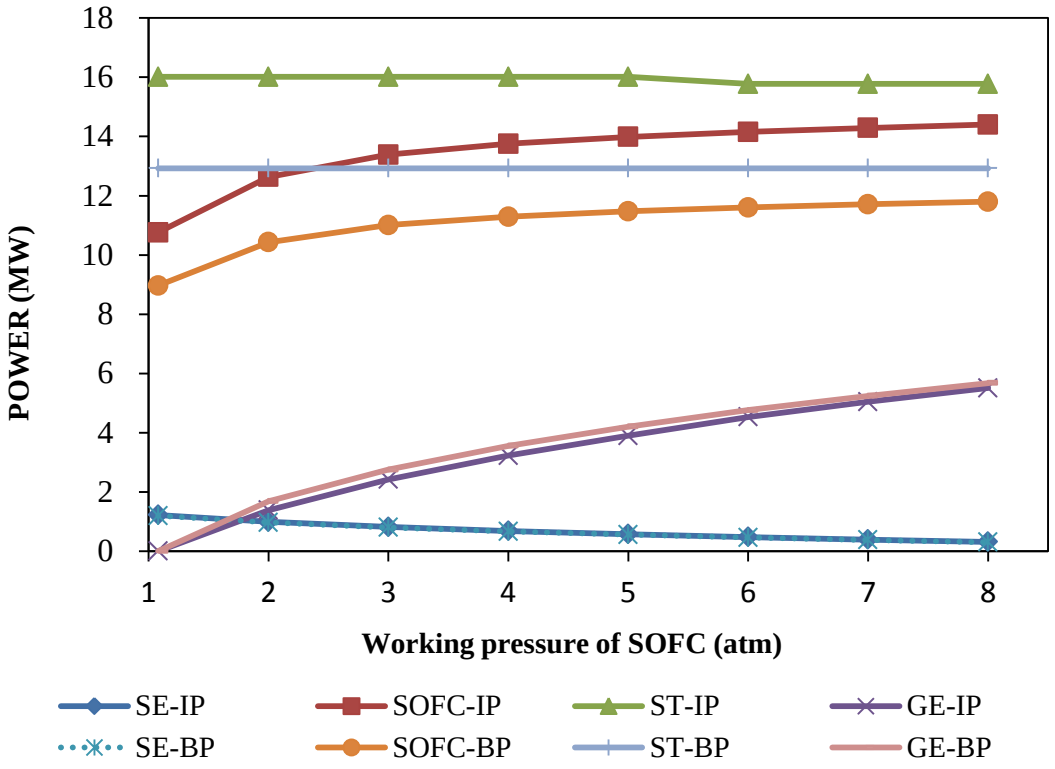

Figure 3.12 Effect of coal moisture content on unit producing power.

(The working temperature SOFC = 800 °C and i = 0.2 A cm^{-2}).

Reducing moisture content of fed coal to 2 wt.% leads to increase the equivalent hydrogen ($jH_{2,equivalent}$) contained in the raw syngas, hence increasing the

performance of SOFC. In this case, the raw syngas composition leaving the gasifier is 44.82 ppm CH_4, 24.29% H_2, 57.55% CO, 5.25% CO_2, 8.04% H_2O, 3.89% N_2, 0.92% H_2S, 489.41 ppm Cl_2, 28.68 ppm NH_3. As for comparisons with BP design, the electrical powers produced by IP design are: 0.82 MW by syngas expander ($W_{SE\text{-}IP}$), 13.38 MW by SOFC ($W_{SOFC\text{-}IP}$) at 3 atm, 16.01 MW by steam turbine ($W_{ST\text{-}IP}$), and 2.42 MW by gas expander ($W_{GE\text{-}IP}$). The net internal energy consumption is 6.51 MW. The net electrical power output is 26.13 MW with electrical efficiency of 60.12% in LHV.

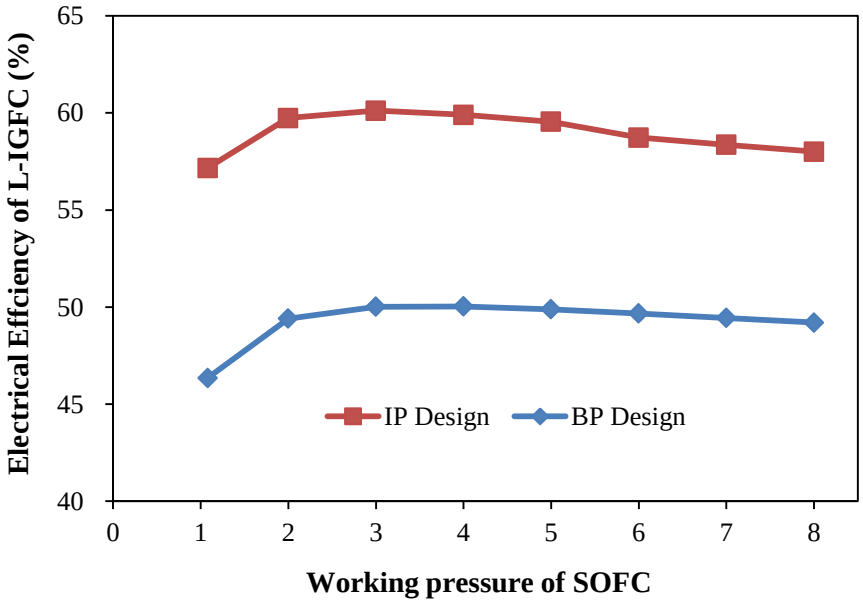

Figure 3.13 Effect of coal moisture content on total electrical plants efficiency. (The working temperature SOFC is 800 °C with i = 0.2 A cm^{-2}).

As coal moisture content decreases, its heating value increases and by assuming constant electric power output of a power plant, less coal needs to be fired. However, having the same quantity of coal fed to the gasifier of L-IGFC plant, this heat rate improvement used to increase the steam turbine power output by increasing the

steam mass flow rate from 55,000 kg hr^{-1} (BP design) to 68,000 kg hr^{-1} (IP design) of L-IGF plant. Therefore, an improved performance of the L-IGFC plant can be realized by a reduction in coal moisture content to 2 wt.% as shown in Figure 3.13.

The effect of the SOFC working pressure on the electrical system efficiency (η) at different current density and constant temperature is shown in Figure 3.14. It can be seen that the system efficiency is considerably improved when increasing the SOFC working pressure from 2 atm to 4 atm. However, it is found that the L-IGFC efficiency decreases when the working pressure SOFC is higher than 4 atm.

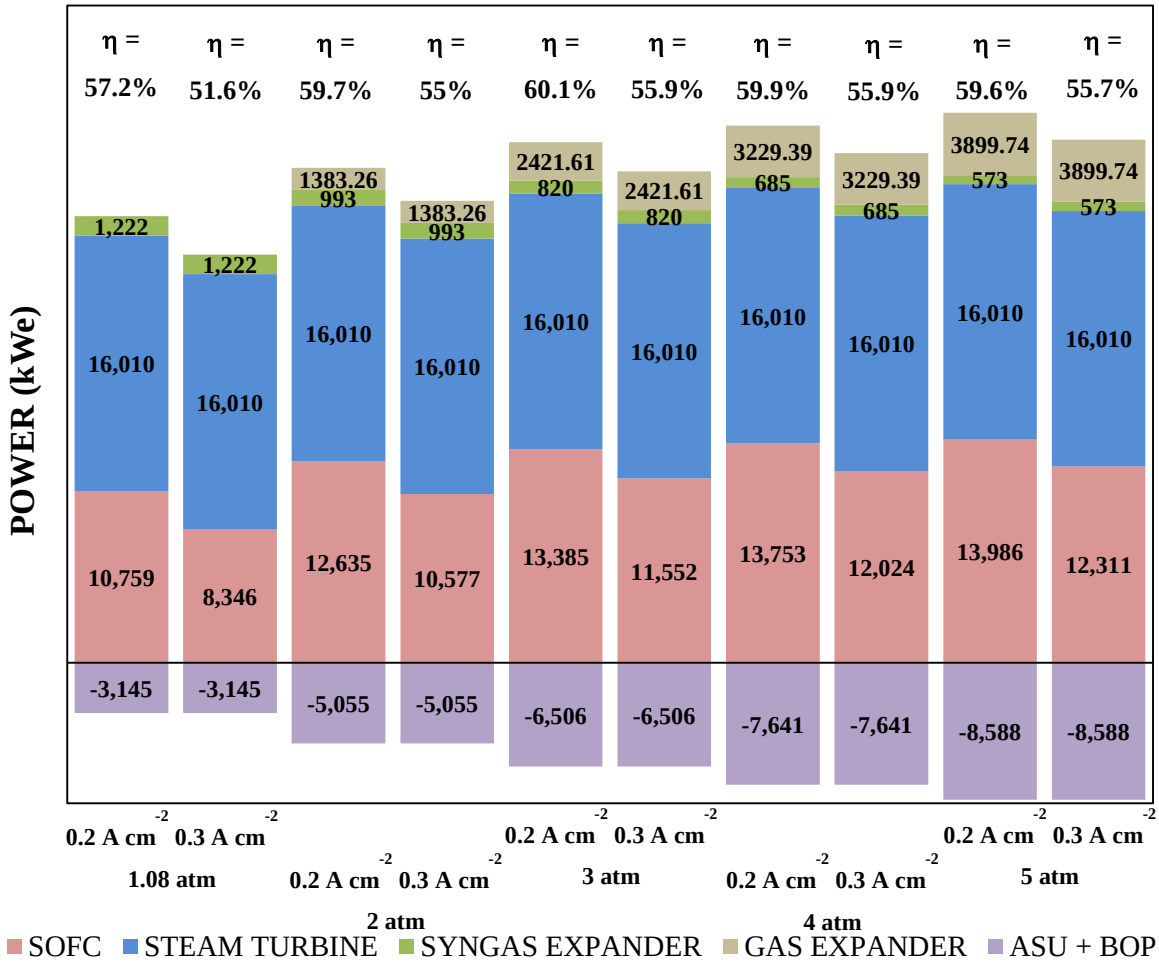

Figure 3.14 Effect of SOFC working pressure on total electrical system efficiency (η) of IP Design.

3.5 Options to Improve L-IGFC System Performance

To increase the efficiency of L-IGFC plant, a higher SOFC working voltage is desirable because of: (i) higher working voltage means the SOFC module is more efficient; (ii) a larger portion of the chemical energy in the syngas fuel is converted into electric power and less is released as heat. The SOFC performance is estimated to improve with increase in working temperature and pressure of SOFC. Increasing the cell working temperature leads to the faster kinetics of elementary processes in the cell while lowers the Nernst voltage. The dependence of SOFC performance on temperature is illustrated in Figure 3.15. The sharp decrease in cell voltage at 800 °C as a function of current density is a manifestation of the high ohmic polarization at this temperature. The ohmic polarization decreases as the operating temperature increases to 1000 °C.

In whole analysis for SOFC module in this study, the fresh clean syngas is fed to the SOFC module being mixed with the recycled anode gas containing the electrochemical reaction products in the ejector block (as descrbed in the Chapter 2). This recycle ratio of anode is defined as the fraction of the anode outlet molar flow that is recirculated back to the ejector block, that is always be less than or equal to 1. Therefore, operating SOFC in different operating temperatures and pressures contribute to different values of the recycle ratio and in the end will change the syngas composition in the inlet of anode. The sensitivity analysis was adopted on this study to find the optimum efficiency for IP design as shown in Figure 3.16. It is found that, the maximum L-IGFC system electrical efficiency realized when SOFC operating condition are 850 °C and 3 atm. The electrical efficiency at this condition is 60.32% in LHV. In this case, the electrical power output produced by syngas expander (W_{SE}), SOFC (W_{SOFC}) at 3 atm, steam turbine (W_{ST}), and gas expander (W_{GE}) are 0.82 MW, 13.48

MW, 16.01 MW, and 2.41 MW, respectively. The net internal energy consumption ($E_{int,consumed}$) by ASU, pumps, air blower, and auxiliaries is 6.51 MW. Thus the net electrical power output is 26.22 MW.

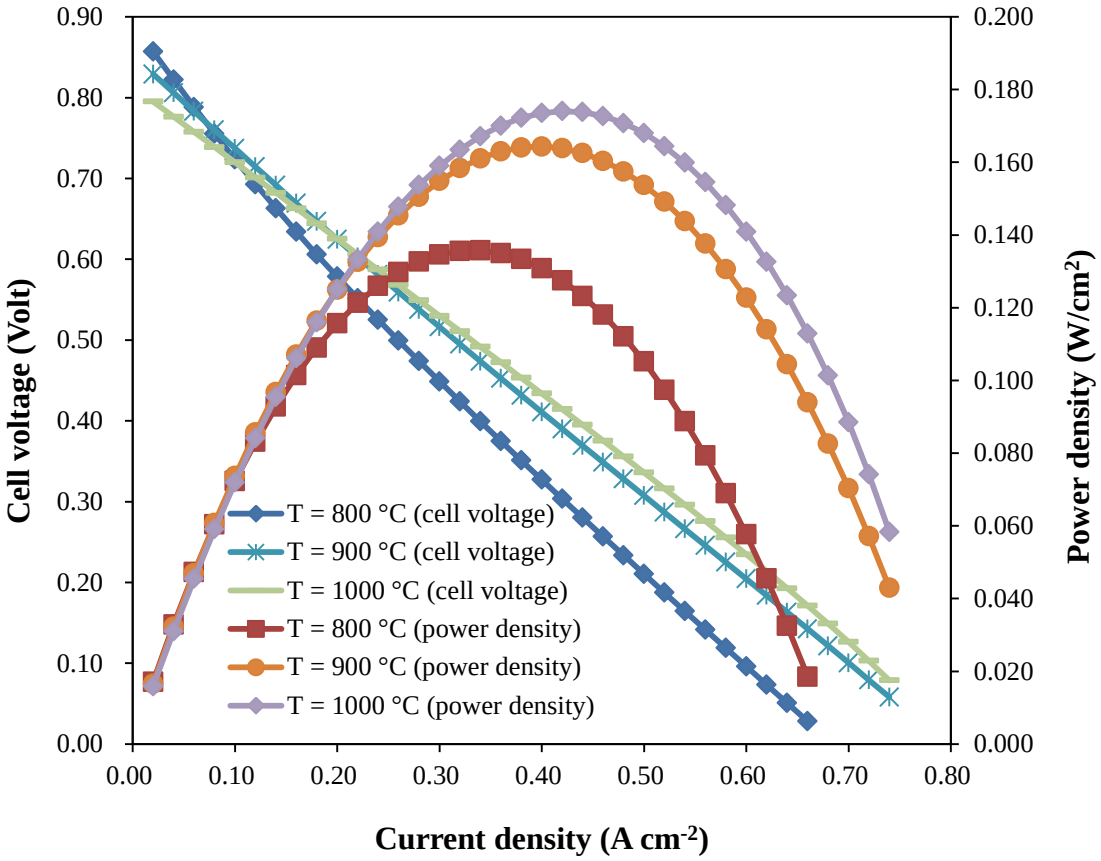

Figure 3.15 Effect of SOFC cell temperature on cell voltage and cell power at current density. (The working pressure SOFC = 1.08 atm, IP design).

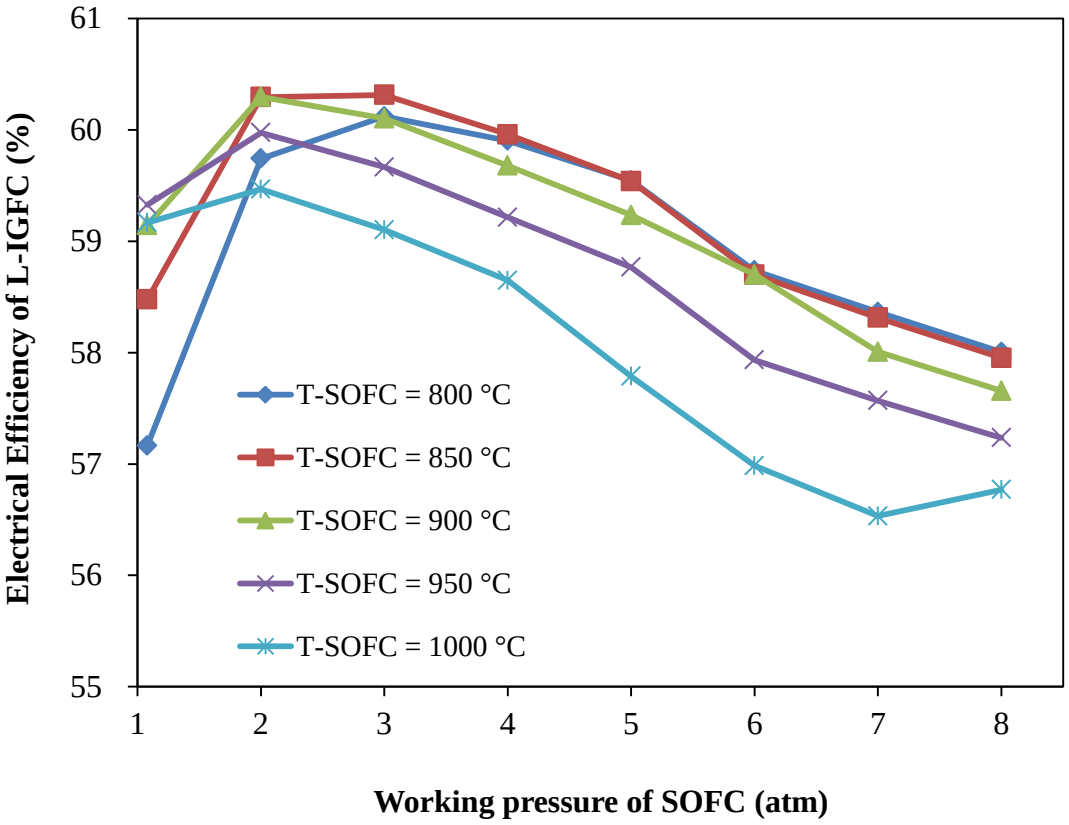

Figure 3.16. Effect of SOFC working temperature and pressure on efficiency of the plant. (SOFC current density = i = 0.2 A cm^{-2}, IP design).

REFERENCES

[57]. Kivisaari T, Bjornbom P, Sylwan C, Jacquinot, Jansen D, de Groot A. The feasibility of a coal gasifier combined with a high-temperature fuel cell. Chem Eng J 2004;100:167-180.

[58]. Zhang W, Croiset E, Douglas PL, Fowler MW, Entchev E. Simulation of a tubular solid oxide fuel cell stack using AspenPlus™ unit operation models. Energy Conv Manag 2005;46:181-196.

[59]. Doherty W, Reynolds A, Kennedy D. Computer simulation of a biomass gasification-solid oxide fuel cell power system using Aspen Plus. Energy 2010;35:4545-4555.

[60]. EG&G Technical Services. Fuel cell handbook. US Department of Energy; 2004.

[61]. Bodo Linnhoff. Introduction to Pinch Analysis. In: Boehm RF, ed. Developments in the design of thermal system. Cambridge University Press, USA; 1997. Pp. 122-137.

[62]. Geldermann J, Treitz M, Rentz O. Integrated technique assessment based on the pinch analysis approach for the design of production networks. Eur J Oper Res 2006; 171:1020-1032.

[63]. Tarroja B, Mueller F, Maclay J, Brouwer J. Parametric thermodynamic analysis of a solid oxide fuel cell gas turbine system design space. ASME J Eng Gas Turbines Power 2010;132:1-11.

[64]. Nikolele A. Investigations into the reduction of moisture in fine coal by plant tests with surfactants. J S A Inst Min Metall 2004: 171-176.

[65]. Burnard K, Bhattacharya. Power generation from coal: Ongoing developments and outlook. IEA information paper. International Energy Agency, Paris, France. https://www.iea.org/publications/freepublications/publication/Power_Generation_from_Coal2011.pdf_

CHAPTER 4

TECHNO-ECONOMIC ANALYSIS OF L-IGFC PLANT

Widespread utilization of any power generation technology depends on its economic viability in addition to its technical benefits. The demonstration of a new power plant's competitive position compared to other potential energy system technologies is essential to attract market attention. In this regard, a techno-economic comparative study was performed to highlight the economic feasibility as well as the advantages/disadvantages of the L-IGFC plant to other competing energy conversion systems. One important of this chapter is to provide a brief description of steps in order to perform the techno-economic evaluation of the selected energy conversion system.

4.1 Cost Estimating Methodology

A Complete analysis of any electricity generating system is carried out by an evaluation of current and future projected costs as well as its performance characteristics. Techno-economic assessments play an important role in determining the competitiveness of a selected technology against existing or reference technologies by evaluate the CAPEX and OPEX in addition to the technical indicators. Such assessments are crucial to investigate whether and under what circumstances investment in the selected technology is economically viable. Estimations of capital costs, operation and maintenance (O&M) costs, and fuel costs are necessary to calculate the cost of electricity (COE).

Economic assessments are not definite and rely on the underlying assumptions as well as on the choice of selected parameters. There are significant differences in the

cost estimating methods and basis of the calculations employed by various researchers performing economic assessments of fossil-fuel power plant with and without CO_2 capture [1]. These inconsistencies complicate a fair comparison between the COEs for different fossil-fuel power plants from various publishing sources. However, a cost comparison between different alternative systems based on the sort of assumptions and methodology is valid even in the presence of uncertainty in absolute costs of the plant's components [2].

Various publicity available reports by different researchers presented their approaches for cost estimation of power plants [2-6]. Amongst these reports, two publicly available reports have been initially selected as sources for equipment cost data and reference cost estimating methodologies. These two reports are from the European Benchmarking Task Force (EBTF) under the EU-FP7 CAESAR project [6] and the National Energy Technology Laboratory (NETL) of the U.S. Department of Energy (DOE) [3,7]. Although these reports share many common features, the final cost estimating method selected for this work is based on the study provide by NETL report [7].

A set of assumptions has then been made in order to evaluate the economic indicators of the L-IGFC plant based on the methodology adopted from references [5,7]. The economic viability of the L-IGFC plant has been measured through the cost of electricity. This cost indicator is a standard metric used in the assessment of project economics, which represents the revenue per unit of electricity that must be met to reach breakeven over the lifetime of a plant. In other words, it is the selling price of electricity that generates a zero profit. Due to large uncertainties in the available cost data for some cost elements, they were excluded from the assessment. Hence, any labor incentives;

cost associated with plant`s decommissioning; costs associated with transmission networks, handling distribution network and administrations of supply; as well as all taxes (with the exception of property taxes) were excluded from the assessment.

4.2 Capital Costs

The following sections firstly present the method and equations used for overall capital costs assessment and then the equations used for costing any component/sub-system of the selected reference plant. The capital cost of L-IGFC plant platforms based on heat and material balances and the relative size of the different unit operations compared to state-of-the art IGCC systems that are fully designed and costed in the NETL report [3,7].

The capital cost level is illustrated in Figure 4.1, showing that there are four main levels, i.e. Bare Erected Cost (BEC), Total Plant Cost (TPC), Total Overnight Cost (TOC) and Total As-spent Capital (TASC). BEC, TPC and TOC are "overnight" costs and are expressed in "base-year" dollars. The base year is the first year of capital expenditure, which for this study is assumed to be 2007. TACS is expressed in mixed-year, current-year dollars over the entire capital expenditure period. The definitions of each level can be described as follows [3,7]:

- The BEC comprises the cost of process equipment, on-site facilities and infrastructure that support the plant (e.g., shops, offices, labs, road), and the direct and indirect labor required for its construction and/or installation.
- The TOC comprises the TPC plus owner`s costs. TOC is an "overnight" cost, expressed in base-year (2007) dollars and as such does not include escalating during construction or interest during construction. TOC is an overnight cost expressed in

base-year (2007) dollars.

- The TACS is the sum of all capital expenditures as they are incurred during the capital expenditure period including their escalation. TASC also includes interest during construction.

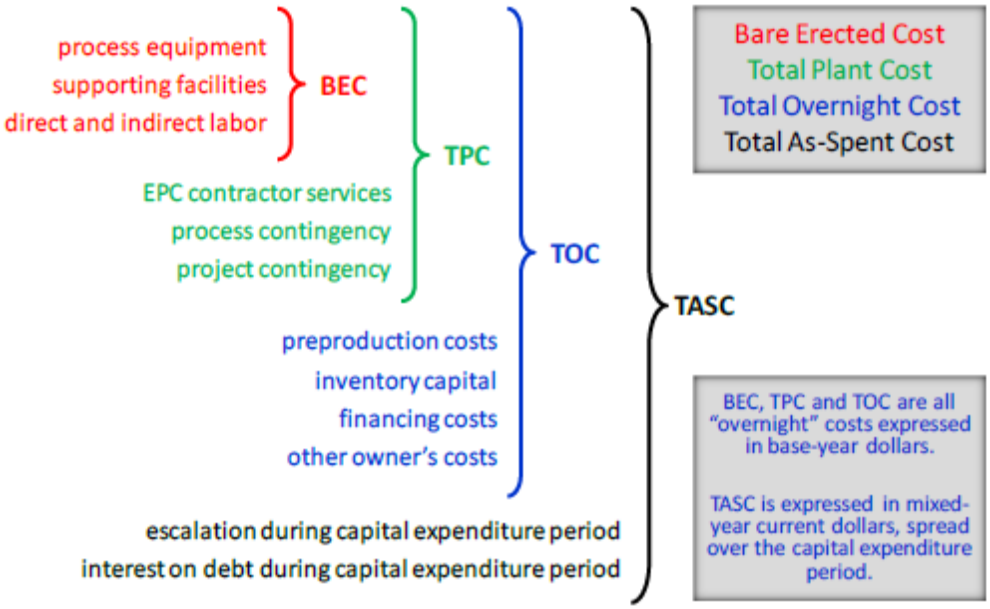

Figure 4.1 Capital cost levels and their elements [3].

The capital costs for plant components could be found in the open literature. However, these data could not be used unless they were made consistent by using correction of size and the reference year [2]. Generally, calculation of the equipment cost for a certain plant, based on utilization of the cost data for different component size, could be performed using the following equation [2,5]:

$$C_i = C_{i,ref}\left(\frac{S_i}{S_{i,ref}}\right)^f \quad \ldots (4.1)$$

where C_i is the cost of an advance component (sub-system), $C_{i,ref}$ is the known cost of a reference component (sub-system) of the same type and of the same order of magnitude, S_i is the scaling parameter, f is the reference cost scaling exponent. Each capital cost category uses a distinct scaling factor based on engineering expertise [3,7]. In this study, all cost data for the reference component (sub-system) of reference plant cases came from the reported data available done by NETL.

The scaling model to estimate the capital cost of component can be described as follows:

- Capital cost associated with coal handling, gasifier, and gas clean-up are scaled using efficiency and the scaling factor as [7]:

$$cost_{adv} = cost_{ref} * \left(\frac{eff_{ref}}{eff_{adv}}\right)^{f} \quad \ldots (4.2)$$

- The cost of the air separation unit (ASU) is scaled both on the efficiency and the oxygen use per ton of coal as [7]:

$$cost_{adv} = cost_{ref} * \left\{\left(\frac{eff_{ref}}{eff_{adv}}\right) * \left(\frac{oxygen_{adv}}{oxygen_{ref}}\right)\right\}^{f} \quad \ldots (4.3)$$

- The steam turbine and HRSG cost are scaled on the percent of power from steam cycle as [7]:

$$cost_{adv} = cost_{base} * \left(\frac{W_{steam\ turbine_{adv}}}{W_{steam\ turbine_{ref}}}\right)^{f} \quad \ldots (4.4)$$

- For the IGCC case, the cost item for gas turbine is scaled to "one minus the percent of power from steam" as shown as [7]:

$$cost_{adv} = cost_{ref} * \left\{\frac{(1-W_{steam\ turbine_{adv}})}{(1-W_{steam\ turbine_{ref}})}\right\}^{f} \quad \ldots (4.5)$$

- For the SOFC cases, the cost is equal to the SOFC`s target cost scaled to "one minus the percent of power from steam plus power from gas turbine" as follow:

$$\text{cost}_{adv} = cost\ of\ SOFC * \left\{1 - \left(W_{steam\ turbine_{adv}} + W_{gas\ turbine_{adv}}\right)\right\}^{f} \quad \ldots (4.6)$$

- For the air centrifugal compressor, the corresponding costs are determined on the basis of a cost function from reference [8], as follows:

$$cost_{comp} = 91562 \left(\frac{W_{comp_{adv}}}{445}\right)^{0.67} \quad \ldots (4.7)$$

- The cost for heat exchangers are calculated based on data provided by reference [9] which is \$1 per cm^2 of cross sectional area required, while for syngas expander are extracted from reference [10].

4.3 Operating and Maintenance Costs

The operations and maintenance (O&M) costs are the costs associated with operating and maintaining the power plants over their expected lifetimes. These costs

usually include [3]:

- Operating labor
- Maintenance (material and labor)
- Consumables
- Administrative and support labor
- Fuel
- Waste disposal
- Co-product or by-product credits (that is, a negative cost for any by-products sold).

Those costs are classified in two categories: the fixed O&M costs, which are independent of power generation, and variable O&M, which is proportional to power generation. The costs for variable O&M are scaled using efficiency as follows [7]:

$$cost_{adv} = cost_{ref} * \left(\frac{eff_{ref}}{eff_{adv}}\right) \quad \ldots (4.8)$$

The fixed O&M costs can be calculated as follows [7]:

$$cost_{ref} =$$
$$cost_{adv} * (1 - 10\%) + \left(1 - W_{steam\ turbine_{adv}}\right) * \text{annualized\_stack\_cost\_perkWh} \quad \ldots (4.9)$$

Another important cost measure for O&M cost is the fuel cost which dependent on the plant output, and can be determined by [7]:

$$cost_{fuel} = \frac{3412}{eff_{adv}} * cost\_of\_coal \quad \ldots (4.10)$$

4.4 Levelized Cost of Electricity

One potentially useful economic figure of merit is the levelized cost of electricity (LCOE). The LCOE is the revenue received by the generator per net megawatt-hour during the power plant`s first year of operation, assuming that the cost of electricity escalates thereafter at a nominal annual rate of 0 percent, i.e., that it remains constant in nominal terms over the operational period of the power plant [3]. The LCOE can be calculated as follows [7,11]:

$$\text{LCOE} = \{(overnight\_capital\_cost * CRF + fixed\_O\&M\_cost)/(8760 * CF)\} + (fuel\_cost * heat\_rate) + variable\_O\&M\_cost \quad \ldots (4.11)$$

where overnight capital cost is measured in dollars per installed kilowatt ($/kW), capital recovery factor is the ratio of a constant annuity to the present value of receiving that annuity for a given length of time, fixed operation and maintenance (O&M) costs in dollars per kilowatt-year ($/kW-yr) and variable O&M costs in dollars per kilowatt-hour ($/kWh). In the denominator 8760 is the number of hours in a year and capacity factor (CF) is a fraction between 0 and 1 representing the portion of a year that the power plant is generating power. The CRF is determining by using:

$$\text{CRF} = \frac{[r_{dis}(1+r_{dis})^n]}{[r_{dis}(1+r_{dis})^{n-1}]} \quad \ldots (4.12)$$

A Microsoft Excel spreadsheet was used to determine the LCOE of the L-IGFC plant. The model was based on the assumptions as listed Table 4.1.

Table 4.1 Key inputs to the LCOE calculation.

Parameters	**Value**	**Unit**
Coal cost [12]	2.31	$/MMbtu
Depreciation period (n)	20	years
Discount rate (r_{dis})	2	%
Fuel cell module cost [13]	657	$/kW
Coal CO_2 emissions factor [7]	95.3	$MMmtCO_2$/qbtu
Fuel cell module replacement cost [7]	175	$/kW
Module life [7]	5	years
Discount rate for module O&M	2	%

A summary of the techno-economic analysis for 4 power plants are presented on Table 4.2. The total capital cost ($/kW net) given in Table 4.2 for each case. For reference and comparison, the results for a Shell-based IGCC power plant are also shown. The thermodynamic performance of the SCPC and IGCC power plants considered here equals that reported in Ref. [3]. However, the levelized cost of electricity (LCOE) was calculated using the economic assumptions used in this study. The power plants configuration analyzed are described as follows:

1. Supercritical pulverized coal (SCPC) with single reheat 241 bar/593 ºC/593 ºC cycle [3].
2. Integrated gasification combined cycle (IGCC) configuration which incorporates Shell dry feed of Illinois No. 6 coal, pressurized, upflow, entrained, slagging gasifiers, operating at 4.2 MPa and processing a total of 4,753 tonnes/day of

as-received coal. The air separation plant supplies 3,614 tonnes/day of 95% oxygen to the gasifiers and the Claust plant. Coal reacts with oxygen and steam at a temperature of 1427 ºC. The configuration also occupied with steam cycle of 124 bar/559 ºC/559 ºC, whereas 2 gas turbines of advanced F Class with 232 MW output each [3].

3. Atmospheric L-IGFC plant with DGC unit configuration where the Illinois No. 6 coal (as received) fed to gasifier, and the SOFC temperature working condition at 800 ºC.
4. Pressurized L-IGFC plant with DGC unit configuration. Two different condition of coal moisture content fed to the gasifier were analyzed; (i) coal as received with 11.12 wt.% of moisture content and, (ii) coal with 2 wt.% of moisture content. The SOFC working temperature and pressure are at 800 ºC and 3 atm, respectively.

Table 4.2 Capital costs and LCOE of power plants.

	SCPC	**IGCC**	**Atm L-IGFC**	**Press L-IGFC**	**Press L-IGFC**
Operating Conditions					
Coal	Illinois No. 6	Illinois No. 6, 5% moist	Illinois No. 6, 11.12% moist	Illinois No. 6, 11.12% moist	Illinois No. 6, 2% moist
Steam cycle (bar/ºC/ºC)	241/593 /593	241/559 /559	100/565, 40/440	100/565, 40/440	100/565, 40/440
Gas turbine	-	2 x Advanced F class	-	-	-
H_2S removal	WGC	WGC	WGC	DGC	DGC

SOFC					
- Temperature (ºC)	-	-	800	800	850
- Pressure (bar)	-	-	1.08	4	3
- Current density (A cm^{-2})	-	-	0.2	0.2	0.2
Net power (kWe)	549,990	628,980	20,145	21,747	26,215
Efficiency (%, HHV)	39.3%	42.1%	44.6%	48.2%	58.1%
Capacity factor (hr/yr/8760 hrs)	60%	60%	60%	60%	60%
% of power from steam cycle	100%	37%	64%	59%	61%
O_2 requirement (lbO_2/lbdry coal)	0.00	0.80	0.96	0.96	0.96
% CO_2 capture	0%	0%	0%	0%	0%
Total CO_2, $kgCO_2$/kWh	0.83	0.77	0.73	0.67	0.56
Cost Data					
Capital cost, $/kW net					
Coal Handling + Preparation	103	326	310	291	248
ASU	0	285	317	297	254
Gasifier	0	627	595	555	469
Gas Clean Up	234	213	203	190	162
Gas Turbine	0	188	0	0	0
Boiler	539	0	0	0	0
HRSG	68	95	147	139	142
Steam Turbine	211	104	166	155	159
Combustor	0	0	0	0	0
Air Compressor	0	0	0	0	0
Syngas Expander	0	0	0	0	0
Heat Exchanger	0	0	0	0	0
SOFC	0	0	235	266	256
Other	495	378	412	412	412
Total capital cost, $/kW net	1,650	2,216	2,386	2,306	2,102
Variable O&M, cents/kWh	0.01	0.65	0.61	0.57	0.47
Fixed O&M, $/kW/yr	59.3	35.3	47.3	48.9	48.4
Fuel cost, cents/kWh	2.01	1.87	1.77	1.64	1.36
LCOE (cents/kWh)	**5.1**	**5.8**	**6.1**	**5.8**	**5.2**

At the assumed target of SOFC module cost of 657$/kW, the pressurized L-IGFC plant with 2 wt.% coal moisture produces electricity at costs below that of IGCC. Among the L-IGFC configurations studied, the lowest LCOE appeared by pressurized L-IGFC using 2 wt.% coal moisture level. Applying the same procedures as described above, Table 4.3 provides another comparison of electricity cost components between IGFC plants. It is shown that the LCOE of L-IGFC plant still has the lowest LCOE among others design of IGFC plants. However, the next target for L-IGFC plant is to couple with CCS unit while keeping less total cost of producing electricity.

Table 4.3 Efficiency and cost of IGFC.

Plant	Electricity MWe	$\eta_{electrical}$ with CCS (%, HHV)	$\eta_{electrical}$ without CCS (%, HHV)[c]	LCOE cents/kWh
IGFC DIRECT[a] [13]	984	51.4	57.4	5.5
IGFC TREMP[a] [13]	905	47.2	53.2	5.7
IGFC HICOM[a] [13]	998	52.1	58.1	5.4
IGFC[b] [10]	253	56.2	60.1[10]	5.3

[a] SOFC cost at 657$/kW AC, with operating temperature and pressure of SOFC are 800 ºC and 20 bar, respectively.

[b] SOFC cost at 657$/kW AC, with operating temperature and pressure of SOFC are 800 ºC and 18 bar, respectively.

[c] Assume the percentage point of the plant efficiency losses due to introducing CCS unit up to 6 for comparison LCOE of related plants.

REFERENCES

[1]. Rubin E, Booras G, Davison J, Ekstrom C, Matuszewki M, McCoy S, Short C. Toward a common method of cost estimation for CO_2 capture and storage at fossil fuel power plants 2013, Global CCS Institute: Canberra, Australia.

[2]. Majoumerd MM, Assadi M. Techno-economic assessment of fossil fuel power plants with CO2 capture-results of EU H2-IGCC project. Int J Hydrogen Energy 2014;39:16771-16784.

[3]. Haslbeck JL, Hamilton BA, Kuehn NJ, et al. Cost and performance baseline for fossil energy plants, Bituminous coal and natural gas to electricity, vol. 1. DOE/NETL-2010/1397.

[4]. Rubin ED, Chen C, Rao AB. Cost and performance of fossil fuel power plants with CO_2 capture and storage. Energy Policy 2007;35:4444-4454.

[5]. DOE/NETL-341/013113 Report, 2013. Capital cost scaling methodology: Quality guidelines for energy system studies.

[6]. CAESAR. European best practice guidelines for assessment of CO_2 capture technologies, in the European Benchmarking Task Force (EBTF) 2011.

[7]. DOE/NETL-402/061308 Report, 2008. The impact of advanced syngas conversion technologies on the cost of electricity from gasification-based power generation platforms.

[8]. Arsalis A. Thermoeconomic modeling and parametric study of hybrid SOFC-gas turbine-steam turbine power plants ranging from 1.5 to 10 MWe. J Power Sources 2008;181:313-326.

[9]. Siefert NS, Litster S. Exergy and economic analyses of advanced IGCC-CCS and IGFC-CCS power plants. Appl Energy 2013;107:315-328.

[10]. Gerdes K, Grol E, Keairns D, Newby R. Integrated gasification fuel cell performance and cost assessment, DOE/NETL-2009/1361, U.S. Department of Energy, Morgantown, WV, 2009.

[11]. http://www.nrel.gov/analysis/tech_lcoe_documentation.html

[12]. http://www.eia.gov/forecasts/steo/report/prices.cfm

[13]. Lanzini A, Kreutz TG, Martelli E, Santarelli M. Energy and economic performance of novel integrated gasifier fuel cell (IGFC) cycles with carbon capture. Int J Greenh Gas Con 2014;26:169-184.

CHAPTER 5

CONCLUSIONS AND FUTURE PERSPECTIVE

5.1 Conclusion

The increasing demand for electricity has been faced with a global concern, i.e. increasing worldwide GHG emissions. Several potential pathways to mitigate the emissions and future energy solutions are diversity in primary energy sources and generation technology, improved the efficiency of energy conversion, and optimally matching energy technologies and resources to specific uses. High power plant efficiency means that the use of fuel, such as coal, can be reduced. That lowers the power generation cost, and also at the same time reducing CO_2 emission. In this thesis, the L-IGFC plant consisting of coal gasifier and SOFC on the top of a steam turbine (ST) has been proposed. Major conclusions drawn from this thesis research work are summarized as the following:

- Employing a WGC unit into the L-IGFC plant poses relatively bigger efficiency penalty due to significant waste of thermal energy and requires complex heat exchanger equipment during syngas cleanup processes. But, the DGC unit that can work at high temperatures and high pressures to remove sulfur compound until less than 0.1 ppm and other species contaminant during the cleanup processes contribute to increase the overall performance of the plant.
- Implementing the DGC unit into L-IGFC plant increase the efficiency and at the same time simplifying the layout of the plant by removing the complexity of heat exchanger network required.
- The SOFC module is the critical part in this L-IGFC plant. Changing the working

conditions of the SOFC will contribute to performance of the plant. It was found that the pressurized L-IGFC system with DGC gives the maximum electrical efficiency of 50.04% in LHV when operated at SOFC working pressure of 4 atm (4.053 bar) and current density of 0.2 A cm^{-2}.

- Further improvement step to the plant is by adding a coal dryer for reducing the moisture content of the fed coal to gasifier until 2 wt. %. The analysis shown that it increase the performance of SOFC due to increasing the equivalent hydrogen contained in the raw syngas. Meanwhile, heat rate improvement occurred in system also contribute to further increasing the steam turbine performance by increasing the steam mass flow rate. Thus, overall electrical efficiency of 60.12% in LVH achieved when SOFC working pressure of 3 atm and current density of 0.2 A cm^{-2}.
- A sensitivity analysis on the different working temperatures and pressures of SOFC conducted where the maximum electrical efficiency of the system realized when SOFC operating conditions are 850 ºC and 3 atm. The electrical efficiency at this condition is 60.32% in LHV.
- The techno-economic estimate presented in this work shown that L-IGFC plant has lowest LCOE compared to IGCC and IGFC plants.

5.2 Future Perspective

There are a number of issues that are still to be addressed for further improvement of L-IGFC plant design:

1. SOFC models are the primary investigation tool in the L-IGFC design and optimization, and the validity of the models should be examined carefully. The SOFC model could be adapted to explore other SOFC designs, such as the

flattened tubular SOFCs or planar SOFCs. Computational fluid dynamic (CFD) modeling of the SOFC module could be employed to explore the internal temperature distributions within SOFC module. The CFD model would reveal the preheat temperature limits as it would display the temperature gradients within the module. Also, experimental data on commercial SOFC performance are very useful in further validating and calibrating the developed SOFC model.

2. Based on literature survey, it is possible to increase the system efficiency by employing a catalytic hydro-gasifier. The catalytic hydro-gasification process operates at relatively low temperature and produces high methane content syngas which benefits both the gasifier efficiency and the SOFC performance.
3. The predictive capability of the integrated system models could be improved by simulating the syngas cleanup process in more detail. The chemical reactions that occur during H_2S, HCl, and HCN removal were not modelled. The processes were modelled using Aspen Plus separator blocks. It would be possible to predict the required flow rate of adsorbent in more details if those processes were modeled.
4. As DGC and SOFC technologies become well establish, more reliable and detailed economic data will become available and it will be possible to reduce the level of uncertainty for developing more accurate techno-economic analysis.